Mechanistic studies on the adverse cardiovascular and cerebral effects of lifestyle and environmental risk factors - e-cigarette vapour, shisha smoke and aircraft noise - in cellular and murine models

A dissertation submitted to attain the academic degree of

Doctor of Philosophy (Ph.D.)

from the Faculties

University Medical Center,

Social Sciences, Media, and Sports,

Chemistry, Pharmaceutical Sciences, Geography, and Geosciences,

and

Biology

of the Johannes Gutenberg University Mainz

Ivana Kuntić

Born 11.03.1992 in Belgrade, Serbia

The present work was performed from November 2020 to November 2024 in the Department of Cardiology, Cardiology I, Laboratory for Molecular Cardiology, University Medical Center of the Johannes Gutenberg University in Mainz.

Date of oral examination: 22.01.2025.

Zusammenfassung

Mit fortschreitenden Verbesserungen in der Hygiene und medizinischen Versorgung gewinnen Umweltrisikofaktoren wie Fluglärm und Lebensstil-Risikofaktoren wie E-Zigaretten und Shisha-Rauchen an Bedeutung für die globale Krankheitslast. Mithilfe eines zuvor etablierten Mausmodells wurde in der vorliegenden Arbeit die Verbindung zwischen neuronalen und kardiovaskulären Systemen unter Lärmbelastung untersucht. Nach der Exposition von Mäusen gegenüber Fluglärm für entweder 4 oder 28 Tage waren der Blutdruck und mehrere oxidative Stressmarker erhöht und die Endothelfunktion war beeinträchtigt. Die Behandlung mit neuroaktiven und blutdrucksenkenden Medikamenten milderte diese Effekte, was die Rolle von psychologischem Stress bei durch Lärm verursachten Herz-Kreislauf-Schäden hervorhebt. Mäuse wurden auch nach 4-tägiger oder 28-tägiger Fluglärmbelastung einer Reihe von Verhaltenstests unterzogen. Nach 4 Tagen Lärmbelastung zeigten die Mäuse keine Verhaltensänderungen, aber nach 28 Tagen Lärmbelastung zeigten sie eine verminderte Gedächtnisleistung und soziale Interaktion. Obwohl Verhaltensänderungen auftraten, entsprachen diese nicht den erwarteten angstähnlichen Verhaltensweisen. Nachdem meine Gruppe zuvor die Auswirkungen von E-Zigaretten-Dampfen auf den kardiovaskulären oxidativen Stress gezeigt hatte, wurden hier kultivierte Endothelzellen und Makrophagen entweder E-Zigaretten-Dampf-Kondensat oder einem toxischen Bestandteil des Dampfes, Acrolein, ausgesetzt, um die mögliche Quelle des durch E-Zigaretten verursachten oxidativen Stresses zu untersuchen. Die Ergebnisse zeigten, dass sowohl das E-Zigaretten-Dampf-Kondensat als auch Acrolein konzentrationsabhängige Effekte auf beide Zelltypen hatte und dass Acrolein die Aktivierung des NADPH-Komplexes und die Erzeugung von Superoxid fördern kann, wie von uns bereits für E-Zigaretten-Dampf publiziert. Die Aktivierung von Stress-Genen (Nrf2-abhängig) wurde auch in DLD1-HO1-Promotorzellen nach Exposition gegenüber E-Zigaretten-Dampf und Acrolein gezeigt. Darüber hinaus wurde ein Mausmodell für Shisha-Rauch-Exposition etabliert. Nach anfänglicher Optimierung der Expositionsbedingungen untersuchte ich die Auswirkungen des Shisha-Rauchens auf die kardiovaskuläre und neuronale Funktion bei Mäusen. Die Endothelfunktion war bei Mäusen, die Shisha-Rauch ausgesetzt waren, beeinträchtigt, und eine marginale Erhöhung des Blutdrucks wurde beobachtet, was wahrscheinlich auf die vasodilatierenden Effekte von CO im Shisharauch zurückzuführen ist. Ausgewählte Marker für oxidativen Stress und Entzündung im Herz-, Aorten- und

Lungengewebe waren erhöht. Im kortikalen Gewebe wurde lediglich eine erhöhte Bildung reaktiver Sauerstoffspezies beobachtet. Erhöhte oxidative Stressmarker wie NQO-1 und HO-1 deuten auf die Aktivierung des Nrf2-Wegs als potenten antioxidativen Abwehrmechanismus hin. Die Aktivierung des Nrf2-Wegs wurde in den DLD1-HO1-Promotorzellen bestätigt, die Feinstaub-Partikeln ausgesetzt waren, wie sie durch die Verbrennung der Kohle bzw. Des Tabaks während einer Shisha-Session generiert werden können. Diese Arbeit ist sowohl für Grundlagenwissenschaftler als auch für medizinische Fachkräfte von Interesse, da sie einen tieferen Einblick in die möglichen Mechanismen bietet, durch die Umwelt- und Lebensstilrisikofaktoren das kardiovaskuläre System und neuronale Prozesse beeinflussen.

Abstract

With improvements in hygiene and medical care, environmental risk factors like aircraft noise and lifestyle choices such as e-cigarettes and shisha smoking gained prominence in global disease burden. This study used an established mouse model to investigate the link between the neuronal and cardiovascular systems under noise exposure. After exposing mice to aircraft noise for either 4 or 28 days, blood pressure and several oxidative stress markers were elevated and endothelial function was impaired. Neuroactive and antihypertensive drugs alleviated these effects, underscoring the role of psychological stress in noise-induced cardiovascular damage. Behavioural tests post-exposure showed that while 4 days of noise did not affect behaviour, 28 days-noise exposure impaired working memory and social interaction, though not consistent with the expected anxiety-like behaviour. After my group previously demonstrated effects of vaping on the cardiovascular oxidative stress, I exposed cultured endothelial cells and macrophages to either e-cigarette vapour condensate or acrolein, to explore the source of e-cigarette-induced oxidative stress. The results showed that both exposures followed the concentration-dependent effects on both cell types, and that acrolein can promote the NADPH-oxidase activation and generation of superoxide, as already published for e-cigarette vapour. The activation of Nrf2-dependent-stress-genes was also shown in DLD1-HO1-promotor cells after exposure to e-cigarette vapour and acrolein. Additionally, we established a mouse model of shisha smoke exposure and tested the effects shisha smoking has on cardiovascular and neuronal function in mice. Endothelial function was impaired in mice exposed to shisha smoke, but interestingly, blood pressure increased only marginally, probably due to the vasodilatory effects of CO in the shisha smoke. Selected markers of oxidative stress and inflammation were elevated in the heart, aortic and lung tissue, whereas only reactive oxygen species formation was elevated in the cortex. Increased oxidative stress markers, such as NQO-1 and HO-1 point to the activation of the Nrf2-pathway as a potent antioxidant response mechanism. This activation was confirmed in the DLD1-HO1-promotor cells exposed to particulate matter as it can be produced by coal and tobacco burning during a shisha session. This work is of interest for both basic scientists and medical professionals, as it provides a deeper insight into the possible mechanisms by which environmental and lifestyle risk factors affect the cardiovascular system.

List of abbreviations

$^{\bullet}O_2^-$ – superoxide radical

$^1O_2$ – singlet oxygen

O_3 – ozone

$^{\bullet}OH$ – hydroxyl radical

4-HNE – 4-hydroxynonenal

8-OHdG – 8-hydroxy-2'–deoxyguanosine

A – adrenaline

ACTH – adrenocorticotropic hormone

Ang II – angiotensin 2

ARE – antioxidant-response element

BH_2 – dihydrobiopterin

BH_4 – tetrahydrobiopterin

cGMP – cyclic guanine monophosphate

CO – carbon monoxide

COPD – chronic obstructive lung disease

COX2 – cyclooxygenase 2

CRF – corticotropin-releasing factor

CRP – C-reactive protein

Cul3-Rbx1-E3 – Cullin-3-ring-box 1-E3 ubiquitin ligase complex

CVD – cardiovascular disease

DAMP – damage-associated molecular pattern

DALY – disability-adjusted life years

DMF – dimethyl fumarate

eNOS – endothelial nitric oxide synthase

ET-1 – endothelin-1

EpRE – electrophilic-response element

FAD – flavin adenine dinucleotide

FBF – forearm blood flow

FMD – flow mediated dilation

FMN – flavin mononucleotide

GCLC – glutamate-cysteine ligase catalytic subunit

GCLM – glutamate-cysteine ligase regulatory subunit

GDP – guanosine diphosphate

GTP – guanosine triphosphate

GSH – glutathione

GST – glutathione-S-transferase

H_2O_2 – hydrogen peroxide

HO-1 – heme-oxygenase-1

HPA axis – hypothalamus-pituitary-adrenal axis

IL-1ß – interleukin-1ß

IL-6 – interleukin 6

IL-8 – interleukin 8

iNOS – inducible nitric oxide synthase

Keap1 - kelch-like ECH-associated protein 1

MC2-R – melanocotrin-2 receptor

MDA – malondialdehyde

NA – noradrenaline

NADPH-oxidase – nicotinamide adenine dinucleotide phosphate oxidase

NF-E2/AP-1 – nuclear factor erythroid 2/activator protein 1

NF-κB – nuclear factor kappa-B

nNOS – neuronal nitric oxide synthase

•NO – nitric oxide

NOS – nitric oxide synthase

NOX2 – nicotinamide adenine dinucleotide phosphate oxidase-2

Nrf2 – nuclear factor erythroid 2-related factor 2

NQO-1 – NAD(P)H dehydrogenase quinone 1

$ONOO^-$ – peroxynitrite

PKC – protein kinase C

PKG – cGMP dependent protein kinase

PAMP – pathogen-associated molecular pattern

PRR - pattern-recognition receptor

Prx - peroxiredoxin

Rac – Rho-related C3 botulinum toxin substrate

ROS – reactive oxygen species

SOD – superoxide dismutase

SRXN1 – sulfiredoxin-1 reductase

TNF-α – tumor necrosis factor alpha

TPR domain – tetratricopeptide repeat

Trx – thioredoxin

TRX1 – thioredoxin 1 reductaseVOC – volatile organic compound

Table of contents

1. Introduction

1.1. General introduction

Concept of stress has significantly changed over the years. Even though the word stress is conventionally used synonymously with the psychological stress, it is actually defined very broadly as "challenging of the homeostasis", and factors with the potential to directly challenge homeostasis are defined as stressors [1]. Because of this broad definition, both stress and stressors may be separated into multiple groups, according to the way homeostasis is challenged. Initially, stress was divided into physiological and psychological stress, with multiple subtypes within each group, such as temperature stress and hypoxia as physiological stresses, and emotional or socioeconomic stress as psychological stresses [2]. At the time, stress was defined as a syndrome that activates pituitary-adrenal cortical system [3]. However, this definition proved to be incomplete, as we are now aware of many more systems activated by stress. The division of stress into physiological and psychological stress is also considered incomplete, as some known stressors could not fit into one of the groups (such as certain environmental stressors) and some stressors may fit into both groups (such as some behavioural stressors). Stress is therefore defined mostly by the stressors that may cause it, such as oxidative stress, nutrient stress, heat stress, shear stress, mechanical stress, etc, and by the systems that it activates, such as cardiac stress, cytoskeletal stress, mitochondrial stress, dopamine neuron-specific stress, telomere stress, etc. [1].

1.1.1. Exposome

Having the need to understand all the stressors that may impede human health, Christopher Paul Wild devised the term exposome [4]. In his words, "exposome encompasses life-course environmental exposures (including lifestyle factors), from the prenatal period onwards" and the biochemical effects of these exposures leading to health outcomes such as chronic disease or death. This concept proved to be much more comprehensive than simply defining certain stressor as an individual factor for stress reaction in the body. Exposome, therefore, includes external factors that one has little control over like air pollution, noise, social surrounding, green spaces and climate, and factors that one can control, such as tobacco consumption, exercise, diet and exposure to household chemicals. This is all combined with the internal factors of genetics, individual metabolism and disease to provide an overarching

set of risk factors that influence one's health. A summary of the concept of exposome and the major obstacles for its implementation in medicine are shown in **Figure 1**.

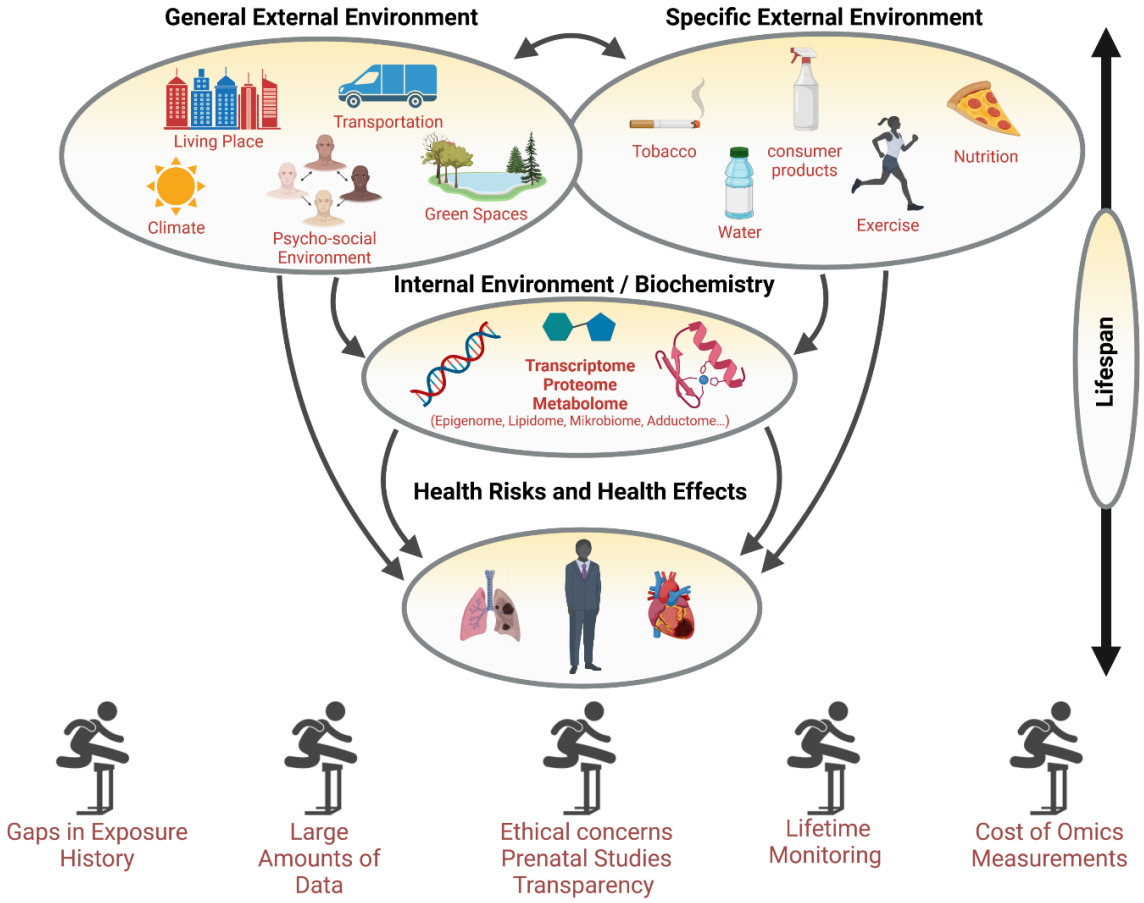

Figure 1. The Exposome concept. The exposome is a term that integrates everything an individual has been exposed to during their lifetime. Presented here are the major exposure factors, as well as major obstacles for a comprehensive exposome study. Reused from [5, 6]. Figure created with Biorender.com

1.1.2. Noise

Environmental noise as a stressor has recently gained much needed attention from the scientific and medical community. World Health Organization (WHO) estimates that in Europe alone, at least 1 million healthy life years are lost each year due to the exposure to environmental noise [7]. However, even though there is significant evidence about the adverse effects that noise poses for human health, not much attention is dedicated to the prevention of noise health effects in everyday human life. All of the human disorders that noise is associated with are shown in **Figure 2**. Even though there are legal recommendations

for the intensity of noise a person should be subjected to (annually, not more than 40 dB outdoor during night-time), more than 1/3 of the European population is exposed to noise levels that exceed these recommendations, according to the WHO Burden of Disease article [8].

There are different types of noise with different effects reported throughout literature. The type of noise depends on its source and can be environmental (such as transportation noise – where aircraft noise falls into, and community noise), occupational (in industrial or construction setting) or self-exposed (loud music at concerts). In addition, noise can be persistent, acute or, like the aircraft noise used in our experiments, it can be sporadic or intermittent noise [9]. From all types of noise, the intermittent noise is the most significant contributor to the human burden of disease [10]. Traffic noise in general is intermittent in nature, with road noise being more dependent on the time of the day, and train and aircraft noise being dependent on the transport schedule. These variations in noise levels are the major cause of annoyance in the areas surrounding airports [11, 12], as well as sleep disturbance [13, 14] and poorer working efficiency [15].

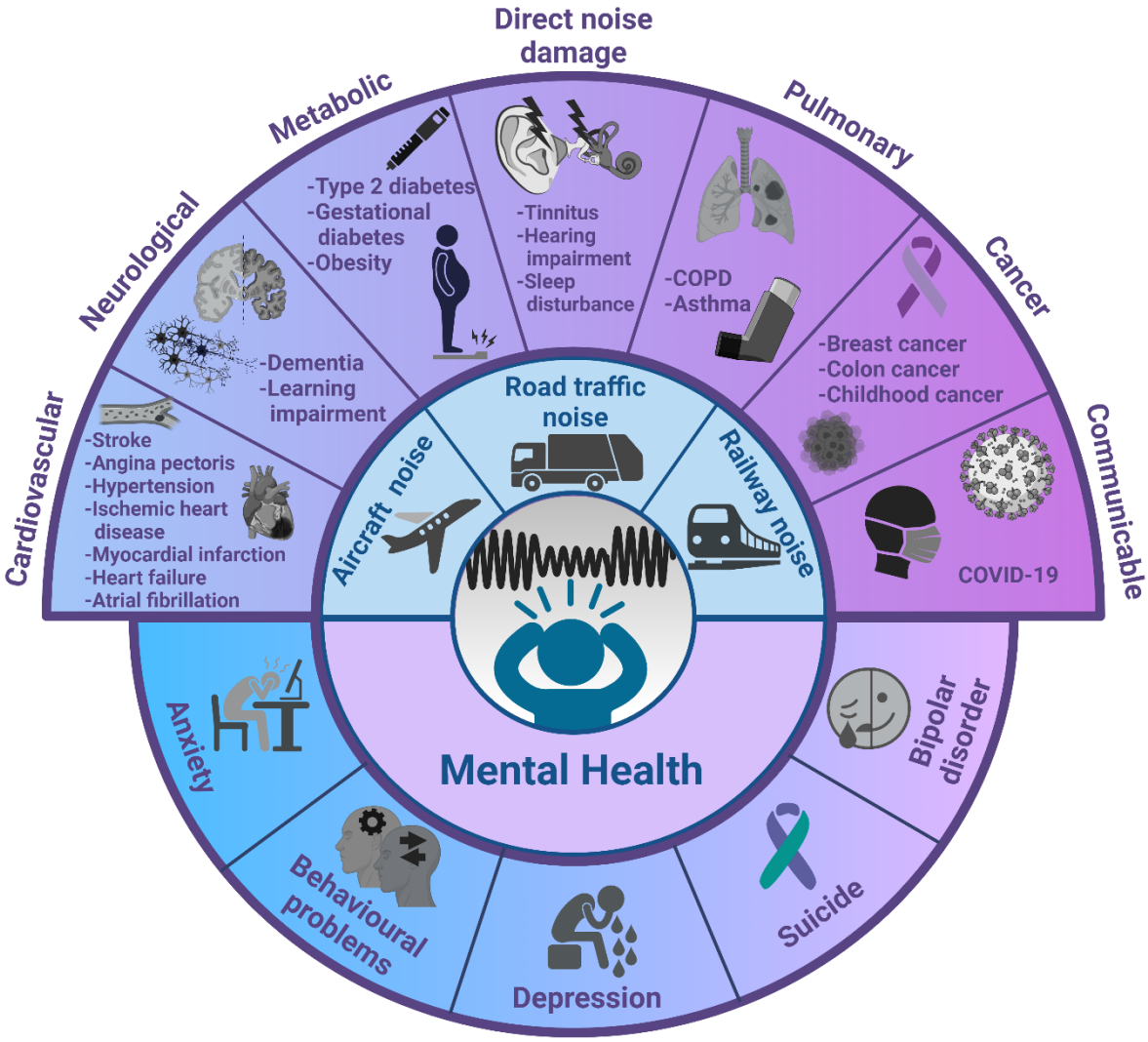

Figure 2. Noise-induced diseases. Overview of all the diseases where noise is an established risk factor, with the emphasis on mental health effects. Figure reused from [16]. Created with BioRender.com

Some studies have positively associated road traffic noise with all-cause mortality with the relative risk ranging from 4.5 % to 8 % per 10 dB increase in noise levels (reviewed in [17]). In contrast, some studies did not observe a positive association between transportation noise and all-cause mortality, although trends towards increasing risk with levels of noise was observed ([18, 19]). In addition to all-cause mortality, transportation noise has an effect on the burden of disease with an estimate that transportation noise is associated with 22 million DALYs (disability-adjusted life years) due to annoyance and 6.5 million DALYs due to sleep disturbance [20].

Noise is also associated with cardiovascular diseases (CVD) [21, 22]. European Environment Agency estimates that 11,000 premature deaths and 40,000 new cases of ischemic heart disease are caused by noise exposure in Europe every year [20, 23]. So far, many studies have shown a link between the incidence of ischemic heart diseases and exposure to noise [24-27]. Additionally, there is evidence from epidemiological studies that long-term exposure to aircraft noise could lead to increased incidence of arterial hypertension [28, 29], a known risk factor for cardiovascular diseases. One of the first studies on the connection between noise and the cardiovascular disease was the Caerphilly study, started in 1984. The study links cardiovascular risk factors, such as elevated systolic blood pressure, total cholesterol and decreased platelet count with the traffic noise exposure [30]. Following this study, others have found that mortality from myocardial infarction increased with the intensity and duration of both traffic noise in general and aircraft noise specifically [31-34]. Furthermore, road traffic noise was associated with higher stroke incidence [32, 35], whereas a study on 5,000 participants associated the railway noise during the night, industrial noise during the day and aircraft noise during both day and night with increased levels of midregional pro-atrial natriuretic peptide, a marker of endothelial dysfunction [36]**.** It is now obvious there are multiple mechanisms involved in the noise-triggered vascular damage, and they are still not fully understood.

1.1.3. E-cigarettes

Tobacco smoke has been a known cardiovascular disease risk factor for decades now and governments around the world are constantly constricting regulations surrounding it.

Significant amount of proof of adverse effects of tobacco cigarettes, negative propaganda and constricting regulations lead to the slow, but constant, decrease of smoking classical tobacco cigarettes in the last few decades [37] (

Figure 3). However, this opened a market for new ways of consuming tobacco and nicotine, such as electronic cigarettes (e-cigarettes), other electronic nicotine-delivered systems and shisha. Electronic cigarettes are devices that heat and vaporize the liquid that contains nicotine (**Figure 4**). This vapour is then inhaled, giving the consumer a sensation of smoking. The system was officially invented by Hon Lik in 2003, even though similar systems were tested since the 1960s. The idea behind the e-cigarettes was to remove negative substances tobacco produces while burning, thus inhaling “pure” nicotine and removing adverse effects

connected to tobacco smoke toxicants. Additionally, as the e-cigarette liquid contains different amounts of nicotine, even none at all, a consumer may ease their way into inhaling less nicotine and eventually quit smoking altogether. The look and feel of e-cigarettes is similar to regular tobacco cigarettes and the inhaling vapour gives similar sensation to inhaling smoke, so the physical and behavioural aspects of smoking are preserved. This is why electronic cigarettes seemed like a good alternative to other nicotine replacement therapies and were marketed as smoking cessation devices. However, even though the transition from tobacco to electronic cigarettes proved to be quite easy and effective, it didn't lead to the complete abandoning of smoking in the end [38-41]**.** Since their introduction to the global market, the popularity they gained was so significant, that, at the moment, 4.5 % of people in the USA use e-cigarettes, almost as half of the people using tobacco cigarettes (11.5 % according to CDC [37]). Although e-cigarettes were supposed to be used by smokers trying to quit nicotine, over half of the people over the age of 18 currently using electronic cigarettes report they have never smoked tobacco cigarettes before [42]. At the same time, e-cigarettes are widely popular among teenagers and young adults, leading to concerns about the effects e-cigarettes may have on the still developing human body, and on the future nicotine addiction [43, 44].

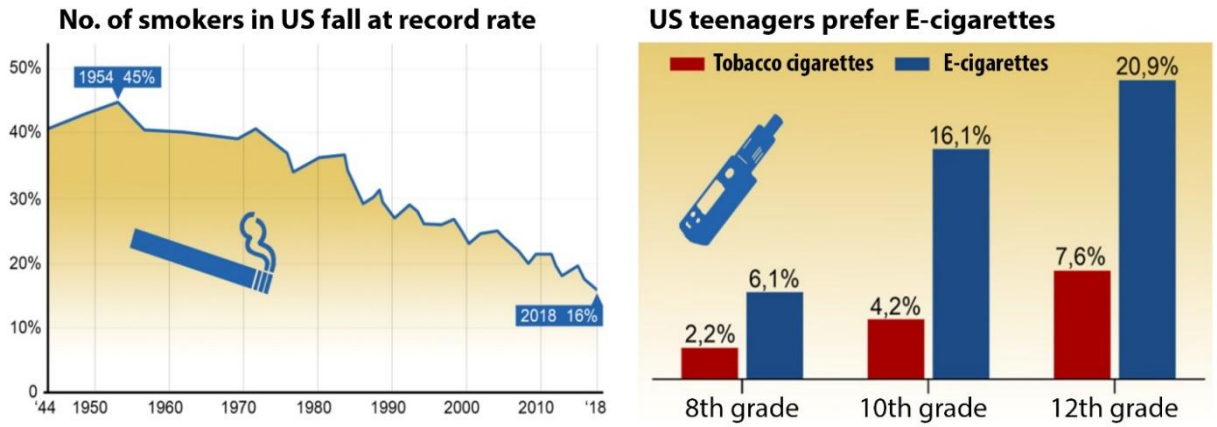

Figure 3. Smoking and vaping popularity. Falling rate of smoking presented together with the raising rate of e-cigarette smoking in teenagers in the USA. Data used from Statista [44, 45]. Adapted from [46].

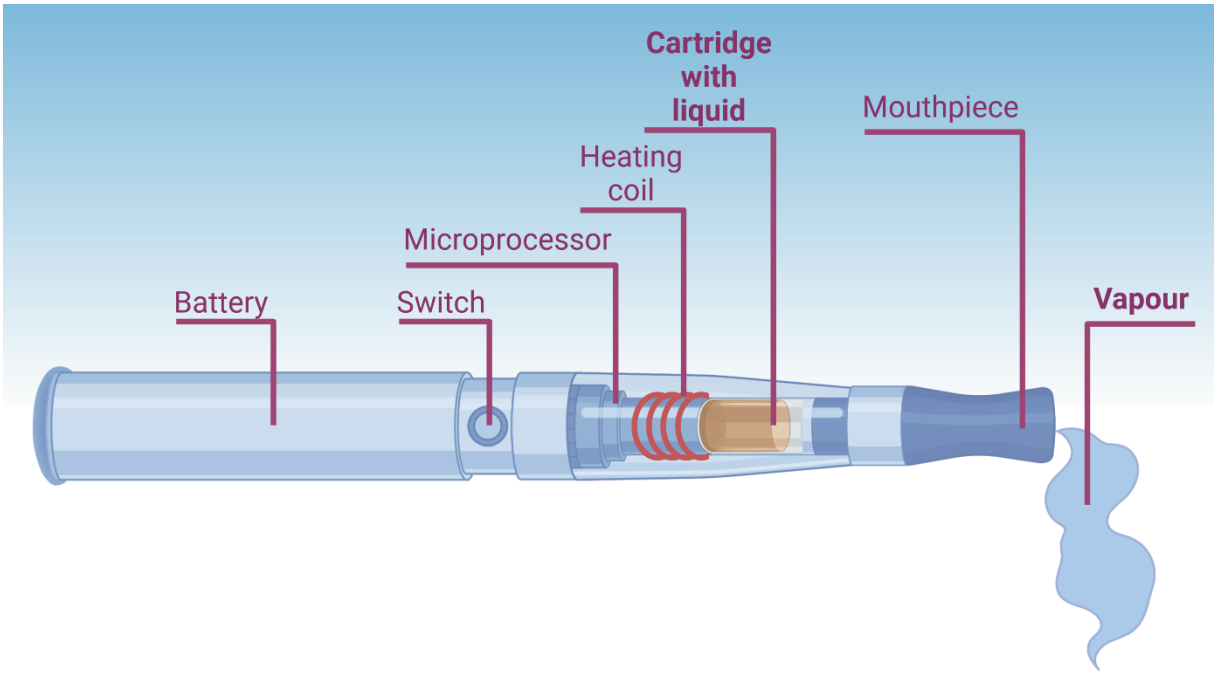

Figure 4. Electronic cigarette scheme. Electronic cigarette (e-cigarette) is a battery-powered system that heats and vaporizes the liquid containing various percentages of propylene-glycol and glycerine, with additions of nicotine and flavours and some other additives. Vapour is than inhaled by the user through a mouthpiece. This way inhaling resembles inhaling smoke from tobacco cigarette but without burning and degrading the tobacco. The system consists of the cartridge (that contains e-cigarette liquid), heating coil connected to the lithium-ion battery and a microprocessor with a switch that activates the heater when pressed or when the user generates negative pressure by taking a puff. Figure created with BioRender.com

Since the literature on e-cigarettes is still sparse, some studies have suggested that the observed negative effects are due to nicotine content in the e-cigarettes [47]. There has still been some evidence that negative effects persist regardless of the nicotine content, even when using liquid that does not contain nicotine. In a recent study by Zhao et al, it was found that heavy metal content in the vapour of e-cigarettes varies significantly with different flavours and nicotine content. However, these variations did not necessarily have the same trend, namely, lead content was significantly higher in vapour from liquid that did not contain nicotine at all [48]. One limitation of the aforementioned study is that nicotine content was not tested, but provided by the manufacturer. However, it was previously reported that most commercial e-cigarette liquids have 1.2 times higher nicotine content than reported [49], with significant variations between manufacturers. In published work from my group, it was found

that a vapour from non-nicotine containing e-cigarette liquid has negative effects on endothelial cells and macrophages, similar to the effects acrolein has on the same cells [50]. It was also shown in human studies that inhaling vapour (or vaping) may have negative impact on the lung and cardiovascular system regardless of the nicotine content [51, 52].

On the other hand, there have been reports where e-cigarette use was not connected to the increased risk for cardiovascular diseases. In a cross-sectional study in 2016 and 2017, no association between myocardial infarction or coronary heart disease and e-cigarette use was found [53]. In a study on 105 healthy smokers, no increase in heart rate or blood pressure was observed, nor any negative respiratory health outcomes. In addition, there were indices that there are some health benefits from switching from tobacco cigarettes to e-cigarettes, such as lower exhaled carbon monoxide (CO) and nitric oxide (NO) levels [54]. When e-cigarettes with and without nicotine were compared, it was shown that only e-cigarettes with nicotine increase cardiac sympathetic nerve activity [55]. Interestingly, a study looking at the efficacy of smoking cessation using e-cigarettes, showed that they are superior to other nicotine replacement products, but the percentage of subjects still using e-cigarette after the trail was much greater than those using other nicotine replacement products (80 % vs 9 %) [38]. It is apparent that the topic of e-cigarette use is not an easy one and there is no black-and-white approach to the effects of vaping. Additional research is needed to understand the mechanisms behind the observed effects, as well as long-term studies on vaping, so that the full scope of effects can be assessed.

1.1.4. Shisha

Another way of enjoying tobacco that became attractive in recent years in the western world is shisha (waterpipe, hookah or narghile) smoking. Since the global epidemic of shisha smoking is still new, most countries do not recognise shisha as a way of consuming tobacco in their statistics. It is estimated that over 10 % of the Middle Eastern population and between 2 % and 10 % of European population smokes shisha regularly, with increasing popularity among young people [56, 57]. Hakim Abul-Fath Gilani invented this method of inhaling tobacco smoke in the 16th century, by purifying it through water [58]. At the beginning, only pure tobacco was smoked in this way. However, when flavours were introduced into the market, they were inevitably used also in the shisha mixtures for inhalation. Introducing different flavoured tobacco, shisha smoking became more attractive for younger generations. Moreover, since

there are limited regulations regarding shisha smoking, it is widely available for teenagers and, in certain parts of the world, it is socially accepted and became a part of café culture. Additional reason for increased prevalence of use among young people is the price of shisha tobacco, which is often lower than the price of cigarettes and/or e-cigarettes [59].

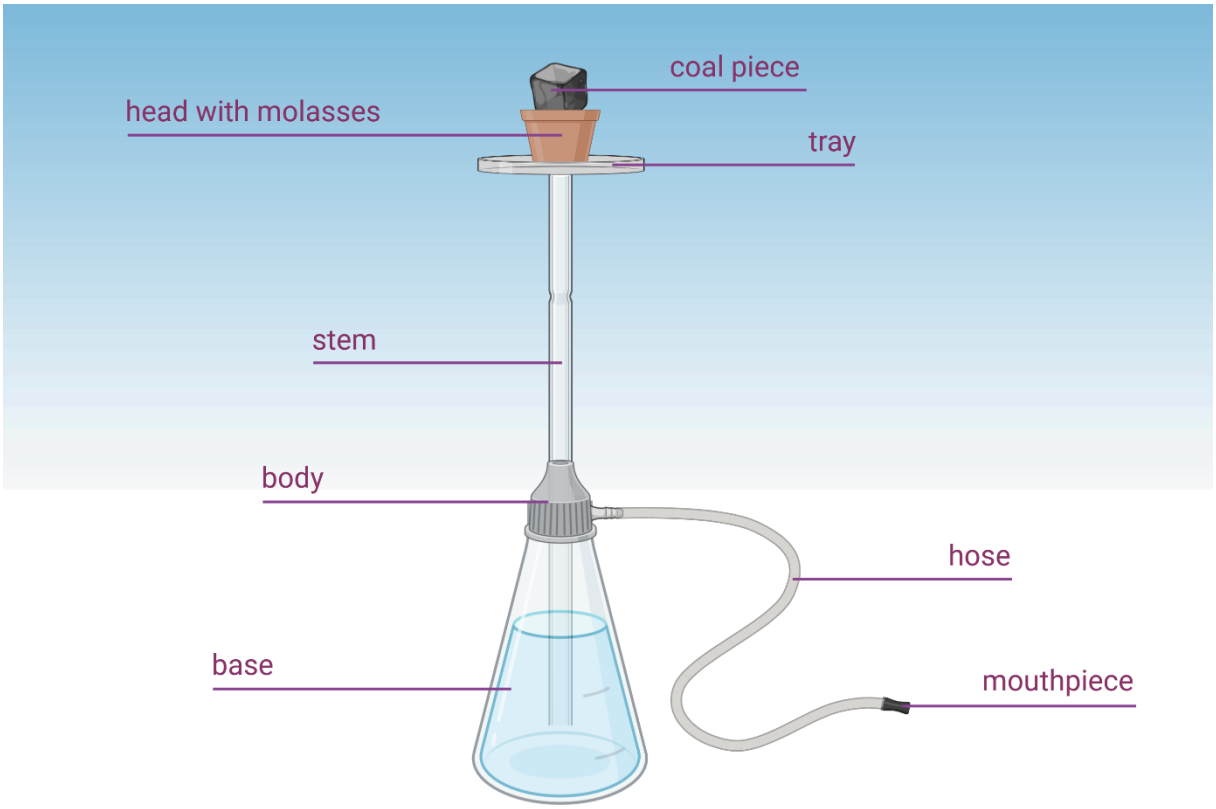

Figure 5. Shisha scheme. Shisha is a device for inhaling tobacco smoke that is passed through water. The system contains a base (bowl filled with water), a body (metal cap that closes the bowl and has one inlet and at least one outlet for a mouthpiece), a head (that is filled with shisha tobacco or molasses and closed with a cap or aluminium foil on top of which a piece of burning coal is added before smoking) and a hose with mouthpiece that is connected to the body. Figure created with BioRender.com

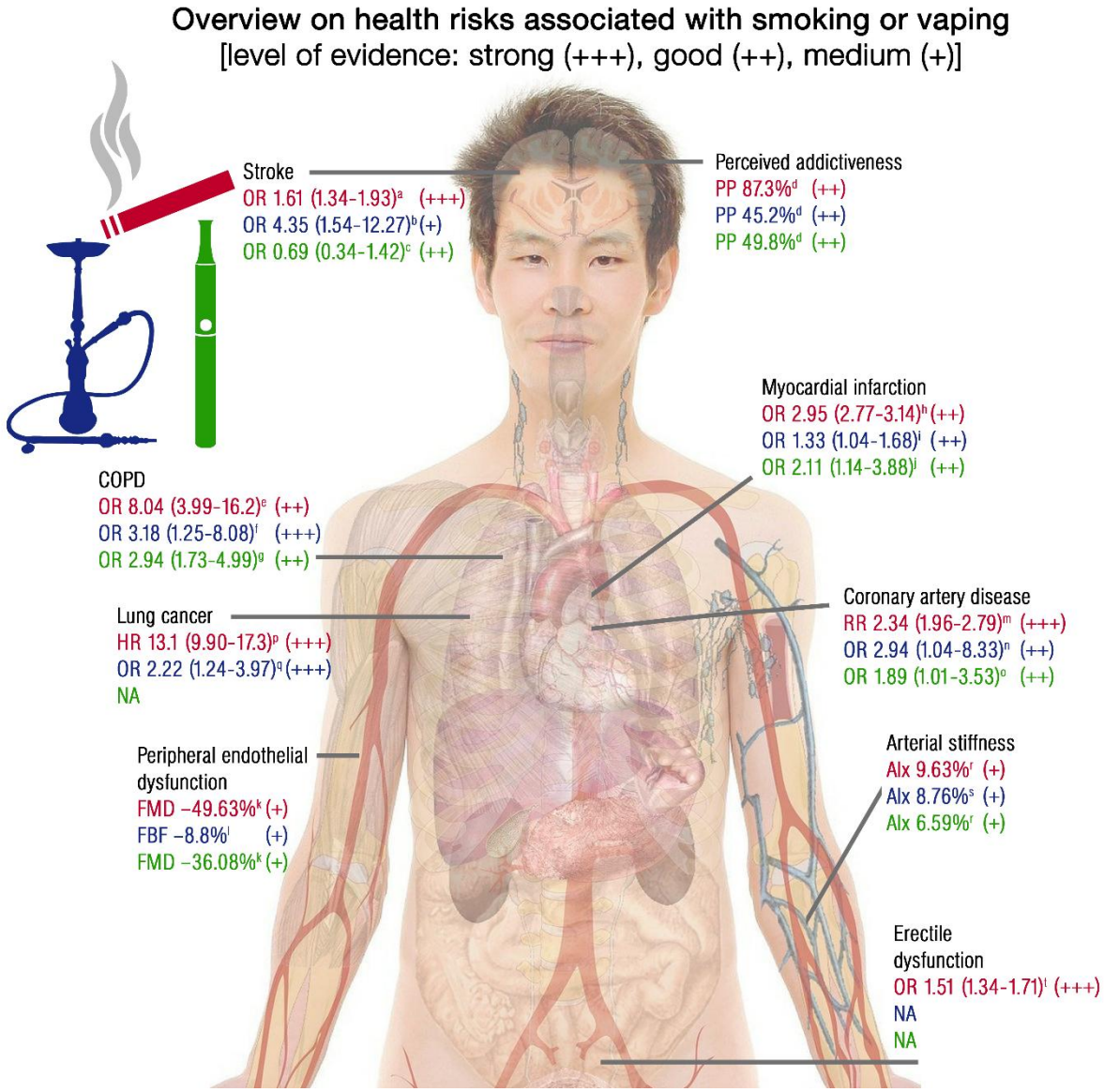

Figure 6. Negative effects of smoking, vaping and shisha smoking. Overview of the negative health effects connected to smoking, vaping and shisha smoking. The results are a representation of published work with different levels of confidence. Originally published in [60]. COPD = chronic obstructive pulmonary disease; N/A = not available; FMD = flow mediated dilation; FBF = forearm blood flow; Aix = augmentation index, OR = odds ratio, RR = relative risk, HR = hazard ratio. Data collected from various sources listed in Supplementary material online of [60].

Shisha tobacco is a flavoured version of tobacco called molasses. It is burned using coal or electronic heater and produces smoke that is passed through water before being inhaled by the user [58] (

Figure 5). The shisha smoke differs from cigarette smoke since the burning technique is different – in cigarettes, tobacco is burned directly and usually does not contain flavours, whereas molasses are burned by coal so the smoke contains components that arise from coal, as well as flavourings added. There are some possible differences between molasses – there are different amounts of nicotine content, sometimes even molasses without tobacco, therefore without nicotine. However, the smoke produced by tobacco-free molasses still contains known carcinogenic compounds that arise mostly from burning coal [61]. Another problem found in investigating effects of shisha on health is the way of smoking. Cigarettes are enjoyed separately and, by a number of cigarettes or packs per day, one can easily calculate the amount of nicotine and other components inhaled. Shisha, on the other hand, is enjoyed in sessions that usually last 30-60 min, is shared among multiple people and the amount of molasses used depends on the preference of the person loading the shisha. So far, there is no ISO standard for shisha smoking (unlike cigarette and e-cigarette smoking), which makes it harder for researchers to compare effects of shisha to the effects of cigarettes or e-cigarettes [60]. Even though there are still misconceptions around inhaling smoke that was passed through water and thus thought to be purified and healthier, it was shown in multiple studies that there are certain negative health effects of smoking shisha, similar to tobacco smoking and that there is almost no filtration of the toxic components [62, 63].

Several studies investigated effects of shisha smoke in preclinical and clinical studies and the observed effects can be separated into several categories – pulmonary effects, cardiovascular effects, increased risk of infection and cancer [58, 64, 65]. Since the work of my group is connected to cardiovascular research, these effects are the only ones that will be discussed here, but the major health effects of shisha, as well as e-cigarettes and classic tobacco cigarettes, are shown in

Figure 6 and

Figure 7. A large prospective study from Bangladesh demonstrated that shisha smoking was associated with all-cause (HR (hazard ratio) = 1.15; 95% CI (confidence interval): 0.93 – 1.43), cancer (HR = 1.30; 95% CI: 0.78 – 2.18) and cardiovascular disease (HR = 1.20; 95% CI: 0.87 – 1.67) mortality [66]. Another study from Lebanon showed that lifetime of shisha smoking was associated with coronary artery disease (OR = 2.94; 95% CI: 1.04 – 8.33) [67]. A recent meta-analysis also provided a significant association between shisha smoking and cardiovascular

disease (OR = 1.67; 95% CI: 1.25 – 2.24) with the primary focus on ischaemic heart disease and heart failure [68].

First study conducted in mice found that shisha smoke, as well as cigarette smoke, elevated total white blood cell count, absolute count of neutrophils, macrophages and lymphocytes in blood, proinflammatory markers in bronchoalveolar lavage fluid and oxidative stress markers in lungs [69]. From then on, other negative cardiovascular effects were found, both in animal and human studies. A study in 2013 found that systolic blood pressure and heart rate in mice were elevated after smoking shisha for one month, and similar results came from human studies at the same time [70-72]. Even though there is evidence that shisha smoking is detrimental to human health almost as much as tobacco cigarettes, it is not clear if the mechanisms behind the observed effects are different from those of classic tobacco cigarette smoking. Since the legislation surrounding shisha is still lacking, it is important to discover as much about this way of inhaling tobacco as possible and provide the background for adequate usage regulation.

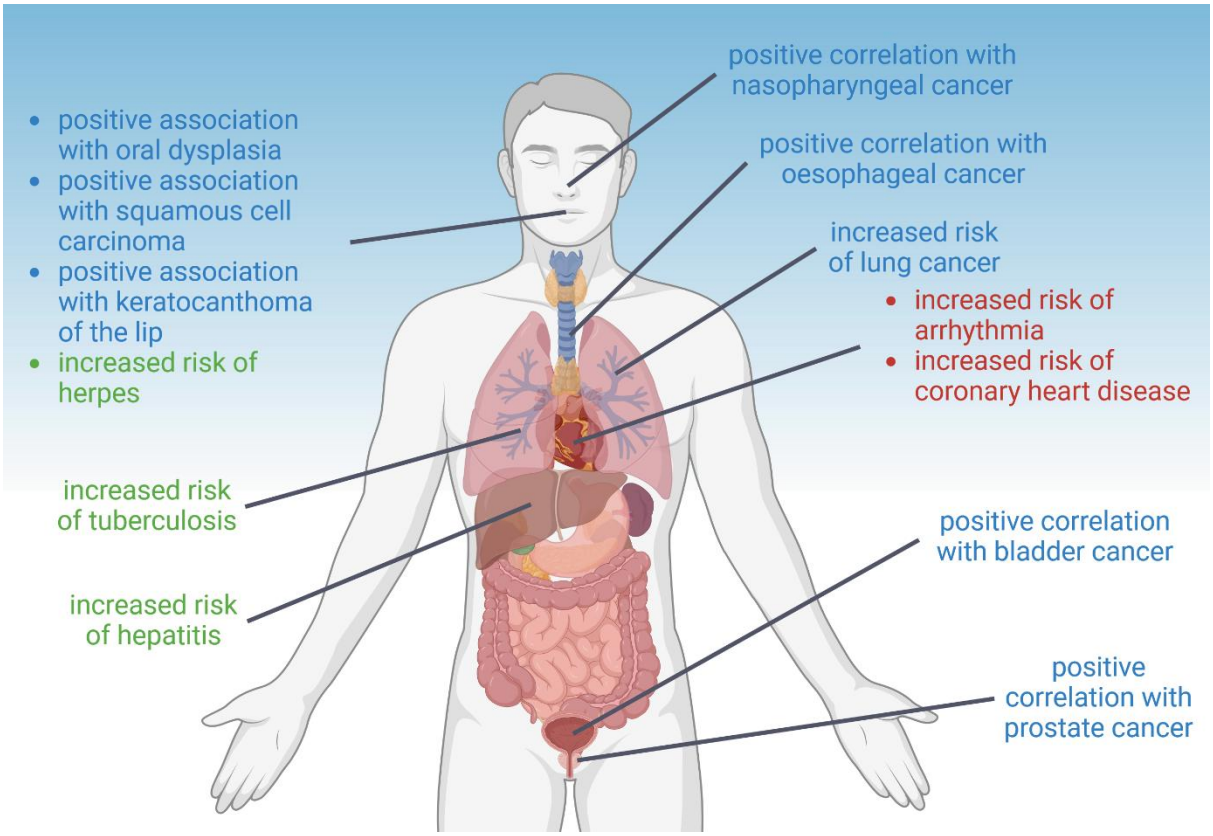

Figure 7. Overview of the negative effects of shisha smoking on different organ systems. Figure created from the data presented in the review article by Kadhum et al. 2015 [73], made in BioRender.com

1.2. Molecular mechanisms behind the detrimental effects of noise, e-cigarette and shisha exposure

Several molecular mechanisms have been connected to the negative effects that noise, e-cigarettes and shisha exert on the cardiovascular system. It seems that, even though these stressors are different, the effects they have and the pathways that are activated in their presence are interconnected. It is therefore important to analyse these stressors both separately and together and define the impact they may have on everyday life.

1.2.1. Stress mechanisms of noise on the cardiovascular pathology

Noise triggers two pathways that lead to adverse effects – direct and indirect pathway [74]. Direct pathway is initiated by intense noise and causes hearing loss and inner ear damage. These effects are fast and very prominent, and they were the first to be investigated. However, the indirect pathway causes other, more subtle effects. Activation of the indirect pathway is caused over time, and is expressed as sleep disturbance and annoyance at first, followed by activation of stress responses, hypothalamus-pituitary-adrenal axis and sympathetic-adrenal-medullary axis [74]. As a proof of the concept, epinephrine, norepinephrine and cortisol are found elevated in noise exposure studies [75-77], with longer exposures to stress hormones leading to increased inflammation and oxidative stress and further to cardiovascular diseases https://doi.org/10.1126/science.7466404[77-79]. Direct and indirect pathways, as well as molecular mechanisms behind them are shown in

Figure 8 and

Figure 9.

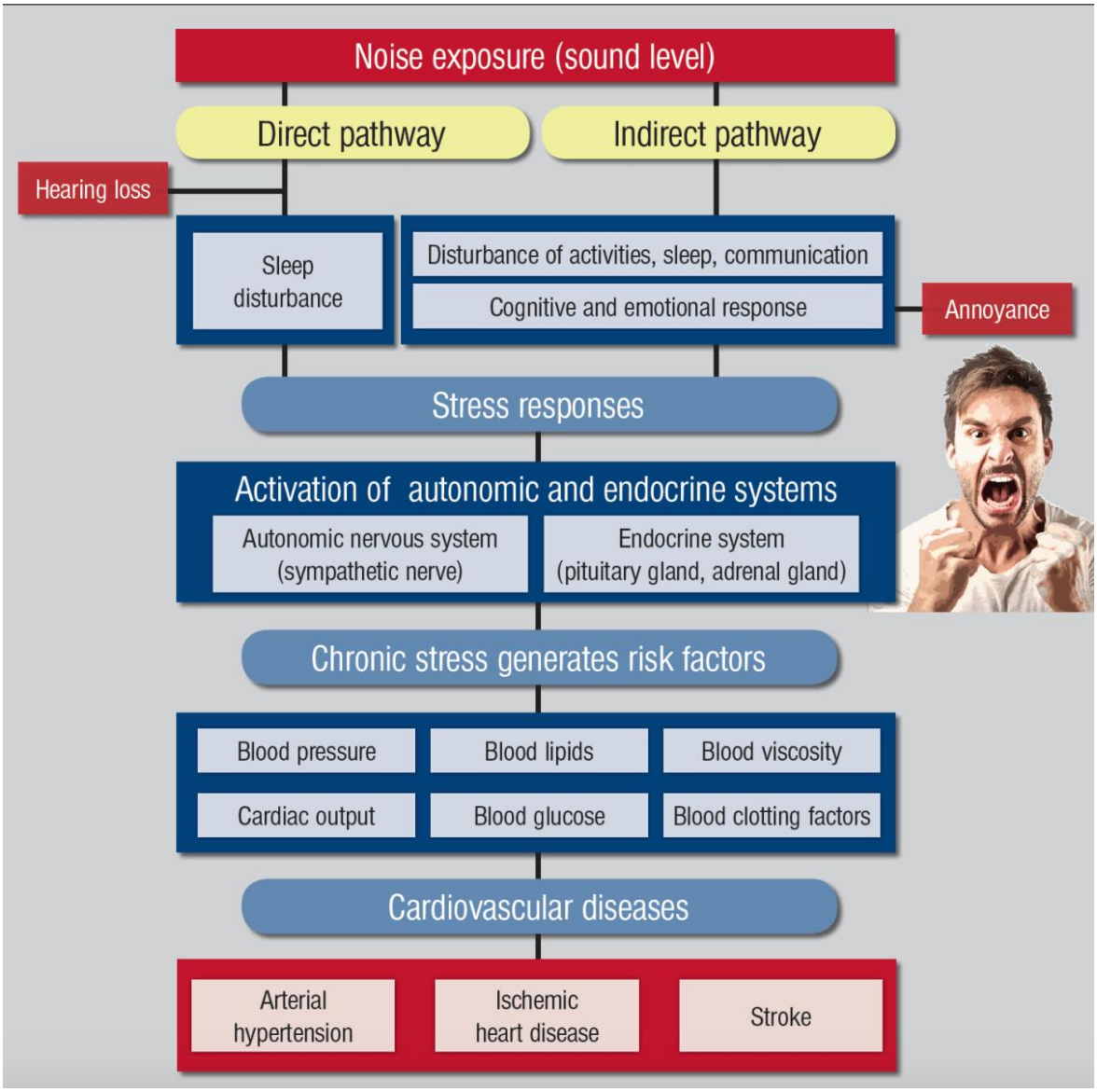

Figure 8. Noise-induced cardiovascular disease pathways. Direct pathway of noise-induced diseases indicates a physical damage to the inner ear and subsequent hearing loss and sleep deprivation. The indirect pathway leads to annoyance and sleep disturbance, than to stress responses and finally risk factors for cardiovascular diseases. Reused from Münzel et al. [24] and Babisch [74].

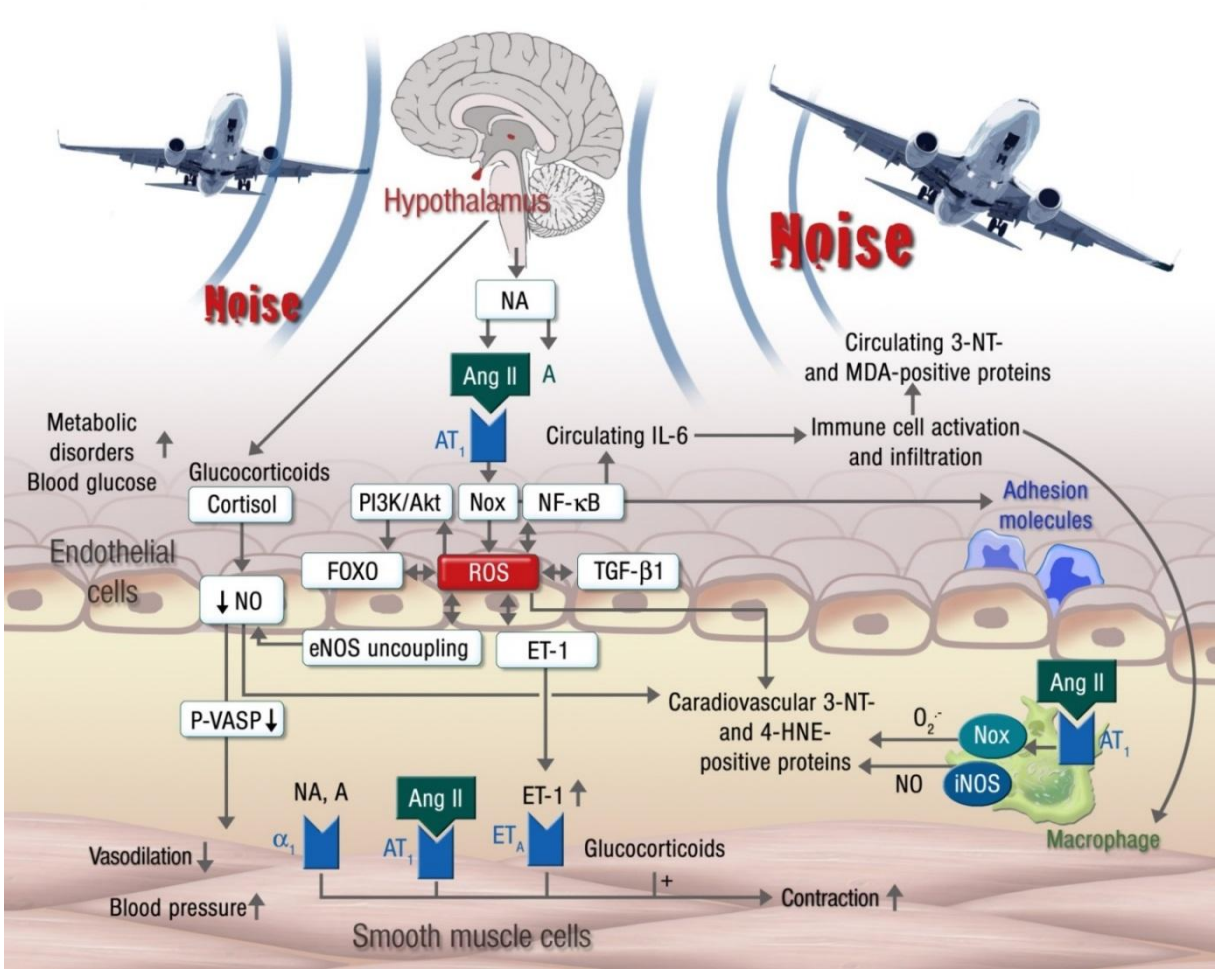

Figure 9. Molecular mechanisms for the vascular dysfunction induced by noise. Activation of the hypothalamus and the sympathetic system results in elevated levels of noradrenalin (NA), adrenalin (A) and angiotensin II (Ang II) which activates NADPH-oxidase and causes oxidative stress and impairment in •NO signalling. Oxidative stress is increased by proinflammatory cytokines and adhesion molecules that promote immune cell infiltration into the (sub)endothelial layer. The picture is reused from Münzel et al. [80].

1.2.2. Toxic components of e-cigarette vapour and shisha smoke

E-cigarettes and shisha are proposed as alternative ways of inhaling nicotine in order to minimize inhalation of toxic compounds. However, in both shisha smoke and e-cigarette vapour, some of those compounds, like aldehydes, metals, N-nitrosamines and volatile organic compounds can still be found, and have negative impact on a person's health, together with nicotine [60]. Nicotine on its own is known to alter cardiovascular function, and is thought to be the main culprit behind negative effects of acute e-cigarette exposure studies [81].

However, nicotine is also connected to the lower incidence of Parkinson's and Alzheimer's disease [82], better patient outcome after myocardial infarction [83] and prevention of ulcerative colitis [84], so it is not fully clear how toxic of a compound it really is. E-cigarette vapour and shisha smoke also contain tobacco specific nitrosamines (TSNAs), although in a lower amount than tobacco smoke [85]. These chemicals attach to DNA molecules and are known carcinogens [86, 87]. Heavy metals in e-cigarette vapour come from the degradation of the heating element, which is made of steel alloys containing nickel, cadmium and chromium [88]. These metals are known to promote inflammation, cancer, cardiovascular and pulmonary diseases [89]. Volatile organic compounds (VOCs) are organic compounds with low boiling point, such as benzene and toluene. They can be found in both shisha smoke and e-cigarette vapour because of the flavours added to the molasses or e-cigarette liquid or because of the extraction of nicotine [90]. The amount of VOCs is therefore bound to the type and the amount of flavour added and differs significantly across the market. Aldehydes found in e-cigarette vapour are degradation products of propylene glycol and glycerine, two components of the e-cigarette liquid base. Acrolein is one of the most detrimental aldehydes present in vapour and it is known to induce oxidative stress and inflammation [91]. Acrolein is also present in shisha smoke, and it is a prominent toxicant in second-hand shisha exposure [92]. The effects of acrolein exposure were previously found in mice after exposure to e-cigarette vapour [93]. Toxic components of e-cigarette vapour, and shisha and classic tobacco cigarette smoke, are shown in

Figure 10.

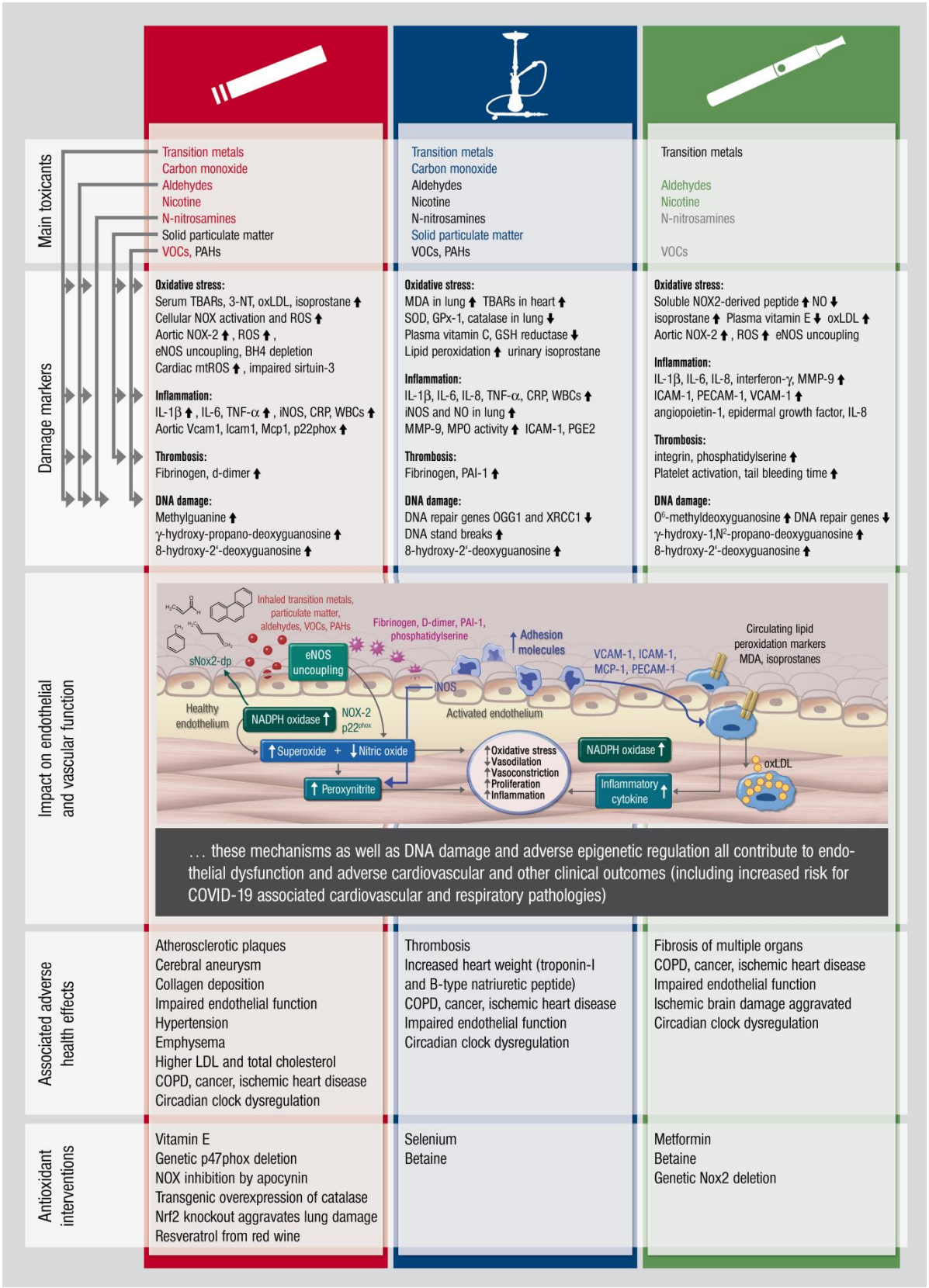

Figure 10. Summarized effects of cigarette, shisha and e-cigarette smoking/vaping. The picture shows toxicants, mechanisms and effects from different types of smoking/vaping. The major toxicants are labelled as red, blue and green = high quantity, black = intermediate quantity, grey = trace amounts. The toxicants are linked to the reported damage markers on

the left side. The molecular scheme is reused from Münzel et al. 2017 and Münzel et al. 2020 [60, 80].

1.2.3. Hypothalamic-pituitary-adrenal (HPA) axis

Main contributors to the stress responses are paraventricular nucleus of the hypothalamus, anterior lobe of the pituitary gland and the adrenal gland, commonly known as HPA (hypothalamic-pituitary-adrenal) axis. Other structures, such as brain stem noradrenergic neurons, sympathetic adrenomedullary circuits and parasympathetic nervous system contribute to the stress responses and are controlled by the HPA axis [94]. Main regulator of the HPA axis is corticotropin-releasing factor (CRF) which is synthesized by hypophysiotropic neurons of the medial parvocellular subdivision of the paraventricular nucleus of hypothalamus. As a response to stress, CRF is secreted by hypothalamus into hypophysial portal vessels and moves towards pituitary gland. After binding of CRF to CRF1 receptor, anterior lobe of the pituitary gland secretes adrenocorticotropic hormone (ACTH) into the systemic circulation. ACTH binds to multiple receptors, but an important one for HPA axis is MC2-R, which is localised on the cortex of adrenal glands. After binding, adrenal gland secretes glucocorticoids from the zona fasciculata of the cortex [94, 95]. Glucocorticoids modulate the inflammatory response in an acute stress scenario, but prolonged stress conditions result in a state called “cortisol resistance” where inflammation is worsened through the release of pro-inflammatory cytokines [96]. An overview of the HPA axis is shown in **Figure 11**.

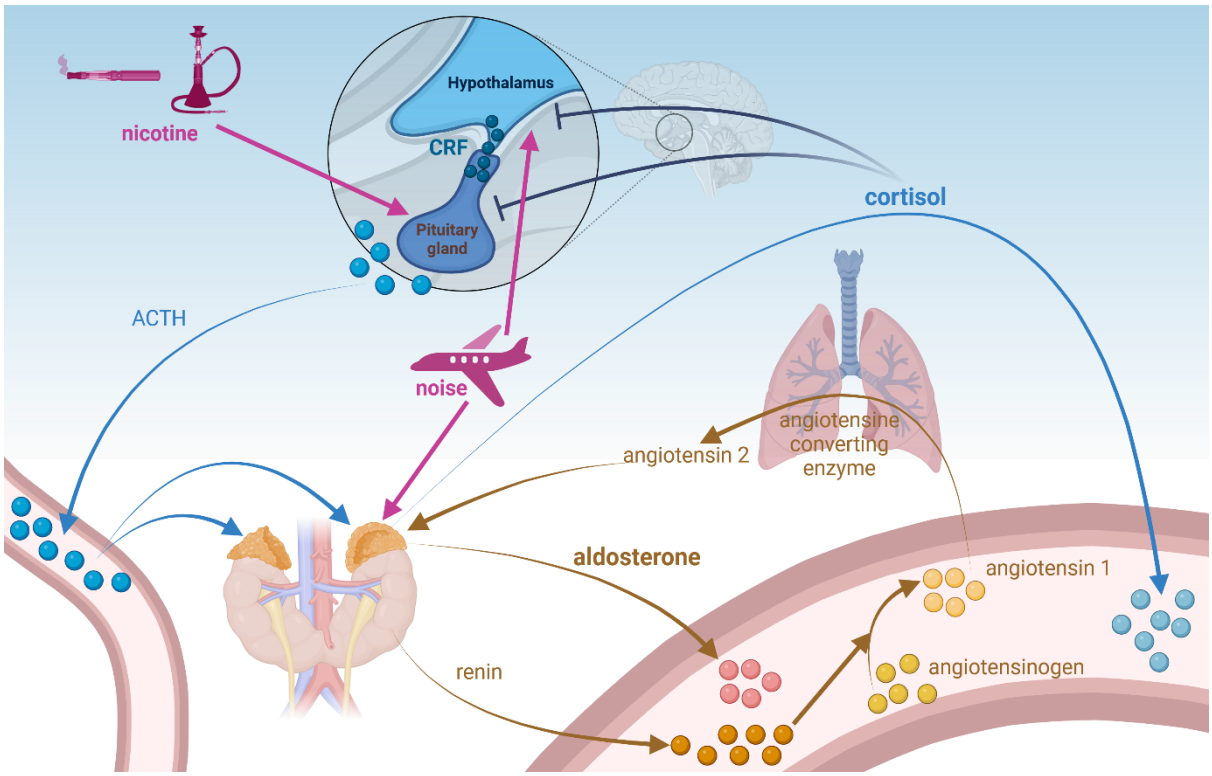

Figure 11. HPA axis and RAAS. A schematic representation of the hypothalamic-pituitary-adrenal axis and renin-angiotensin-aldosterone system. CRF - corticotropin-releasing factor, ACTH – adrenocorticotropic hormone. Figure created with BioRender.com

Activation of HPA axis by noise as a stressor is shown to induce the release of stress hormones (glucocorticoids and catecholamines), as well as secondary activation of renin-angiotensin-aldosterone system (RAAS) and increased expression of ET-1 [97]. These are potent triggers of inflammation and oxidative stress, mediated by activation of NOX2 via angiotensin II signalling [80]. Oxidative stress additionally activates sympathetic nervous system [98], which also activates the renin-angiotensin-aldosterone system and leads to negative vascular effects. Nicotine is a substance that is known to activate HPA axis [99]. However, it was also shown that, in smokers, structures of the HPA axis may be altered even more than expected by the sheer inhalation of nicotine [100]. Unfortunately, there is a lack of evidence of vaping and shisha smoking effects on the HPA axis directly, but similar mechanisms may be expected in vaping and shisha smoking as they contain nicotine.

1.2.4. Reactive oxygen species and oxidative stress

Reactive oxygen species (ROS) are small, very reactive molecules derived from oxygen. Most prominent ROS are superoxide radical ($^{\bullet}O_2^-$), hydroxyl radical ($^{\bullet}OH$), ozone (O_3), singlet oxygen ($^1O_2$) and hydrogen peroxide (H_2O_2). ROS are very reactive and may interact with vast number of small organic molecules, proteins, lipids, carbohydrates and nucleic acids. When interacting with them, the function of molecules is changed or completely impaired, which is why ROS are acknowledged as contributors to many illnesses and damages an organism faces [101]. However, ROS also play an important role in cellular signalling and host defence [102]. There are many mechanisms by which ROS can be removed from the organism. Some of them are enzymatic (like superoxide dismutase that converts superoxide radical into hydrogen peroxide) and some are direct oxidation reactions (like the antioxidant capacity of glutathione) [103]. Because there are both positive and negative effects of ROS in a single cell, as well as organism in total, the term oxidative stress was coined by Helmut Sies in 1985. Oxidative stress is a condition in which there is an imbalance of ROS production and antioxidant defence mechanisms [104]. A state of oxidative stress is achieved by a higher production of ROS, or by lesser activity of antioxidant mechanisms, or both, which finally results in the accumulation of oxidative damage by insufficient repair capacity. The concept of oxidative stress is now fully accepted and has found its way into virtually every part of biomedicine. It is important to note that ROS are not only produced intracellularly, but may also come in contact with the extracellular environment and contribute to systemic oxidative stress. There is significant amount of known contributors to oxidative stress, both from the side of producing ROS and from the side of reducing antioxidant defence, some of which are already well connected to the noise and e-cigarettes and shisha consumption [105, 106].

1.2.5. NADPH-oxidase

NADPH-oxidase is a membrane bound enzyme complex that catalyses superoxide production via the reaction:

$$2\ O_2 + NADPH \rightarrow 2\ ^{\bullet}O_2^- + NADP^+ + H^+$$

The complex is present on the plasma membrane and on the membrane of phagosomes and is found in most cells of the body. There are many different isoforms of the catalytic

subunit named NOX/DUOX (NOX1, NOX2, NOX3, NOX4, NOX5, DUOX1, and DUOX2) [107]. The phagocytic NADPH oxidase variant consists of several subunits – gp91phox (or NOX2), p22phox, p67phox, p47phox, p40phox and Ras-related C3 botulinum toxin substrate, the Rho GTPase Rac1. Gp91phox and p22phox subunits are bound to the membrane, and form the flavocytochrome b_{558} [108]. Gp91phox contains six transmembrane α-helix domains, a domain for binding FAD and NADPH, and this subunit alone can produce $^{\bullet}O_2^-$ [109]. P22phox subunit contains three transmembrane α-helix domains and PxxP domain that binds p47phox subunit when the complex is activated. In the resting state, p22phox stabilizes gp91phox subunit [110]. P47phox, p67phox and p40phox are cytosolic subunits that bind to the flavocytochrome b_{558} when the complex is activated. P47phox contains PX domain that recognizes phosphatidylinositol-3,4-bisphosphate, and is therefore important in activation of the complex [111, 112]. P67phox contains TPR domain that binds the Rac subunit of the complex and PB1 domain that binds the p40phox subunit, as well as the activation domain that reacts with the flavocytochrome b_{588} and regulates electron transfer [113]. P40phox contains PB1 domain that interacts with p67phox and SH3 domain that interacts with p47phox [114]. Rac subunit is a cytosolic GTPase and its binding to the flavocytochrome b_{588} is essential for the functioning of the complex. There are two isoforms of this subunit that appear in cells, Rac1 and Rac2. The difference between the isoforms is only in the tissue expression – Rac1 is present in all cells, while Rac2 is present only in haematopoietic cells. When inactive, Rac binds GDP, and when activated it binds GTP and translocates to the membrane and attaches to the p67phox subunit of the complex [115]. Since the phagocytic NADPH oxidase (NOX2) isoform is mostly associated with cardiovascular oxidative stress during inflammation, that is the form of NADPH-oxidase complex that will be discussed further in the text. In addition, the NOX2 (and NOX1) isoform shows a quite different activation mechanism as compared with the other isoforms, which involves protein kinase C-dependent p47phox phosphorylation, also enabling redox-dependent activation of NOX2 [116].

In leukocytes (e.g. neutrophils, monocytes, macrophages), NADPH-oxidase complex may be found in four different states – a resting state, a primed state, a fully-activated state and a hyperactive state. The resting state of NADPH-oxidase has only NOX2 and p22phox subunits bound to the membrane, while all other subunits are distributed in a cytosol, thus the complex is inactive [117]. The primed state of NADPH-oxidase is also an inactive state of the complex, with only NOX2 and p22phox subunits bound to the membrane. It becomes primed after

encountering certain stimuli, such as IL-1ß, GM-CSF, zymosan and lipopolysaccharide (LPS), which activate tyrosine kinase that phosphorylates p47phox subunit only on Ser345 and does not promote binding of the cytosolic subunits to the membrane. PhosphoSer345 binds proline isomerase Pin1 which induces conformational change of p47phox and facilitates the full activation of p47phox when an activating agent is encountered [118-120]. The active state of NADPH-oxidase is achieved when serine kinase is activated by strong stimuli, such as acrolein and angiotensin 2, which phosphorylates p47phox subunit on Ser303, Ser304, Ser359, Ser370 and Ser379 and promotes the binding of all subunits of the complex. When the complex is activated, NOX2 subunit uses NADPH as electron donor to reduce oxygen (O_2) to superoxide radical ($^{\bullet}O_2^-$). Hyperactive state is reached when NADPH-oxidase is activated from the primed state, when both tyrosine kinase and serine kinase phosphorylate p47phox subunit, which leads to a rapid generation of ROS and damage of the surrounding tissue [119, 120]. Overview of the structure and different states of the NADPH-oxidase is shown in **Figure 12**.

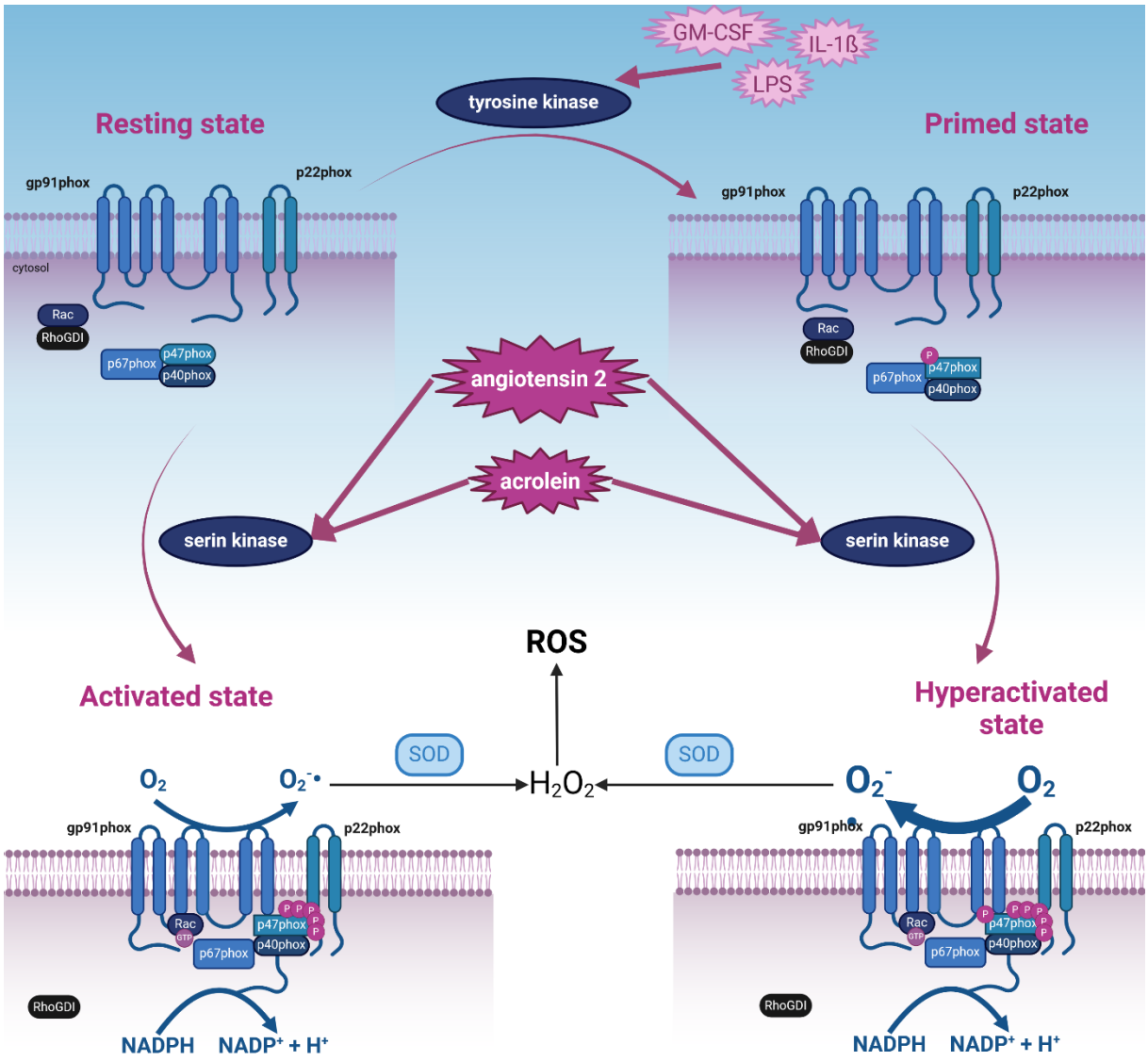

Figure 12. Mechanisms of phagocytic NADPH oxidase-induced oxidative stress. Toxic constituents of vapour, e.g. acrolein, or noise-dependent stress reactions via HPA/SNS-RAAS pathways activate NADPH oxidase complex and its subunits (p47phox, p67phox, p40phox and Rac1) are translocated from the cytosol to the membrane-bound gp91phox (NOX2) and p22phox subunits. When the complex is activated, it generates superoxide radicals, which contribute to the total ROS burden. The scheme was generated using data from [118, 119]. Figure created with BioRender.com

Increased activation of NADPH oxidase leads to increased production of superoxide radical, and consequentially, all other ROS, pushing a cell towards oxidative stress. It was proposed that one of the mechanisms behind adverse effects of noise is activation of NADPH oxidase

[121]. My group investigated the molecular mechanisms of aircraft noise exposure in rodents using aircraft noise exposure [80]. In the study, oxidative stress and inflammation were found to be central players in impeding vascular function. They also found that noise caused an increase in systolic blood pressure and the release of stress hormones, such as adrenaline, noradrenaline, dopamine and angiotensin 2, connecting noise to the hypothalamic-pituitary-adrenal (HPA)-axis [80]. Additionally, Kröller-Schön et al. indicated that aircraft noise induces cerebral oxidative stress and a neuroinflammatory phenotype. This signalling is upstream of the observed adverse cardiovascular effects and points to mechanisms along the brain-heart axis being involved in the cardiovascular damage by noise. All of the negative effects were normalized by genetic deletion of NADPH-oxidase subunit NOX2 [121]. After even a short-term noise exposure, sympathetic nervous system is overstimulated, which leads to increased levels of noradrenaline and adrenaline, which may further cause cross-activation of the RAAS to produce angiotensin II. Angiotensin II is known to activate NADPH-oxidase-dependent production of $^{\bullet}O_2^-$ in endothelial cells [122]. Similar mechanism is proposed for some of the adverse effects behind shisha smoking and e-cigarette vaping. Vaping is shown to upregulate and activate NOX2, while Nox2 knockout mice were protected from this effect [106]. Acrolein, as a toxic compound found both in e-cigarette and shisha smoke, is also one of the proposed activators of NOX2, together with other aldehydes and nicotine [123]. A study found that smoking shisha for 5 days causes an impairment of the fibrinolytic system and prothrombotic effects, as well as increased ROS and lipid peroxides formation in the mouse heart [124]. It is apparent that there is not a single component that leads to activation of NADPH oxidase and ROS production, but multiple components that work in synergy as they push the cell together into the state of oxidative stress.

1.2.6. Endothelial function

Endothelial dysfunction is a change in the physiology of endothelium, which leads to an imbalance of vasodilators and vasoconstrictors resulting from impaired endothelial cell signalling and it is an early prognostic marker for formation and progression of atherosclerotic plaques [125]. Nitric oxide ($^{\bullet}NO$) is one of the main signalling molecules responsible for healthy endothelial function. It is synthesised in the endothelial cells from L-arginine through a reaction catalysed by NOS enzymes:

$$3H^+ + 2\ \text{L-arginine} + 3\ \text{NADPH} + 4\ O_2 \rightarrow 4\ H_2O + 2\ \text{L-citrulline} + 3\ NADP^+ + 2\ {}^\bullet NO$$

After synthesis, $^\bullet$NO diffuses through the plasma membrane into the smooth muscle cell layer where it binds to the soluble guanylyl-cyclase, which further catalyses the formation of cyclic guanosine-monophosphate (cGMP) which is a secondary messenger that activates cGMP-dependent protein kinase (PKG) leading to the inhibition of Ca^{2+} entry into the vascular smooth muscle cells resulting in vasorelaxation [126]. NOS enzymes are a group of calcium-calmodulin controlled isozymes named endothelial, inducible and neuronal NOS. Endothelial NOS, or eNOS, is the one that is primarily involved in physiological vasodilation and prevention of adhesion of platelets and immune cells to the vascular wall. Inducible NOS, or iNOS, is connected to the immune response and inflammation as it is induced by pro-inflammatory stimuli. Neuronal NOS (nNOS) is linked with cognitive and memory functions of the brain [127, 128]. The three isoforms share most of the domains. Near the N-terminal they contain zinc-binding motif and haem domain (responsible for tetrahydrobiopterin (BH_4) and L-arginine binding), and FMN-containing flavodoxin region (responsible for calmodulin binding), FAD-bearing region and NADPH-binding region on the C-terminal [129]. As calmodulin is modulated by intracellular Ca^{2+} levels, the process of $^\bullet$NO synthesis is activated by rising Ca^{2+} levels in the cell [130, 131]. eNOS and nNOS are calcium-dependent isoforms, as the binding of calmodulin is reversible and depends on the intracellular levels of Ca^{2+}. After an increase in calcium levels in the cell, activation of eNOS and nNOS leads to increased production of $^\bullet$NO. The increased production of $^\bullet$NO can contribute to cell damage through oxidative stress (e.g. by conversion to peroxynitrite), but it mostly helps with increased blood flow and vasodilation [132]. On the other hand, iNOS is not regulated by calcium, as the calcium/calmodulin complex is tightly bound. This isoform is activated by cytokines or pathogens [129], so the $^\bullet$NO that is produced by iNOS functions as part of the host defence. In addition to maintaining vascular tone, $^\bullet$NO also helps to reduce vascular smooth cell and immune cell migration and proliferation, and inhibits adhesion of platelets and monocytes [127, 133]. eNOS, and therefore the $^\bullet$NO synthesis, is sensitive to oxidative stress, as it can lead to many redox modifications, one of which is oxidation of tetrahydrobiopterin (BH_4), an important eNOS cofactor, to dihydrobiopterin (BH_2), resulting in uncoupled eNOS. Uncoupled eNOS produces $^\bullet O_2^-$ instead of $^\bullet$NO, increasing the total ROS burden [134]. $^\bullet$NO on its own is also sensitive to oxidative stress as it can react with $^\bullet O_2^-$ and produce peroxynitrite ($ONOO^-$), which has pro-atherogenic,

pro-thrombotic and vasoconstrictive effects. $ONOO^-$ can also nitrate protein tyrosine residue, resulting in 3-nitrotyrosine positive proteins, a marker of nitro-oxidative stress [135].

Dysregulation of eNOS has been linked to multiple cardiovascular diseases both in animal and human studies. It has been shown that, in murine model, increase in NADPH-oxidase activity leads to an increased superoxide production that, in turn, impairs eNOS signaling and leads to eNOS uncoupling and endothelial dysfunction [136, 137]. Endothelial dysfunction caused by oxidative stress is connected to hypertension [137], diabetes mellitus [138], atherosclerosis [139, 140] and dyslipidemia [141, 142], all known risk factors for cardiovascular diseases.

eNOS uncoupling and endothelial dysfunction was directly connected to noise exposure numerous times. Recent review papers and original publications from my group show this connection in details, both in animal and human subjects [80, 97, 143, 144]. Connection between eNOS, endothelial dysfunction and e-cigarette usage is also well established, and was previously demonstrated by my group in exposed mice [106]. The molecular mechanism was recently confirmed and described by El Mahdy et al [145]. However, the role of eNOS uncoupling in shisha smoking-caused cardiovascular effects is not yet clear [146]. Human studies found, aside from elevated blood pressure and heart rate, elevation in CO levels in blood, higher than levels observed after smoking tobacco cigarettes [58, 147]. The proxy measurements of endothelial function in humans, flow mediated dilation (FMD), could be influenced by the presence of CO in the shisha smoke, as demonstrated previously by Rezk-Hanna et al. [147]. The vasodilator properties of CO could also mask the molecular response to particulate matter or other chemicals coming from shisha smoke in an acute exposure scenario. On the other hand, a study in humans found lower FMD in shisha smokers, that was comparable to that of classic tobacco cigarette smokers [148]. Therefore, additional research is warranted, especially regarding shisha exposure, as to establish the importance of eNOS uncoupling in endothelial dysfunction and cardiovascular effects caused by the aforementioned environmental and behavioural risk factors.

1.2.7. Inflammation

Inflammation is a defence mechanism of the immune system in a response to harmful stimuli [149]. Immune system removes the damaging stimuli and initiates healing, with minimizing injury or infection and restoring homeostasis as the main goal. However,

prolonged exposure and uncontrolled inflammation may become chronic and can lead to various diseases [150]. Normally, pattern-recognition receptors (PRRs) on the cell membrane of all cell types recognize pathogen-associated molecular patterns (PAMPs) of the stimulus or damage-associated molecular patterns (DAMPs) as endogenous signals from the damaged tissue [151]. When PRRs are stimulated, they activate enzymatic cascades that lead to activation of transcription factors like nuclear factor kappa-B (NF-κB) and mitogen-activated protein kinase (MAPK). These transcription factors then induce production of pro-inflammatory cytokines, such as interleukin-1beta (IL-1β), interleukin-6 (IL-6) and tumour necrosis factor alpha (TNF-α) [152]. Non-immune cells produce both pro-inflammatory and anti-inflammatory cytokines with the end-goal to attract leukocytes and activate immune response. However, leukocytes themselves produce pro-inflammatory cytokines and may exacerbate the inflammation above the necessary levels [153].

Inflammation in general, but especially chronic inflammation, is a key factor that leads to cardiovascular disease [154, 155]. Specifically, NF-κB activation is thought to have serious implications in endothelial injury through oxidative mechanism, leading to impaired $^{\bullet}NO$ signalling [156]. Additionally, redox-triggered mitochondria-derived superoxide and hydrogen peroxide activate NOX2 subunit of NADPH oxidase complex [157]. This also leads to increased inflammation response and promotes expression of C-reactive protein (CRP), iNOS and cyclooxygenase 2 (COX2) [158]. NF-κB is known to be regulated by ROS, but also products of oxidative damage, such as malondialdehyde (MDA), 4-hydroxynonenal (4-HNE) and DNA oxidation products (8-OHdG) [159, 160]. Expression of pro-inflammatory cytokines like IL-1β and IL-6 is also known to be regulated by ROS [160, 161]. Most common inflammatory pathways in the vasculature are shown in

Figure 13.

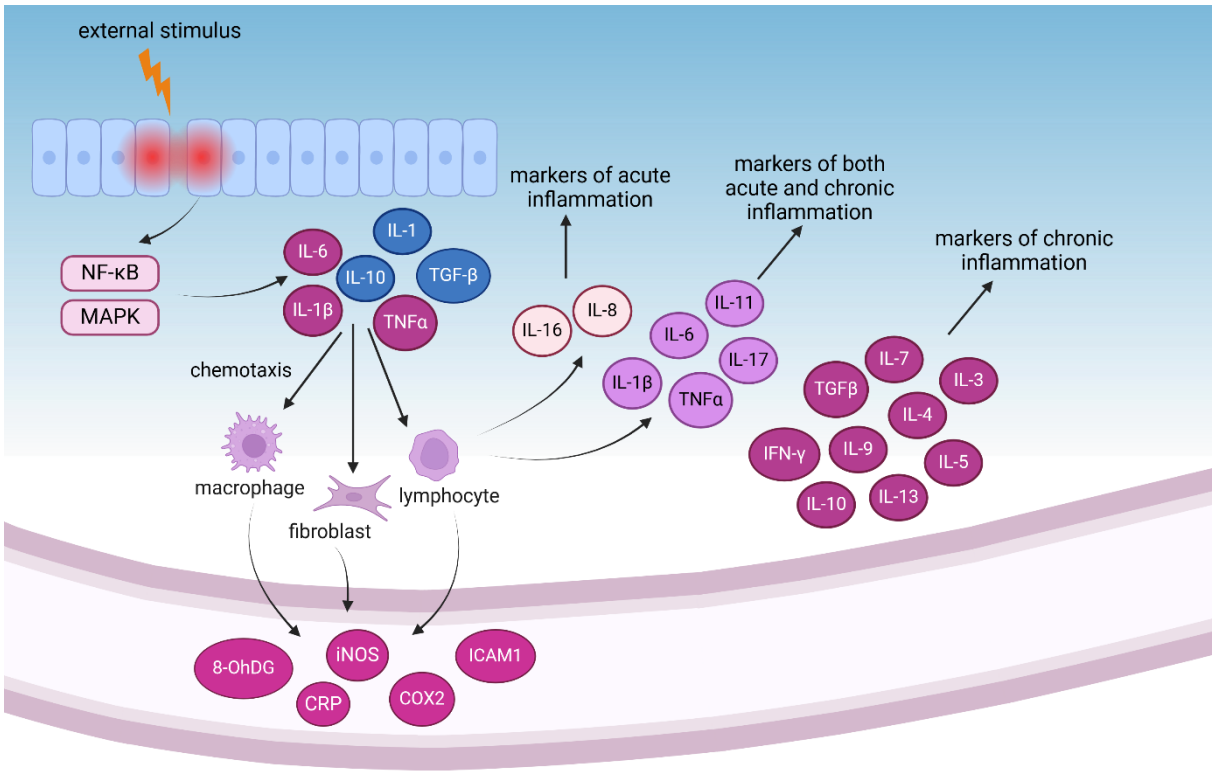

Figure 13. Scheme of the inflammatory mechanisms and cytokine production. Inflammatory pathways are activated when an external stimulus signals that the organism is under threat or is damaged. Most of the inflammatory signalling is done through the NF-κB transcription factor. The scheme was generated using data in [156-160]. Figure created with BioRender.com

Night-time aircraft noise was previously associated with a pro-inflammatory phenotype of the plasma proteome [144]. The first mechanistic proof of association between individual noise exposure levels and vascular inflammation and major adverse cardiovascular events (MACE) in humans was put forward by Osborne et al. [162]. In their paper the authors used ^{18}F-fluorodeoxyglucose (^{18}FDG) positron emission tomography-computed tomography (PET–CT) imaging, to show an association between stress (amygdala activity, envisaged by higher uptake of ^{18}FDG into amygdalar tissue by PET) and arterial inflammation (envisaged by atherosclerotic plaque formation by CT). In animal studies, aircraft noise was shown to induce systemic inflammation, as envisaged by circulating IL-6 and CD68 levels [80, 163] and prevention of noise damage by genetic ablation of myelomonocytic inflammatory cells such as monocytes and macrophages using the LysMCre^{iDTR} mice [164]. Another interesting fact is the importance of the NOX2 in the noise-induced cardiovascular effects observed in mice

[165]. Since NOX2 is a phagocytic isoform of the NADPH oxidase, it is clear that macrophage infiltration, and inflammation in general, plays an important role in noise-induced vascular dysfunction, which we have previously proven in noise-exposed LysMCre^{iDTR} mice [164]. Neuronal inflammation is also a prominent factor in the observed noise effects, as astrocytes and microglia can be activated by the stress response through the HPA axis activation and catecholamine release [17, 164, 166].

Cardiovascular pro-inflammatory effects of e-cigarette usage are still understudied. Human studies mostly focus on acute exposure, which can mostly show inflammation at the level of lung injury [167]. However, there are indices that vaping also could lead to systemic inflammation as a result of both acute and chronic exposure. Studies found increase in human plasma levels of CRP [168], ICAM-1 [168, 169], S100A8, HMGB1 ligand and myeloperoxidase [169]. In a 20 subject trial, an increase in phagocytic NADPH-oxidase-derived peptide, 8-isoprostaglandine F2α, CD40 ligand and P-selectin was observed, as well as platelet aggregation, which all points to the oxidative stress and vascular inflammation [170, 171]**.** On the other hand, a 5-day suspension from electronic cigarettes increased serum club cell-protein 16, pointing to a decrease in lung inflammation and a possible protection against chronic obstructive pulmonary disease [172]**.** Animal studies provide a better mechanistic insight into the inflammation response to vaping. It was found that, after acute exposure of mice, IL-6 and IL-1β levels in plasma were increased, and these observations were connected to flavoured e-cigarette liquids [93, 173]. However, in other animal studies, circulatory pro-inflammatory cytokines such as leukaemia inhibitory factor, angiopoietin 1 and CXC-motif chemokine ligand 5 were elevated even with e-cigarette liquid that did not contain flavourings [174]. Some studies investigated the effects of vaping on the offspring of exposed female mice where it was found that inflammatory pathways of the offspring were dysregulated, not only after birth but also after maturing [150, 175]. It is apparent there are multiple factors contributing to the inflammatory response connected to vaping and the contributing mechanisms are still to be fully disclosed.

For shisha smoking, studies are even scarcer. Studies have found an increase in circulating and pulmonary 8-OhDG in humans [176], and IL-6, IL-8, IL-1β and TNFα in both mice and humans [69, 177, 178] in acute exposure scenario. The findings are thought to be associated with the nicotine and CO exposure, as well as heavy metals and other toxicants comparable to cigarette smoke [62, 69, 124, 179].

1.2.8. NRF2 pathway

Nuclear factor erythroid 2-related factor 2 (NRF2) is a transcription factor that is in humans encoded by the *NFE2L2* gene. It is a protein capable of inducing transcription through the binding of the nuclear factor erythroid 2/activator protein 1 (NF-E2/AP-1) motif of the hypersensitive site-2 in the β-globin locus control region. Under homeostatic conditions, NRF2 is in complex with its cytosolic repressor Keap1, a substrate and binding partner of the Cullin-3-ring-box 1-E3 (Cul3-Rbx1-E3) ubiquitin ligase complex that primes NRF2 for proteasomal degradation. Under oxidative stress, NRF2 is not degraded via the KEAP1 regulator, but instead travels to the nucleus where it binds to antioxidant-response elements (ARE) or electrophilic-response elements (EpRE) within the promoter region of cytoprotective genes, inducing their transcription. Binding to ARE initiates the expression of downstream phase II gene detoxification and antioxidant enzymes, such as heme-oxygenase-1 (HO-1), NAD(P)H dehydrogenase quinone 1 (NQO1), glutathione-S-transferase (GST), superoxide dismutase (SOD), aldehyde dehydrogenase-1 and -2, UDP-glucuronosyltransferase, glutamate-cysteine ligase, and regulatory subunits including thioredoxin reductase 1, sulfaredoxin, glutathione reductase (GR), peroxiredoxin (Prx), thioredoxin (Trx), catalase, and glutathione peroxidase. After exerting its function, NRF2 is phosphorylated by the tyrosine kinase that, upon GSK-3β-dependent activation, enters into the nucleus promoting NRF2 retrotranslocation and subsequent cytosolic degradation. NRF2 activation scheme is shown in **Figure 14**.

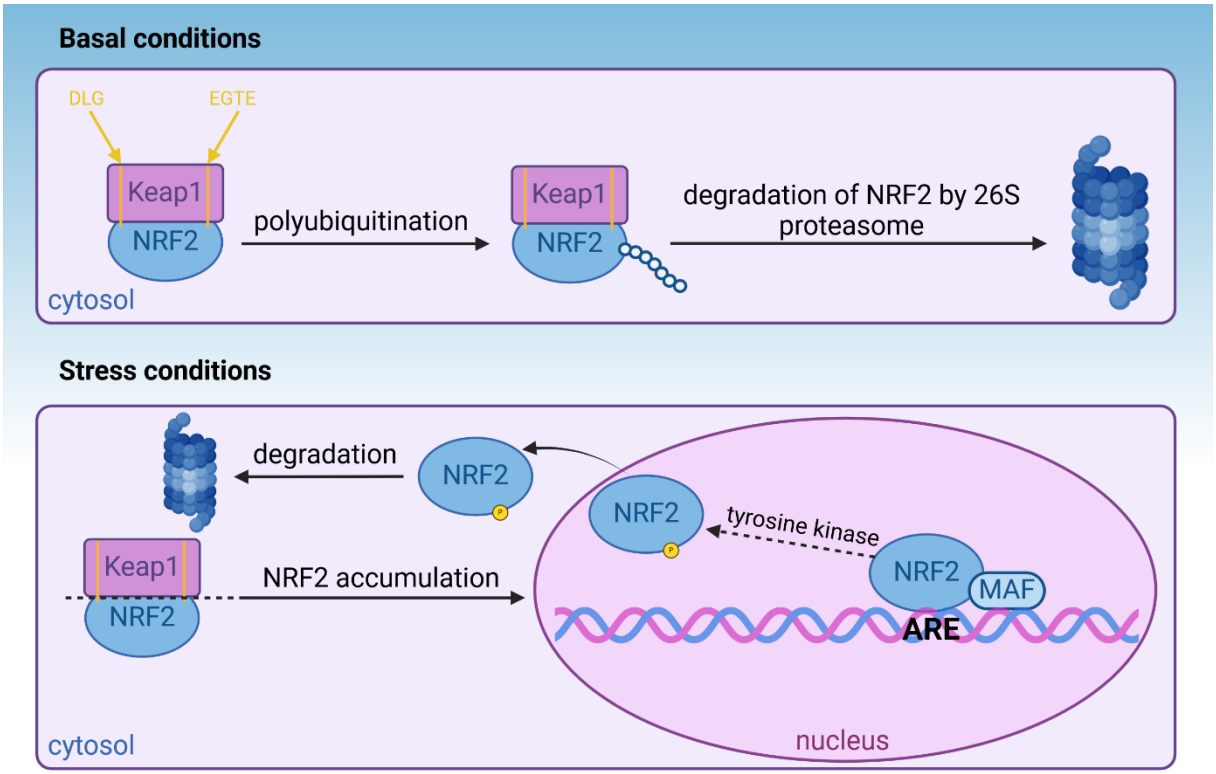

Figure 14. NRF2/Keap1 binding and regulation. Under homeostatic conditions, KEAP1 interacts with NRF2 in the cytosol, promoting its polyubiquitination and subsequent proteasomal degradation, resulting in minimal or absent NRF2 transactivation. In contrast, under different stress conditions, the binding of KEAP1 to NRF2 is strongly impaired, decreasing the likelihood of NRF2 ubiquitination. As a consequence, a large fraction of NRF2 molecules in the cytosolic pool can translocate into the nucleus, wherein it interacts with small MAF proteins and induces the transcription of several cytoprotective genes. The figure was generated using data from [180, 181] Figure created with BioRender.com

As a heterogeneous transcription factor, NRF2 has target genes that encode multiple proteins. Nqo1 is a prototypical NRF2 target gene that catalyzes the reduction and detoxification of highly reactive quinones that can cause redox cycling and oxidative stress. HO-1 is the rate-limiting enzyme in the process of haem catabolism; it catalyzes the breakdown of haem into the antioxidant biliverdin that is further converted to bilirubin, the anti-inflammatory agent carbon monoxide, and iron. HO-1 is a NRF2 target gene that has been shown to protect from a variety of pathologies, sepsis, hypertension, atherosclerosis, acute lung injury, kidney injury, and pain. Glutamate-cysteine ligase catalytic subunit (GCLC) and glutamate-cysteine ligase regulatory subunit (GCLM) form a heterodimer, which is the rate-

limiting step in the synthesis of glutathione (GSH), an important endogenous antioxidant. Sulfiredoxin-1 reductase (SRXN1) and thioredoxin-1 reductase (TRX1) support the reduction and recovery of peroxiredoxins and glutathione peroxidase 2, proteins important in the detoxification of highly reactive peroxides. NRF2 also transcribes superoxide dismutase 3 (SOD3) that catalyses conversion of extracellular superoxide radical into oxygen and hydrogen peroxide.

Noise exposure has been linked with NRF2 pathway in several ways. Nqo1, HO-1 and GSH were downregulated in murine model after noise-induced hearing loss [182], and treating mice with HO-1 or NRF2 activators showed partial normalisation of negative cardiovascular events linked to the noise exposure [163]. Other preclinical studies on mice and rats showed protective effects of activation of the NRF2 pathway on other adverse effects of noise [183, 184].

Connection between NRF2 pathway and e-cigarettes is not as studied as NRF2 pathway and noise. However, there are some indices that e-cigarette usage may induce NRF2 pathway, with increased Nqo1 [185] and HO-1 expression in cell cultures [50, 185], and in animal studies [106].

Shisha effects on NRF2 pathway, as well as on all of the aforementioned pathways, were not yet examined deeply as effects of noise, but this topic is slowly gaining attraction. A recent study in mice tested effects of both occasional and regular shisha usage on cardiovascular system and found increase in NRF2 as one of the main mechanisms behind increased systolic blood pressure, cardiac damage, inflammation and oxidative stress [186]. HO-1 was also observed to be increased in mouse heart after shisha exposure [187]. Other works showed increased NRF2 expression after shisha exposure, which was normalised after gum arabic intake [188, 189]. Same papers link increased NRF2 expression to lung and cardiac injury, as well as increased systolic blood pressure and impaired coagulation. Interestingly, regulation of NRF2 is not clear in the classic tobacco cigarette smoking literature, with some studies pointing to upregulation [190] and some to downregulation [191]. This could be an artefact stemming from the translocation of NRF2 into the nucleus, leading to reduced cytosol concentrations often observed in tissue homogenates.

2. Materials and methods

2.1. Materials

Table 1. Chemicals

Product	**Company**	**Prod. No.**
2-Mercaptoethanol	Sigma-Aldrich	M6250
Acetonitrile	Honeywell	34967
Acetylcholine chloride	Sigma-Aldrich	A6625
Acetaldehyde	Merck	8000040500
Acrolein	Sigma	89116
Acrylamide/Bis solution 40%, 29:1	Bio-Rad	1610146
AEM1 (NRF2 inhibitor, CAS: 1030123-90-0)	Sigma	SML1556
Albumin Fraktion V (BSA)	Carl Roth GmbH	8076.3
Ammonium persulfate (APS)	Sigma	A3678
Aprotinin	Sigma-Aldrich	A6279
Aqua-Phenol	Roth	A980.4
Bromophenol Blue sodium salt	Sigma	B8026
Chloroform - isoamyl alcohol mixture, 49:1	Sigma	25668
Coenzyme A	Cayman	21499
DEPC (diethylpyrocarbonate)-treated water, nuclease-free and autoclaved	Roth	T143.3
Dihydroethidium 95% (DHE)	Sigma	37291
DMSO (dimethyl sulfoxide)	Honeywell	34943
D-luciferin	Abcam	Ab145164
EDTA (Ethylenediaminetetraacetic acid)	Sigma	E9884
Ethanol	Sigma	32205
E-cigarette liquid 50% PG 50% VG	German Flavours	
Formaldehyde	Merck	1.040.031.000
Glycerol	Roth	3783.1
HEPES (4-(2-hydroxyethyl)-1-piperazineethanesulfonic acid) sodium salt hydrate	Sigma	H2393
Isofluran	Abbott	B506
Isopropanol	AppliChem	A3465
K_2HPO_4 (Di-potassium hydrogenphosphate trihydrate)	Carl Roth GmbH	16788-57-1
KCl (potassium chloride)	AppliChem	7447-40-7
Ketamine hydrochloride/xylazine hydrochloride solution	Sigma	K113

L-012 (8-Amino-5-Chloro-7-Phenylpyrido[3,4-d]pyridazin-1,4-(2H,3H)Dion), Luminol Analogon	Wako Chemicals GmbH	120-04891
Cytotoxicity Detection Kit^{PLUS} (LDH)	Roche	4744926001
Leupeptin-Hydrochlorid (min. 90%(HPLC))	Sigma-Aldrich	L0649
Lucigenin (*N*,*N*'-dimethyl-9,9'-biacridinium dinitrate)	Sigma	M8010
Methanol, 99.8 %	Sigma-Aldrich	322415
$MgSO_4$ (magnesium sulfate)	Carl Roth GmbH	7487-88-9
Milk powder	Roth	T145.2
ML385 (NRF2 inhibitor, CAS: 846557-71-9)	Sigma	SML1833
N,N,N,N-Tetramethylethylene-diamine (TEMED)	Sigma	T9281
Na_2HCO_3 (sodium hydrogencarbonate or bicarbonate)	AppliChem	131638
$NaCH_3COO$ (sodium acetate)	Merck KgaA	127-09-3
NaCl (sodium chloride)	Carl Roth GmbH	7647-14-5
Na-Hepes (sodium 4-(2-hydroxyethyl)-1-piperazineethanesulfonate)	Carl Roth GmbH	75277-39-3
NaOH (sodium hydroxide)	Merck KgaA	106462
Nitroglycerine	G. Pohl-Boskamp GmbH & Co. KG - Hohenlockstedt (ots)	
NIST SRM1648a (mixture of urban particulate matter from St. Louis)	National Institute of Standards and Technology (NIST)	
OCT-resin Tissue-Tek®	Sakura	4583
Passive Lysis Buffer	Promega	E1941
PBS (1x), Dulbecco's Phosphate Buffered Saline without calcium and magnesium	Sigma-Aldrich	D8537

PDBu (phorbol ester, phorbol 12,13-dibutyrate)	Sigma-Aldrich	37558-16-0
Phenylmethanesulfonyl fluoride (PMSF)	Sigma	P7626
PEG-Catalase (polyethylene glycol modified)	Sigma	C9322
Pepstatin A	Sigma-Aldrich	P5318
Peroxidase from horseradish Type VI	Sigma-Aldrich	9003-99-0
Phenol	Sigma-Aldrich	108-95-2
Phosphatase Inhibitor Cocktail 1	Sigma-Aldrich	P2850
Ponceau S	Sigma-Aldrich	P5288
Precision Plus Protein TM Dual Color Standards (50µl)	BIORAD Laboratories GmbH	1610374S
Prostaglandin F 2alpha	Sigma-Aldrich	16010
Protease Inhibitor Cocktail	Sigma-Aldrich	P8340
Proteinase K	QIAGEN GmbH, Hilden	19157
RNase AWAY™	Thermo Scientific	7002
Roti® -Quant	Carl Roth GmbH	K015.1
ROTI®Aqua-Phenol	Carl Roth GmbH	A980.1
SDS (Sodium dodecyl sulfate)	Merck	822050
Sucrose	Sigma-Aldrich	57-50-1
TEMED (N,N,N',N'-tetramethylethylendiamine)	Sigma-Aldrich	110-18-9
Tricin	Sigma/Merck	T0377
Tris(tris(hydroxymethyl)-aminomethane)-base	Sigma-Aldrich	252859
Tris(tris(hydroxymethyl)-aminomethane)-HCl	Carl Roth GmbH	9090
Triton X-100	Fluka & Riedel	93420
Tween-20	SERVA Electrophoresis GmbH	P2287

Wash buffer (IHC), 10x	Dako	S3006
Zymosan A	Sigma-Aldrich	Z4250

Table 2. Consumables

Product	**Company**	**Prod. No**
Adhesive Towel (OP Abdecktuch)	Mölnicke Health Care	63603
Cellstar® PP-Test tubes, 15 ml steril	Greiner Bio-One GmbH	188271
Cellstar® PP-Test tubes, 50 ml steril	Greiner Bio-One GmbH	227261
CO detection tubes	Dräger Safety AG & Co KGaA	CH20601
Coal for shisha TOM COCO Gold	TOM Cococha GmbH	/
Eppendorf-epT.I.P.S. Standard 0.1-10µl	Eppendorf AG, Hamburg	0030000811
Eppendorf-epT.I.P.S. Standard 2-200µl	Eppendorf AG, Hamburg	0030000889
Eppendorf-epT.I.P.S. Standard 50-1000µl	Eppendorf AG, Hamburg	0030000927
Eppendorf® Safe-Lock microcentrifuge tubes; volume 0.5 mL	Eppendorf	0030121023
Eppendorf® Safe-Lock microcentrifuge tubes; volume 1.5 mL	Eppendorf	0030120086
Eppendorf® Safe-Lock microcentrifuge tubes; volume 2.0 mL	Eppendorf	0030120094
Gel Blotting Paper GB 002	Whatman GmbH	9057077
Glass petri dish	Duran	237554805
Micro Amp Optical Well Reaction plate	Applied Biosystems, Foster City,California, USA	N8010560
Microplate, 96 well, F-bottom, transparent	Greiner	655101
Microplate, 96 well, U-bottom, transparent	Greiner	650101

Microscope slide	Paul Marienfeld GmbH & Co KG, Lauda-Königshofen	1000000
Mini-Trans-Blot Filterpaper	BIORAD Laboratories GmbH, München	1703932EDU
Nitrocellulose Blotting membrane Amersham™Protran® 0.45µm	GE Healthcare	GE10600002
PCR tubes, 0.2 mL	Kisker Biotech	G003-A
Petri dish, sterile	Greiner	632181
Pipette tip 1000µl, blue	SARSTEDT AG & Co., Nümbrecht	70.3050.020
Pipette tip 200µl, yellow	SARSTEDT AG & Co., Nümbrecht	70.3030.020
TipOne 0,1-10µl Extended Length Natural Tips	STARLAB GmbH, Ahrensburg	S1012-3610
TipOne 100-1000µl Filter Tips	STARLAB GmbH, Ahrensburg	S1126-7810
TipOne 1-20µl Bevelled Filter Tips	STARLAB GmbH, Ahrensburg	S1120-1810
TipOne 200µl Graduated Filter Tips	STARLAB GmbH, Ahrensburg	S1120-8810
Tobacco for shisha Core Doppelgänger	Darkside	/
Nunc™ MicroWell™ 96-Well	Termo Fisher Scientific	167008

Table 3. Technical devices

Product	**Company**
Applied Biosystems 7900HT Fast Real-Time PCR System	Applied Biosystems, Darmstadt
BioPhotometer	Eppendorf
Benchtop centrifuge ROTOFIX 32	Hettich
Sound level meter - Casella CEL-246	
Chemiluminescence plate reader Mithras2 LB 943	Berthold Technologies, Bad Wildbad, Germany
Chemilux Imager	Intas, Göttingen, Germany
Cryostat CM3050 S	Leica Biosystems
Dot blot device	Whatman® Schleicher&Schuell
E-cigarette device eVic-VTC Mini	Joyetech, Shenzhen, China
Exposure system for mice InExpose	Emka Technologies, Montreal, QC Canada

Fluorescence microscope Axiovert 40CFL with Axiocam MRm	Zeiss, Germany
Noise exposure device - Grundig MS 540 with a total output of 65 W	
HPLC-column C18-Nucleosil	Macherey & Nagel
HPLC-System	Jasco
Lumat LB 9507 (luminometer)	Berthold Technologies
Micro-osmotic pump Model 1007D	Alzet
Mini Trans-Blot Electrophoretic Transfer Cell (Blotting apparatus)	Bio-Rad
Mini ProteanTM System 3 Cell (Electrophoresis apparatus)	BioRad laboratories, Hercules, California
MiniSpin® Centrifuge	Eppendorf
MRXII plate reader	Dynex Technologies, Berlin, Germany
Noninvasive Blood Pressure System (NIBP) CODA®	Kent Scientific
Organ bath chambers	Radnoti
Organ bath force transducers	Kent Scientific / ADInstruments
Pipette Eppendorf Research 0,1 -2,5 µl	Eppendorf AG, Hamburg
Pipette Eppendorf Research 0,5 -10 µl	Eppendorf AG, Hamburg
Pipette Eppendorf Research 100-1000 µl	Eppendorf AG, Hamburg
Pipette Eppendorf Research 10-100 µl	Eppendorf AG, Hamburg
Pipette Eppendorf Research 20-200µl	Eppendorf AG, Hamburg
Pipette Eppendorf Research 2-20 µl	Eppendorf AG, Hamburg
PowerPac™ Basic power supply	Bio-Rad
Refrigerated benchtop centrifuge Mikro 22R	Hettich
Rotary microtome RM2145	Leica Biosystems
Shisha - Minya	Smokezilla
StepOnePlus™ Real-Time PCR Systems	Applied Biosystems
Stereomicroscope MSZ 5400	Krüss
Thermomixer Comfort	Eppendorf AG, Hamburg
TissueLyser QIAGEN	Retsch GmbH, Haan
Transferpette Eppendorf 200 µl	BRAND GMBH + CO KG, Wertheim
Vortex-Genie (G560E) 2, 230V,50Hz 0.5 amps	Scientific Industries,New York USA
Western Blot Imager, CHEMICAM HR 16	Intas - Science Imaging Instruments, Göttingen

Table 4. Surgical instruments

Product	**Company**	**Prod. No**

Extra Fine Bonn Scissors Straight, 8.5 cm	Fine Science Tools	14084-08
Extra Fine Graefe Forceps Curved 10 cm	Fine Science Tools	11152-10
Graefe Forceps Straight, 10 cm	Fine Science Tools	11050-10
Noyes Spring Scissors Curved 12 cm	Fine Science Tools	15011-12
Scissors Curved BluntBlunt 12 cm	Fine Science Tools	14003-12
Strabismus Scissors Tungsten Carbide Curved 9 cm	Fine Science Tools	14575-09

Table 5. Reagents and kits

Product	**Company**	**Prod. No**
A1CNow+Professional Test	PTS Diagnostics	3038
Pierce™ ECL Western Blotting Substrate	Thermo Scientific	32106
RNeasy mini kit	Qiagen	74104
QuantiTect® Probe RT-PCR Kit	Qiagen	204445
SuperSignal™ West Femto Maximum Sensitivity Substrate	Thermo Scientific	34095

Table 6. Media and buffers

Media / Buffer	**Composition**
BMDM growth medium, day 1	RPMI 1640, 25 mM HEPES and L-glutamine, 1 % (v/v) PenStrep, 20 % (v/v) FCS, 30 % (v/v) L929 cell-conditioned media
BMDM growth medium, day 4	RPMI 1640, 25 mM HEPES and L-glutamine, 1 % (v/v) PenStrep, 20 % (v/v) FCS, 15 % (v/v) L929 cell-conditioned media
Dulbecco's modified Eagle's medium	10% fetal calf serum, 2 mM L-glutamine, 100 IU/mL penicillin, 100 µg/mL streptomycin
DMEM	10 % foetal calf serum, 1 % penicillin and streptomycin, and 2 mM pyruvate
GIT (guanidinium thiocyanate) buffer	4 M guanidinium thiocyanate, 25 mM sodium citrate (pH 7.0), 0.5 % (w/v) *N*-lauryl sarcosine, 0.1 M 2-mercaptoethanol
Homogenization buffer	20 mM Tris-HCl, 250 mM sucrose, 3 mM EGTA, 20 mM EDTA
Homogenization solution (Hg-solution)	20 mM Tris-HCl, 250 mM sucrose, 3 mM EGTA, 20 mM EDTA, 0.5 mM PMSF, 1 % (v/v) protease inhibitor cocktail, 1 % (v/v) phosphatase inhibitor cocktail, 1 % (v/v) TritonX-100
KH (Krebs-Hepes) buffer	99 mM NaCl, 4.7 mM KCl, 2.5 mM $CaCl_2$, 1.2 mM $MgSO_4$, 25 mM $NaHCO_3$, 1 mM K_2HPO4, 20 mM HEPES, 11.1 mM D-glucose, pH 7.35
KH buffer including protease inhibitors	KH buffer, 1 % (v/v) aprotinin, 5 µg/ml leupeptin, 8 µg/ml pepstatin

Krebs-Henseleit buffer	118.3 mM NaCl, 4.69 mM KCl, 1.87 mM $CaCl_2$, 1.2 mM $MgSO_4$, 25 mM $NaHCO_3$, 1.03 mM K_2HPO_4, 11.1 mM D-glucose
Laemmli buffer, 3x	188 mM Tris-HCl (pH 6.8), 6 % (w/v) SDS, 30 % (v/v) glycerol, 0.01 % (w/v) bromophenol blue, 15 % (v/v) 2-mercaptoethanol
Luciferase assay solution	D-luciferin 12.5 µM, coenzyme A 27 mM, ATP 100 mM, Tricin 0.5 M, MgSO4 1 M, EDTA 0.5 M, DTT 1 M
PBS, 10x	1.37 M NaCl, 100 mM Na_2HPO_4, 27 mM KCl, 17.6 mM KH_2PO_4, pH 7.4
PBS-T, 1x	1x PBS, 0.1 % (v/v) Tween 20
SDS-PAGE resolving gel buffer	1.5 M Tris-HCl, pH 8.8
SDS-PAGE running buffer, 10x	250 mM Tris-base, 192 mM glycin, 35 mM SDS
SDS-PAGE stacking gel buffer	0.5 M Tris-HCl, pH 6.8
TAE (Tris-Acetate-EDTA) buffer, 50x	0.5 M Tris-base, 1.5 M acetic acid (glacial), 50 mM EDTA, pH 8.5
TBS, 10x	200 mM Tris-base, 1.5 M NaCl, pH 7.6
TBS-T, 1x	1x TBS, 0.1 % (v/v) Tween 20
Tris Mem buffer	50 mM Tris-HCl, 1 tablet EDTA-free Protease Inhibitor Cocktail (per 50 ml buffer), pH 7.4
Western blot transfer buffer, 10x	250 mM Tris-base, 192 mM glycine, 25 % (v/v) methanol

Table 7. Enzymes and standards

Product	**Company**	**Prod. No**
100 bp DNA ladder	New England Biolabs	N3231L
BenchMark™ Unstained Protein Ladder	Invitrogen	10747012
Bovine Serum Albumin Standard Ampules	Thermo Scientific	23209
Precision Plus Protein™ WesternC™	BioRad	1610376

Table 8. Primary antibodies

Product	**Company**	**Prod. No**
monoclonal anti-α-actinin (*mouse,* 1:2500 in 3 % BSA / TBS-T)	Sigma	A5044
polyclonal anti-β-actin (*rabbit*, 1:2500 in 5 % BSA / TBS-T)	Sigma	A5060
monoclonal anti-CD68	Abcam	ab31630

(*mouse*, 1:1000, 3 % BSA / PBS-T)		
monoclonal anti-COX2 (*rabbit*, 1:1000 in 3 % BSA / TBS-T)	Cell Signaling	12282S
monoclonal anti-Cu-Zn-SOD (*rabbit*, 1:1000, 3 % BSA / PBS-T)	Abcam	ab183881
Monoclonal anti-GAPDH (*rabbit*, 1:1000, 5 % BSA / TBS-T)	Cell signaling	2118
monoclonal anti-eNOS (*mouse*, 1:1000 in 3 % BSA / TBS-T)	BD Biosciences	610297
polyclonal anti-endothelin-1 (*rabbit*, 1:5000, 3 % BSA / PBS-T)	Abcam	ab117757
monoclonal anti-GCLC (*mouse*, 1:1000 in 1 % BSA / PBS-T)	Novus biologicals	NBP2-45830
monoclonal anti-gp91phox (Nox2) (*mouse*, 1:1000 in 5 % BSA / PBS)	BD Biosciences	611414
monoclonal anti-HO1 (*rabbit*, 1:1000 in 3 % BSA / PBS-T)	Abcam	Ab68477
polyclonal anti-IL-6 (*rabbit*, 1:1000 in 3 % BSA / TBS-T)	Abcam	Ab6672
monoclonal anti-p-MARCKS (*rabbit*, 1:1000 in 5 % BSA / TBS-T)	Cell signalling	2741S
monoclonal anti-MCP-1 (*rabbit*, 1:5000 in 3 % BSA / PBS-T)	Biorad	AAM43
polyclonal anti-nitrotyrosine (*rabbit*, 1:1000 in 3 % milk / PBS)	Millipore	06-284
monoclonal anti-p67phox (*mouse*, 1:500, 3 % BSA / TBS-T)	BD Bioscience	610913
monoclonal anti-PKCα (*mouse*, 1:1000, 3 % BSA / TBS-T)	BD Bioscience	610107
monoclonal anti-Rac1 (*mouse*, 1:1000 in 3 % BSA / TBS-T)	BD Bioscience	610651
monoclonal anti-VCAM1 (*mouse*, 1:200 in 3 % BSA / PBS-T)	Santa Cruz	sc-13160

Table 9. Secondary antibodies

Product	**Company**	**Prod. No**
anti-mouse IgG produced in horse, peroxidase-labelled (1:10,000, same conditions as primary antibody)	Vector lab	PI-2000
anti-rabbit IgG produced in goat,	Vector lab	PI-1000

peroxidase-labelled (1:10,000, same conditions as primary antibody)		

Table 10. Primers used in rtPCR

Primers	Gene Name	Order Number
BNP	Natriuretic peptide B	Mm01255770_g1
Ccl2	Monocyte chemoattractant protein 1	Mm00441243_g1
COX2	Cyclooxygenase 2	Mm00478374_m1
CD68	Macrosialin	Mm00839636_g1
Cybb / Nox2	cytochrome b-245, beta polypeptide / NADPH oxidase 2	Mm00432775_m1
Gclc	Glutamate-Cysteine Ligase Catalytic Subunit	Mm00802653_g1
Gpx-1	Glutathione peroxidase 1	Mm00656767_g1
Hmox1	Haemoxygenase 1	Mm00516005_m1
IL-1β	Interleukin 1 beta	Mm00434228_m1
IL-6	Interleukin 6	Mm00446190_m1
Nos1	nNOS	Mm01208059_m1
Nos3	eNOS	Mm00435204_m1
Nox1	NADPH Oxidase 1	Mm_00549170_m1
Nqo1	NADPH-quinone dehydrogenase 1	Mm_01253561_m1
Prdx-5		Mm00465365_m1
Tbp	TATA box binding protein	Mm00446973_m1
Txnrd-1		Mm00443675_m1
VCAM1	vascular cell adhesion molecule 1	Mm00449197_m1

Table 11. Software

Adobe Photoshop CS2	Adobe Systems GmbH
7900HT Fast Real Time System	Applied Biosystems,D-64293 Darmstadt
Axiovision Rel 4.3	Carls Zeiss Vision GmbH
BioRender (Medical illustrations)	BioRender
CODA data Acquisition Software	Kent Scientific corporation
ChromPass Chromatography Software	JASCO
FlexiWare 8.0	Scireq
Gel-Pro Analyser 6.0	Media Cybernetics, Bethesda, MD
ImageJ	Wayne Rasband (NIH), Public Domain, BSD-2
GraphPad Prism 8	GraphPad Software, Inc.
Microsoft Office 2016	Microsoft 365
Organbad, Chart 5	ADInstruments GmbH

Revelation 4.25	Dynex Technologies

2.2. Methods

2.2.1. Animals

All animals were treated in accordance with the Guide for the Care and Use of Laboratory Animals as adopted by the U.S. National Institutes of Health and approval was granted by the Ethics Committee of the University Hospital Mainz and the Landesuntersuchungsamt Rheinland-Pfalz (Koblenz, Germany; permit numbers: G 20-1-055, G 20-1-078 and 18-1-084). All of the mice were C57BL/6 inbred strain acquired from either Janvier or Charles River at an age of 6-10 weeks old. Mice were fed with standard chow ad libitum and kept in the ventilated cabinets with 12 hour light cycle. Depending on the experiment, mice were divided into following groups: control mice (without treatment), 4 days (24/7) noise exposed mice, 28 days (24/7) noise exposed mice, 4 days (24/7) noise exposed mice treated with citalopram (0,1 mg/kg/day i.p.), 4 days (24/7) noise exposed mice treated with diazepam (0,2 mg/kg/day i.p.), 4 days (24/7) noise exposed mice treated with propranolol (10 mg/kg/day osmotic minipump), 4 days (24/7) noise exposed mice treated with phenoxybenzamine (1 mg/kg/day osmotic minipump), 3 days shisha exposed mice (6 × 20 min/day). During the 28 days of noise exposure, mouse weight was recorded twice per week. After treatments, animals were sacrificed under deep ketamine/xylazine (120 mg/kg body weight) anaesthesia by transection of the diaphragm and exsanguination from the heart.

2.2.2. Cell culture

EA.hy 926 cell line (immortalized human endothelial cells), DLD1-HO1-prom cell line (human colorectal adenocarcinoma cell line transfected with a human HO-1 promoter region attached to a luciferase reporter gene) and RAW 264.7 (immortalized murine macrophages) were used in the experiments. All cell culture experiments were performed with help from [redacted] EA.hy cell line was a kind gift by C.-J. S. Edgell (the University of North Carolina, Chapel Hill, USA). RAW 264.7 cell macrophages were obtained from LGC Standards (Wesel, Germany). DLD1-HO1-prom cell line is a continuous culture at the Department of Pharmacology, University Medical Center Mainz, Germany and was established in our lab with help from [redacted] Department of Pharmacology, University Medical Center Mainz, Germany. EA.hy 926 and RAW 264.7 cells were seeded in 6-well plates in Dulbecco's

modified Eagle's medium as previously described [192, 193]. DLD1-HO1-prom cells were seeded in 96-well plates in DMEM. Cells were kept at 37 °C and 10 % CO_2 until they were 70–80 % confluent, as previously described [194]. For the experiment, they were incubated with either 1 % DMSO (control) or increasing concentrations of acrolein (0.33, 1, 3.3, 10, 33 µM; these concentrations were estimated to match concentrations in the e-cigarette vapour condensate) or e-cigarette vapour condensate (1:150, 1:100, 1:75, 1:50, 1:25; ratio of condensate to the cell medium) or air-derived particulate matter (NIST - 2.5, 7, 22, 66 or 200 µg/mL). All solutions of acrolein or e-cigarette vapour condensate were prepared in 1 % DMSO. Cells were incubated for either 3 days (EA.hy 926 and RAW 264.7 cells) or 2 days (DLD1-HO1-prom cells). The exposure medium with acrolein or e-cigarette vapour condensate was changed every 24 h. Treatment solutions were heated up to 37 °C, added to the medium, mixed well and then added to the cells under sterile conditions. Microscopic images of the wells were taken each day while changing the exposure medium. After the images were taken, cells were flash-frozen for further use.

2.2.3. Noise exposure

Noise exposure protocol was previously established Münzel et all 2017 [80] and described here. During exposure, mice were kept in an isolated room with the same housing conditions as the institutional animal facility and checked daily. Mice were left for two days in the room prior to exposure, to acclimate to the new surroundings. The loudspeaker system used for noise exposure was positioned about 30 cm above open mouse cages. Noise exposure used in the study consisted of airplane landing and take-off events, irregularly distributed during 2 hour sequence and repeated constantly throughout the day, for either 4 or 28 days. Every noise event was 43 seconds long, with a maximum sound pressure level of 85 dB(A) and a mean of 72 dB(A). Used sound pressure levels are below the threshold for cochlear damage [195]. Background level of noise in the room was 48 dB. Sound pressure levels were previously calibrated using a sound level meter within one of the cages at initial setup, and maintained constant throughout all exposure protocols.

2.2.4. Shisha exposure

Mice were exposed to shisha smoke using a modified inExpose exposure system acquired from emka Technologies S.A.S (Paris, France). The scheme of the modified system is shown in the

Figure 15. The system consists of a commercially available shisha device connected to the intake pump via a pinch valve that allows fresh air to be drawn when the smoking puff ends. The intake pump brings the shisha smoke into the mouse exposure chamber. The exposure chamber has a total volume of 5 L, and can fit up to 16 mice. The exhaust pump draws the smoke out of the chamber facilitating constant flow. A light scattering particle monitoring device (Casella Microdust Pro™, Diatec, Auckland, New Zealand) was used to ensure consistency between exposures. The whole system is controlled by a proprietary software (flexiWare 8.0, emka Technologies S.A.S). The system was established with help from Dr Marin Kuntić.

The exposure protocol consisted of 6 x 20 minute sessions per day for 3 days, and mice were returned to their cages with access to food and water during brakes. The puff profile used to draw in smoke was set as 6 seconds in duration every 60 seconds and 300 mL in volume. The puff protocol was chosen based on input from a human study [196], and considerations made with the stability and consistency in the presently used system. After testing the number of coal pieces, a single coal piece was used for the mouse exposures. 15 g of shisha tobacco was used in each session. Tobacco was apple flavour (Doppelgänger), a common choice among shisha users.

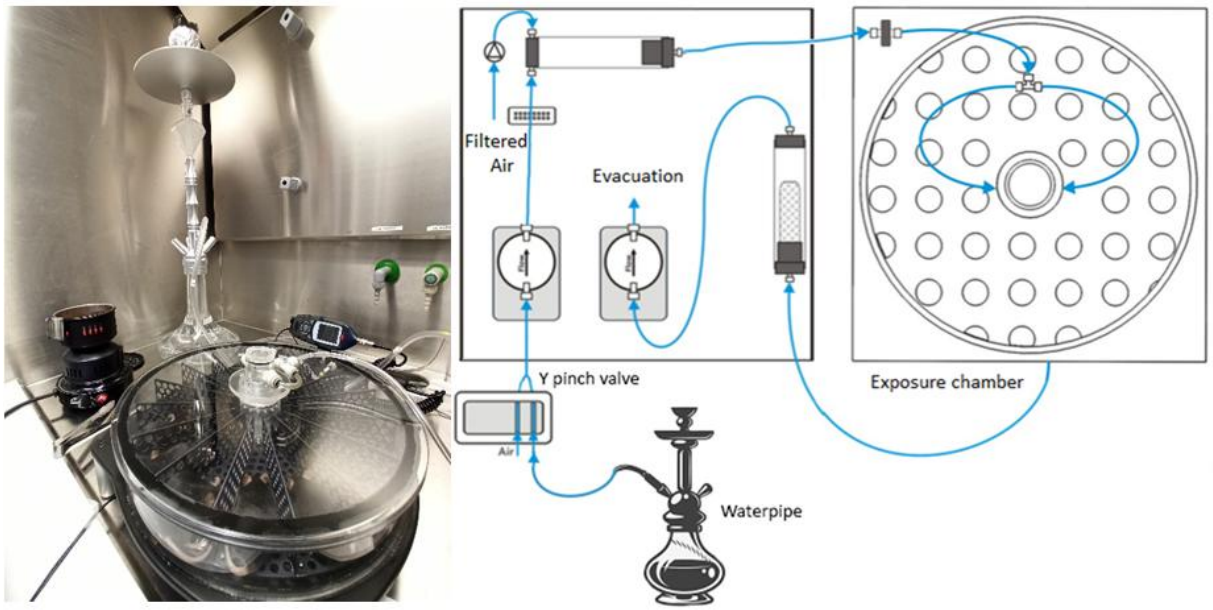

Figure 15. Shisha exposure system. The photograph of the shisha exposure system with a schematic representation of the system with labelled airflow. Figure created with BioRender.com

2.2.5. Pharmacological treatments

Two groups of mice were injected *i.p.* either with diazepam (0.4 mg/kg/day) or citalopram (0.2 mg/kg/day) twice a day and then exposed to the noise as described above. Another two groups of mice were treated with either propranolol (20 mg/kg/day) or phenoxybenzamine (2 mg/kg/day) by implanting osmotic minipumps underneath the skin on the back of each mouse, and then subjecting the mice to noise for four days the same way as described before. The treatments started a day before noise exposure, and they lasted for five days in total.

2.2.6. E-cigarette liquid and e-cigarette vapour condensate

E-cigarette liquid used in the experiments was obtained from German Flavours. The liquid is a 1:1 mixture of 1,2-propylene glycol and glycerine without added aromas or nicotine. The liquid was heated with an e-cigarette device custom designed to fit an e-cigarette exposure system shown in

Figure 16. The exposure chamber was disconnected from the system and the condensate was collected directly from the condenser (the modified flow is shown in red arrows in **Figure 16**). The vapour was produced every 30 seconds for 3 seconds (puff volume 55 mL), condensed to a liquid and used as such for further experiments. The rate of e-cigarette vapour condensate production was around 300 µL/h. The collected condensate was kept at 4 °C in the dark for up to 24 h before cell exposure. Before mixing with cell medium the condensate was warmed to 37 °C.

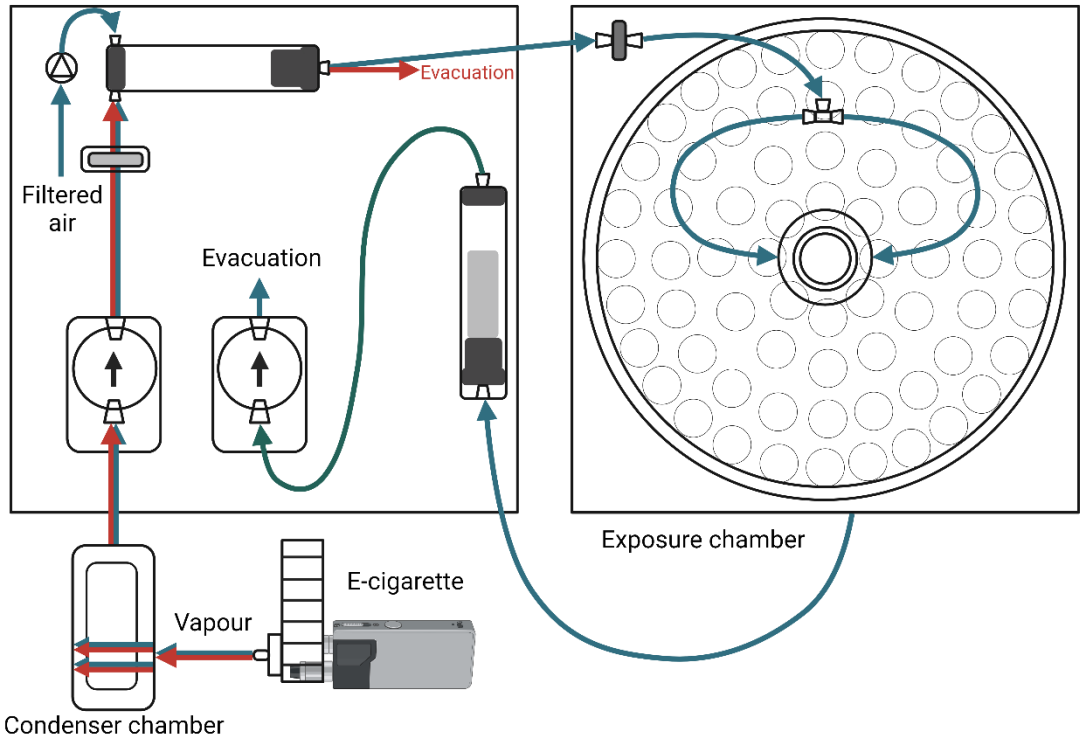

Figure 16. Scheme of the e-cigarette exposure system. Blue arrows show the airflow when the exposure chamber is connected. Red arrows show the airflow when the exposure chamber is disconnected and used for condensing e-cigarette vapour into condensate for use in this work. The condensate was collected from the condenser chamber. The exposure system is operated by flexiWare 8.0 software (emka Technologies, France). Own figure reused from [50].

2.2.7. HBA1c

Glycosylated haemoglobin (HbA1c) was measured from the whole blood of mice, using the A1C Now+ system as described by the manufacturer. One drop of blood was placed into a tube that contains buffer, mixed well, then placed onto the cartridge. The cartridge with sample was inserted into the measuring device and the result was recorded after 5 min. After every measurement, the used cartridge was discarded and new one was used for each sample.

2.2.8. Cell viability

EA.hy 926 cell viability was determined by manually counting adherent cells from light microscopy images at 20 × zoom. Cells were counted at 24 h, 48 h and 72 h of the treatment during medium change, after removal of the old medium. The old medium was collected each day, stored at -80 °C and used after the end of experiment for LDH assay. Since RAW 264.7 cells tend to overlap while growing, light microscopy couldn't be used for determination of viability. The viability of RAW 264.7 cells was therefore determined using a haemocytometer on the last day of exposure and supplemented by images of adherent cells using light microscopy.

2.2.9. Lactate dehydrogenase (LDH) assay

Cytotoxicity Detection Kit was used for determination of EA.hy 926 cell death, as described by the manufacturer. Cell medium was collected every 24 h of the treatment from each well, pooled together and frozen at − 80 °C. Diluted cell medium (1:5) was mixed in a 96-well plate with LDH detection mix and incubated for 30 min in the dark. After incubation, stop-solution was added and the plate was shaken for 10 s. The absorbance was measured at 490 nm using a Mithras2 plate reader.

2.2.10. Luciferase-dependent heme-oxygenase-1 promoter activity reporter assay

DLD1-HO1-prom cells were used to assess the promoter activity of heme-oxygenase-1 dependent on Nrf2 activation, after acrolein exposure. The method was adapted with help from [redacted] from the Institute for Pharmacology, University Medical Center Mainz, Germany. Cells were treated with different concentrations of acrolein (0.33 µM, 1 µM, 3.3 µM, 10 µM or 33 µM) for 2 days and then lysed using Passive Lysis Buffer for 30 min at 37 °C. The lysate was then treated with a luciferase assay solution and the chemiluminescence was measured with a 10 s acquisition time on a plate reader. The detailed protocol of the assay was published previously by prof Kleinert's group [197].

2.2.11. CO levels in the air

Levels of carbon monoxide in the smoke within the exposure chamber were measured using single use cartridges. Smoke coming from the shisha was vacuumed directly through the proprietary glass cartridge, for either one puff (for the smoke of three coal pieces) or ten puffs

(for the smoke of electrically heated shisha, one piece or two pieces of coal). The smoke was vacuumed using a hand-held compression device. The sample of the used cartridge is shown in the **Figure 33** A.

2.2.12. CO-Hb in blood

Levels of carboxyhaemoglobin in blood were measured via spectrophotometry. Whole blood samples were treated with EDTA and haemolysing solution and set at room temperature for 5 min. Diluting solution was added to the samples and set at room temperature for 10 min. After the incubation, absorbance was read at 420 nm and 432 nm with pure diluting solution as a blank. The fraction of carboxyhaemoglobin is calculated as:

$$Sco = \frac{1 - \mathrm{AR} * \mathrm{F1}}{\mathrm{AR} * (\mathrm{F2} - \mathrm{F1}) - F3 + 1}$$

Where AR is the ratio of the absorbance measured at 420 nm and 432 nm of each sample. F1 (1,3330), F2 (0,4787) and F3 (1,9939) are constants calculated from the published molar absorptivities of reduced haemoglobin and carboxyhaemoglobin and 420 nm and 432 nm [198].

2.2.13. Non-invasive blood pressure (NIBP) measurement

Blood pressure of mice was measured once per week via non-invasive tail-cuff method. Mice were constricted in plastic retainers size S (for mice up to 50 grams of weight), in a way that the tail remained completely free, outside of the retainer. The mice were trained for at least two times before acquiring the basal blood pressure measurement, to get used to the retainers. During each training and measurement session, the mice were kept for 10 minutes on warming platform at 32 °C and in the dark. The occlusion cuff was then placed on the base of the tail, closest to the body of the mouse, followed by volume pressure recording cuff. The cuffs were connected to the CODA system either with two or four channels. The original data have been acquired by CODA Data Acquisition Software. Every measurement was repeated 10 times per mouse, with a minimum volume of 15 µL and minimum flow of 5 µL/min. If the measurement did not fit the minimum volume and/or flow requirements, it was discarded. The measurements that were used are mean values of 10 repeated cycles per mouse. Pulse

pressure was calculated as a difference between systolic blood pressure and diastolic blood pressure for each mouse.

2.2.14. Isometric tension studies

Vascular function in aortic segments was tested using isometric tension study, as previously described [80, 121]. This method was performed with help from [redacted] The device consists of organ bath chambers, filled with a buffer (Krebs-Henseleit solution bubbled with carbogen gas (95% O_2, 5% CO_2)) and preheated to 37 °C, a force transducer on top of the chambers and a fixed support at the bottom of the chamber. Substances are added into the chamber to the preheated buffer and washed out after a defined period. Force transducer registers changes in the vascular tone of the aortic rings submerged into the buffer. Aortic rings from the mouse thoracic aorta (4 mm in length), carefully cleaned of the surrounding adipose tissue, were first stretched gradually to reach a resting tension of 1,1 g, then the constant isometric tension of the vessels was induced by increasing concentrations of KCL (potassium chloride; 5, 10, 20, 40 and 80 mM), to create a dose-response curve. Afterwards, the vessels were washed and the resting tension was gradually reestablished, than 3 µM prostaglandin $F_{2\alpha}$ was added to constrict the vessels to 80 % of the maximal tone observed by preconstruction with KCl. In the end, the aortic rings were subjected to a titration by endothelium-dependent vasodilator (acetyl-choline, ACh; 10^{-9} to $10^{-5,5}$ M) and endothelium-independent vasodilator (nitroglycerine, NTG; 10^{-9} to $10^{-4,5}$ M).

2.2.15. Detection of oxidative stress via chemiluminescence

To determine superoxide production in aorta lucigenin-enhanced chemiluminescence was used. Lucigenin reacts with superoxide and the product is chemiluminescent dioxetane intermediate. Aortic rings cleaned of the surrounding tissue (5 mm in length) were incubated first with KH-buffer for 20 min on 37 °C, and then transferred to a vial with 5 µM lucigenin solution. The vial was kept from the light and transferred directly to the luminometer (Lumat LB 9507), where the chemiluminescence was recorded over 20 min at 1 min intervals. Only the last measurement was used in further analysis. The aortic rings were collected after the measurements and placed on room temperature to dry overnight. Then, dry aortic rings were measured and the chemiluminescent values were normalised to the dry mass of the aortic rings.

2.2.16. Oxidative burst

Oxidative burst is used to measure leukocyte–dependent hydrogen-peroxide formation. Myeloperoxidase converts oxidative burst-derived hydrogen peroxide to oxygen-metal complexes that react with a luminol derivative L-012 and oxidizes it, so it emits chemiluminescent light that can be detected. The assay was previously described in whole blood or isolated human granulocytes [194], and additionally modified for the usage on the RAW 264.7 macrophages. Whole blood samples were treated with fresh citrate, while macrophage samples were diluted into matching cell numbers (106 cells/mL) using PBS/Ca^{2+}/Mg^{2+} (1 mM). The reaction was induced using zymosan A (50 µg/mL), as well as direct activator of protein kinase C, phorbol 12,13-dibutyrate (PDBu, 10 µM). Chemiluminescent probe L-012 (100 µM) was added to the mixture and the activated chemiluminescence was measured using a plate reader (Mithras2 LB 943) every 5 min for a total time of 60 min. Oxidative burst was done only in RAW 264.7 macrophages and not in the EA.hy 926 endothelial cells as only phagocytic cells are capable of producing reliable and measurable oxidative burst.

2.2.17. Total oxidative stress

In EA.hy 926 and RAW 264.7 cell cultures dihydroethidium (DHE) oxidation product-dependent fluorescence was used to assess oxidative stress. ROS oxidise DHE into 2-HE (superoxide-specific oxidation product) and E+ (unspecific oxidation product), and the fluorescence of the products can be observed and quantified, but not separated, under fluorescent microscope. This method was performed with help from [redacted] Plates with cell cultures seeded to 70-80 % confluence were washed two times with pre-warmed PBS and then incubated with 1 µM DHE (in PBS) for 30 min at 37 °C. After incubation, cells were washed with PBS again to remove background fluorescence, and imaged under the fluorescence microscope. The excitation wavelength used was 510–520 nm, while the emission wavelength was set at 580–610 nm. Images were quantified with the ImageJ software. After imaging, cells were additionally incubated with 25 µM DHE (in PBS) for 30 min at 37 °C. The PBS fraction was collected and used to determine DHE oxidation by extracellular superoxide and H_2O_2 via HPLC-based fluorescence detection of 2-hydroxyethidium (2-HE, superoxide specific oxidation product of DHE) and ethidium (E+, unspecific oxidation product of DHE). Cells were then lysed with acetonitrile and water solution (1:1), and the lysate was

used to determine the intracellular DHE oxidation products. HPLC system with fluorescent detection uses a C18-Nucleosil 100–3 (125 × 4) column. A gradient of 90 % acetonitrile / 10 % water solvent and 50 mM citrate buffer (pH 2.2) was used as a mobile phase, with percentages of organic solvent as follows: 0 min — 36 %, 7 min — 40 %, 8 min — 95 %, and 13 min — 36 %. The flow was 1 mL/min, with DHE detection at 355 nm (absorbance), and 2-HE and E+ detection at 480 nm excitation and 580 nm emission (fluorescence). The retention time of 2-HE was around 3.2 min and the retention time of E+ was around 3.7 min. The signal was compared to a 1 µM standard.

2.2.18. Cryo conservation and ROS detection by dihydroethidium microtopography

Dihydroethidium (DHE)-dependent fluorescence microtopography was used for determination of ROS formation in cryo-sections of cortex, lung, aortic and heart tissues, as previously described [199, 200]. Small sections of cortex, aorta and lung were incubated in the Krebs-Henseleit buffer for 10 min at 37 °C and then submerged into 1 mL of viscous compound Tissue Tek® and frozen in liquid nitrogen. The samples were kept on -80 °C until cut in the cryo-microtome at -25 °C into 8 µm-thick sections and placed on the microscopic slides. The slides were then kept at -80 °C until used for fluorescent imaging. The slides were incubated with 1 µM DHE (in PBS with 0.5 % DMSO) for 30 min at 37 °C, guarded from light. DHE is able to penetrate tissues and react with superoxide and other ROS. Oxidation products of DHE, 2-HE and E+, were detected via fluorescence microscopy at excitation/emission wavelength of 520/610 nm. DHE oxidation products fluorescence was quantified from images using ImageJ software.

2.2.19. Western blot

For the analysis of specific protein content in aortic and heart tissue, as well as cell cultures, western blot was used, as previously described [106, 121]. Tissue pieces were homogenised using mortar and pestle with liquid nitrogen, then diluted in Hg-solution. The mixture was kept for one hour over ice, with vortexing every 10 min, then centrifuged at 10,000 × g for 10 min at 4 °C. The protein containing supernatant was used for further western blot. Cell cultures were dried, then shock-frozen under liquid nitrogen and scraped from the plates with ice-cold Hg-solution without Triton-X100. This mixture was centrifuged at 100,000 x g for 10 min at 4 °C and the supernatant was discarded. The pellet was re-suspended in Hg-solution with Triton-

X100 and kept over ice for one hour while vortexing every 10 min, then centrifuged at 10,000 × g for 10 min at 4 °C and the membrane-protein contained supernatant was collected. Concentration of protein samples was determined by Bradford protocol described previously [201]. All protein concentration measurements were compared to a bovine serum albumin (BSA) standard curve at dilutions of 0, 1, 5, 10, 20 and 30 µg/ml in H_2O. Cell and tissue lysates were diluted in H_2O to assure that the protein concentration falls into the standard curve range. 80 µl of each sample was transferred to a 96-well plate in, at least, triplicates and 200 µl of the Bradford reagent (ROTI®-Quant, 1:5 diluted) was added to each well and the plate was shaken for 5 seconds. Absorption values of the plate were measured at 595 nm. The results were assessed using the associated application program Revelation. Protein samples were charged with 3 × Laemmli buffer (protein:buffer = 2:1) and denaturised at 95 °C for 5 min. Proteins from the samples were first separated by their molecular weight via SDS-PAGE gel electrophoresis. Depending on the concentration of the samples, they were loaded onto either 10-well or 15-well gels, so that the total protein amount was at least 20 µg per well. The gel ran on a 10 % polyacrylamide-loading and 4 % stacking gel, at 130 V and 4 °C for around 2 hours. After separation, proteins were transferred to the nitrocellulose membrane at 80 mA and 4 °C overnight. Nitrocellulose membranes with transferred proteins were first stained with the Ponceau-S, to visualize the proteins on the membrane and label the molecular weight markers (10 kDa protein ladder). Ponceau-S staining was then washed out and the membranes were blocked with appropriate blocking buffer (either 3 % bovine serum albumin or 5 % bovine serum albumin in either PBS-T or TBS-T) for 1 h. Afterward, the membranes were incubated with appropriate primary antibody, with either alpha-actinin, beta-actin or GAPDH used as housekeeping protein for normalisation of loading and transfer (all used antibodies are listed in the materials section). After washing three times (5 min each) with washing buffer (PBS-T or TBS-T), the membranes were incubated with appropriate horseradish peroxidase (HRP)-conjugated secondary antibodies for 2 h at room temperature. After additional washing steps the antigen-antibody binding complexes were visualized with enhanced chemiluminescence (Pierce™ ECL Western Blotting Substrate or SuperSignal™ West Femto Maximum Sensitivity Substrate). Chemiluminescence of protein-bands were captured with ChemiLux imager. Densitometric quantification was performed using Gel-Pro Analyzer.

2.2.20. Dot Blot

Analysis of total protein content was performed by dot blot, for plasma, lung and heart tissues of shisha exposed mice. For this, equal amounts (usually ~20 µg) of protein homogenates were diluted in PBS and each sample was applied to a buffer-soaked nitrocellulose membrane using a dot blot device with a 96-well top frame. The device was connected to a water pump jet that generated a vacuum, which allowed the absorption of the samples through each well to the membrane. Subsequently, the membrane was removed from the dot blot device and dried for 1 h at 60 °C to fix the proteins on the membrane surface. Equal loading of protein amounts per well/dot was then verified by staining the membrane with Ponceau S. Afterwards, blots were blocked with suitable blocking buffer for 90 min at room temperature before incubation with primary antibodies at their appropriate dilution in blocking buffer over night at 4 °C. The next day, following three washing steps (5 min each) with correspondent buffers, membranes were incubated with horseradish peroxidase (HRP)-conjugated secondary antibodies (diluted in the same blocking buffer as the primary antibody) for 120 min at room temperature. Afterwards, membranes were washed again three times for 5 min with correspondent buffers. ECL Western blotting substrate was used as visualising agent and antibody-specific chemiluminescent dots on the membranes and were captured with ChemiLux imager. Densitometric quantification was performed using Gel-Pro Analyzer. All antibodies, dilutions and buffers that were used are listed in the Materials section.

2.2.21. Quantitative RealTime-reverse transcriptase Polymerase Chain Reaction (qRT-rtPCR)

Quantification of RNA fragments was performed by qPCR analysis using the primers listed in the Materials section. Cortex, heart and lung tissues of shisha exposed mice were used for extraction of RNA. Small pieces of tissue were mixed with 600 µL of GIT-buffer and 4.32 µM of 2-mercaptoethanol and homogenized with steel beads in tissue lyser for 6 minutes. 60 µL Na-acetate and 600 µL of phenol were added and vortexed, before placing at -20 °C for 2 hours. The mixture was then centrifuged at 13000 rpm for 30 minutes at 4°C and the aqueous phase was mixed with isopropanol to precipitate clean RNA. The samples were stored at -20 °C overnight and centrifuged again at 13000 rpm for 30 minutes at 4 °C. The remaining RNA-pellet was washed with 80 % ethanol and then dried. The RNA was then re-dissolved in 30-50 µL of sterile H_2O and used for further analysis. RNA concentration in the samples was

determined by BioPhotometer (Eppendorf) and the samples were stored at -80 °C until further use.

For specific RNA quantification, QuantiTect Probe RT-PCR Kit was used as previously described [202]. As housekeeping gene TaqMan® Gene Expression assays for TATA box binding protein was used. Reaction mix consisted of 10 µL of 2x QuantiTect Probe RT-PCR Master Mix (contains buffer, nucleotide, Taq polymerase, reverse transcriptase), 6.8 µL of RNAse-free water, 1 µL of suitable primer, 0.2 µL of QuantiTect Probe RT Enzyme and 2 µL of sample with 125 ng of RNA. The reaction mix was pipetted into a 96-well PCR plate, which was sealed and then briefly centrifuged to collect components at the bottom of the plate. Templates were amplified using the thermal cycler "StepOnePlus Real-Time PCR Systems". The initial denaturation phase was set to 15 min at 95 °C, followed by 40 cycles of 15 sec denaturation at 95 °C and 1 min of primer annealing and nucleotide extension at 60 °C. Gene expression was normalised to TATA box binding protein and the amount of target gene in each sample was expressed relative to the control sample (using the ΔΔCt method).

2.2.22. Behavioural tests

Behavioural experiments were performed in collaboration with [redacted] from the Laboratory of Neuroanatomy, Institute of Anatomy, Johannes Gutenberg University Mainz, Germany. Most of the tests were previously described in publication by his group [203].

2.2.22.1. Open-field

Open-field is an experimental test that is generally used to assess general locomotor activity, anxiety and willingness to explore in animals. The test was performed in a custom white square Plexiglas box (arena 40 x 40 cm) that is divided into a periphery zone (8 cm away from the edges), a central zone (20 x 20 cm) and a mid-zone (part in between the edge zone and central zone). The animal is placed in the centre of the arena and allowed to explore the open field for 10 min, while being recorded by an overhead camera. The video footage is analysed by an automated tracking system for the total distance travelled and time spent in each of the zones of the open field. The results determine general activity and gross locomotor activity and exploration habits [204].

2.2.22.2. Light-dark test

Light-dark test is an experimental test to determine unconditioned anxiety responses in mice. It was performed in a Plexiglas box divided into two zones connected to each other. One zone is 1/3 of the total box size and kept in the dark and the other zone is 2/3 of the total box size and is kept illuminated. The animal is placed into the dark part of the box first and allowed to freely move between the zones for 10 min, while being recorded with an overhead camera. The footage is analysed by an automated tracking system for the latency until the first entry into the illuminated zone and the time spent in each of the zones. The ratio of the times spent into two zones is used to assess fear-related behaviour [205, 206].

2.2.22.3. Three-chamber social interaction test

Three-chamber social interaction test is an experimental test that assays sociability of mice and their interest in social novelty. Social interaction test was performed in a rectangular Plexiglas box divided into three chambers (each 20 x 40 x 22 cm in size) connected to each other in a row and divided with sliding doors. Side chambers include cylindrical cage each and one of the cages holds an unknown object, while the other holds an unknown and untested mouse. Tested animal is firstly placed into the central chamber closed with the sliding doors and left to move freely for 10 min. After 10 min, the doors open and tested mouse is left for another 10 min to move freely between all three chambers. The movement of the mouse is recorded with an overhead camera and the recording is analysed for the time spent in each of the chambers, number of initiated contacts with an unknown mouse (stranger mouse), duration of the contacts with an unknown mouse and duration of the contacts with an object. A social index is then calculated as follows:

$$\textbf{Social index} = \left(\left[\frac{\textbf{Time stranger mouse}}{(\textbf{Time stranger mouse} + \textbf{Time object})}\right] * \textbf{100}\right) - \textbf{50}$$

Calculated social index determines general sociability and interest in social novelty. Rodents are considered as social animals and they normally prefer to spend time with another rodent as opposed to unknown objects [207].

2.2.22.4. Y-maze test

Y-maze test is an experimental test used to define short term memory in mice. The Y-shaped maze is made from white opaque plastic arms at a 120° angle from each other. Animal is placed into the centre of the maze connected to all three arms and left to freely explore all three arms of the maze for 10 min and recorded with an overhead camera. The footage is analysed for the number of alternating entries (entering the arm of the maze that was not explored in the previous entry, labelled as "correct entry") as well as total number of entries. Each entry is counted when all four limbs are within one of the arms of the maze. Number of correct entries determines cognitive power while total number of entries may refer to the activity level [208].

2.2.23. Statistical analysis

GraphPad Prism 9 was used for the statistical analysis of all the data and visualization of all the graphs. One-way ANOVA (with Tukey post hoc test for comparison of multiple means) or, where appropriate, equivalent non-parametric Kruskal–Wallis test (Dunn multiple comparisons) was used where multiple groups were present. Two-way ANOVA (with Tukey post hoc test) or, when applicable, a mixed-effects model (with Tukey post hoc test) was used for all vascular function graphs. A two-tailed *t*-test was used when only two groups were present, like in the shisha study. When analysed, data are presented as mean ± range as a jitter plot, and a *p*-value ≤ 0.05 is considered statistically significant. Standard deviation (SD) was shown where applicable.

3. Results

3.1. Effects of noise on the cardiovascular system, the metabolic status and the behaviour of mice

3.1.1. Noise effects on vascular function, glycosylated haemoglobin and body weight

Vascular function was tested using functional clinical parameters blood pressure and vascular relaxation. Systolic blood pressure was measured using non-invasive tail-cuff method before and after noise exposure, as well as weekly for the 28 day noise exposure and after behavioural tests were finished (**Figure 17** A and B). Blood pressure was significantly increased after 4-days noise exposure, as well as during the 28-day noise exposure (after weeks 1, 3 and 4 significantly and during week 2 of noise exposure not significant, but still elevated). After behavioural studies, blood pressure remained elevated in the noise-exposed group, however, it also rose in the control group removing the difference between groups (**Figure 17** A). Endothelial function was measured using isometric tension method. Parts of the aorta were isolated and their relaxation pattern was tested using acetylcholine as an endothelium-dependent vasodilator and nitroglycerine as an endothelium-independent vasodilator. Endothelium-dependent relaxation curve was dose-dependent significantly shifted to the right for both short-term and long-term noise exposures (**Figure 17** C). Endothelium-independent relaxation curve also slightly shifted to the right, but this shift was only statistically significant for highest concentrations of nitroglycerine in long-term noise exposure (**Figure 17** D).

Glycosylated haemoglobin (HbA1C) was assessed after 28-days noise exposure using A1C Now+ system [209]. Noise-exposed mice showed significantly lower levels of glycosylated haemoglobin than control mice (**Figure 17** E). Body weight of mice was tested twice a week during long-term exposure, as well as after the end of behavioural studies and no difference was observed between control and noise-exposed mice (**Figure 17** F).

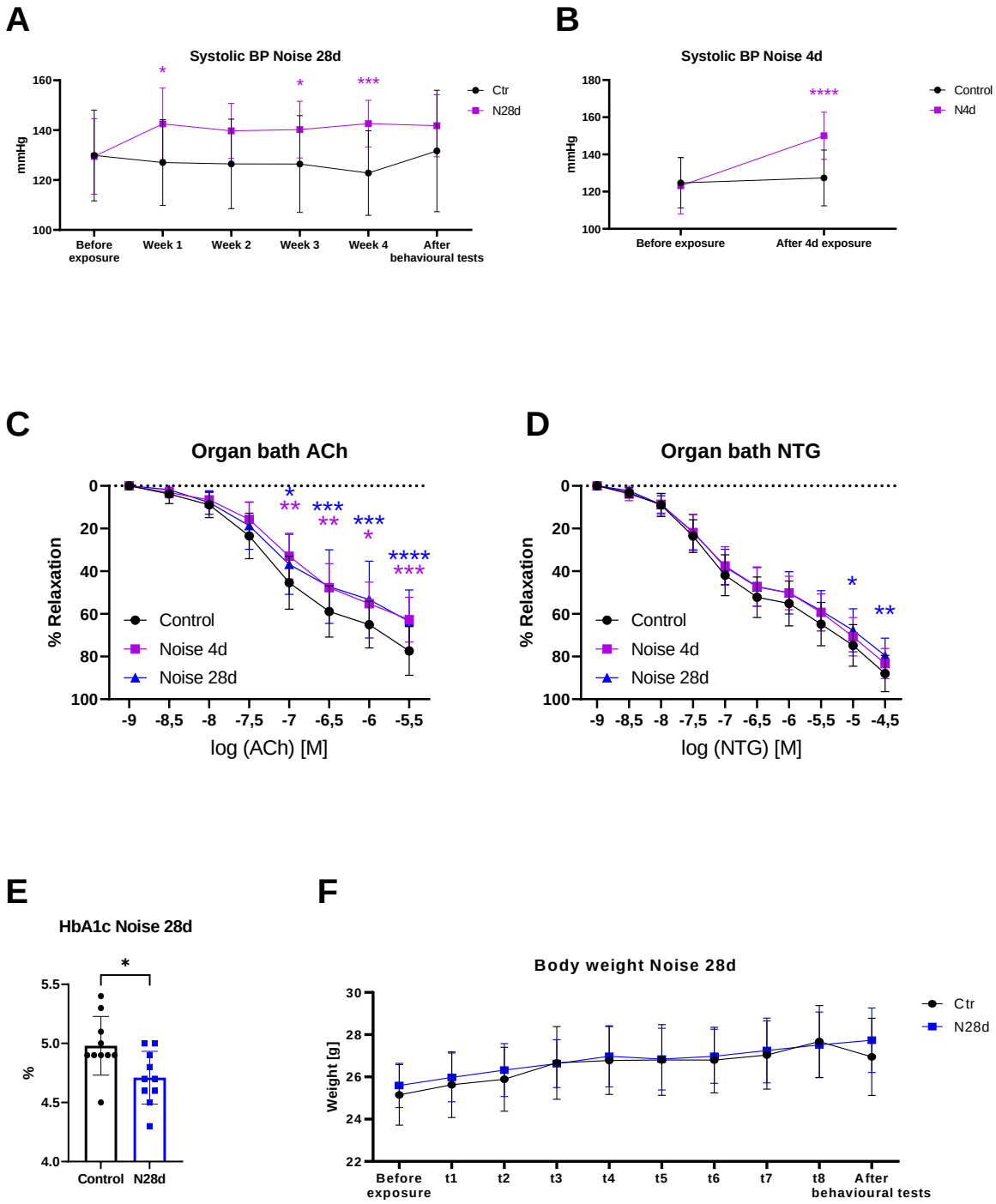

Figure 17. Effects of noise on blood pressure, vascular function, blood sugar and body weight. (A) Blood pressure was measured via tail-cuff method, once a week, during 28 days exposure and once after the end of behavioural tests, as well as (B) before and after 4 days exposure. (C) Vascular function tests were defined as percentage of relaxation of the preconstricted aortic rings with acetylcholine (endothelium-dependent) and with (D) nitroglycerine (endothelium-independent) after both 4 days and 28 days of noise exposure. (E) Glycosylated haemoglobin (HbA1C) was measured after 28-day noise exposure (t1 - t8). (F) Body weight was measured twice a week during 28 days exposure and once after the end of behavioural tests. The data are shown either as an XY graph (A, B, C, D, and F, mean ± SD, n =

20-30) or as a jitter-plot (E, mean ± SD, n = 10). Significance is indicated as *, **, ***, and **** when $p < 0.05$, $p < 0.01$, $p < 0.001$ and $p < 0.0001$ respectively.

3.1.2. Effects of noise on the relative expression of oxidative stress-related proteins in vascular tissue

Oxidative stress markers in heart were determined by quantitative polymerase chain reaction (qRT-rtPCR), western blot and dot blot methods, while oxidative stress markers in aortic rings were determined using western blot only. Relative expression of mRNA that codes stress-related proteins, such as B-type natriuretic peptide (BNP), NOX2 and heme-oxygenase-1 (HO-1), were measured in heart using PCR. The results were unaltered after 28-day noise exposure (**Figure 18** A).

Relative expression of stress-related proteins Cu/Zn-SOD, ET-1 and p-MARCKS were measured in heart (**Figure 18** B) and relative expression of eNOS, HO-1, p67phox, PKCα and CD68 were measured in the aorta (**Figure 18** C) after 28-day noise exposure via western blot. The targets in the heart, as well as PKCα, eNOS, CD68 and p67phox levels in the aorta were only increased by trend. However, relative expressions of HO-1 in aorta was significantly higher in the noise-exposed group.

Relative expressions of oxidative stress-related markers, 3-NT positive proteins, were measured in heart of 4-days noise exposed mice using dot blot technique (**Figure 18** D) and the levels remained increased only by trend.

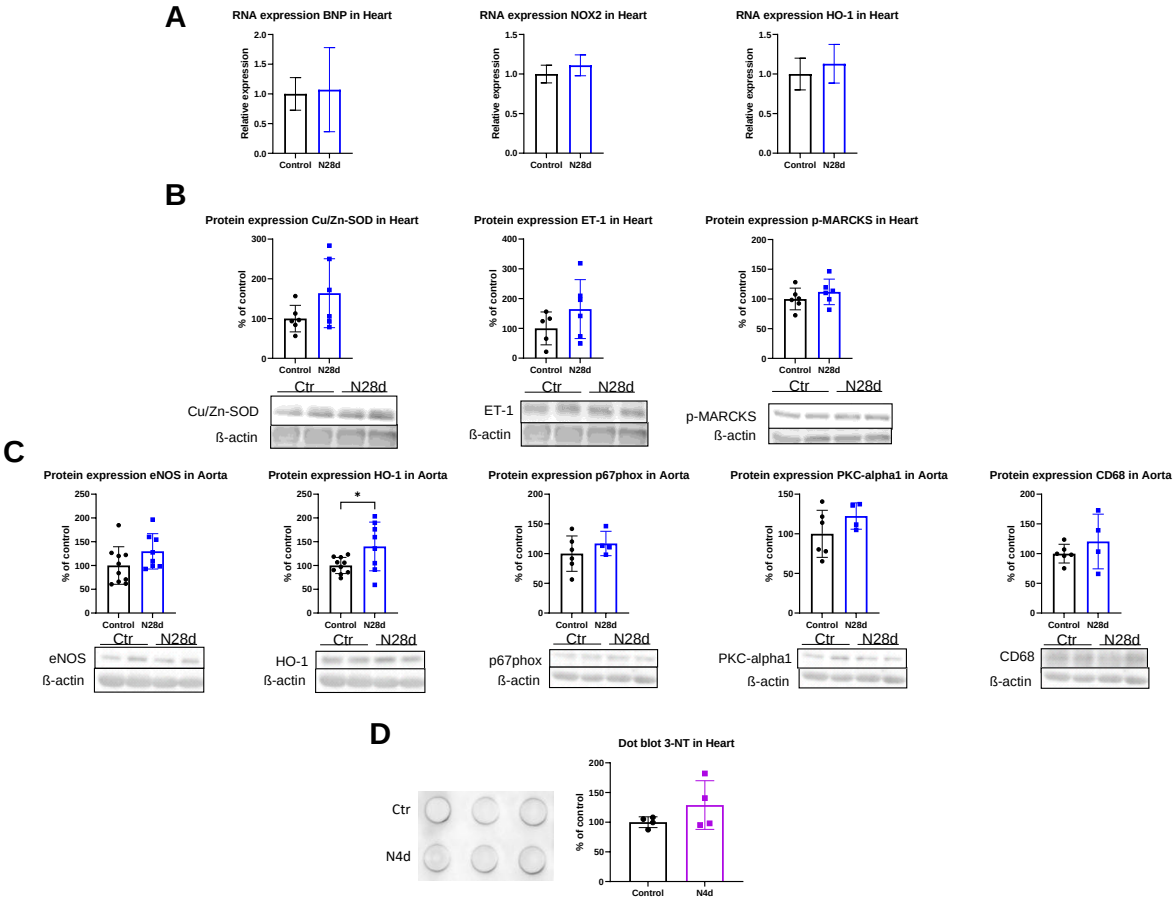

Figure 18. Effects of noise on relative expressions of stress-related proteins and mRNA in the heart and aorta of mice. (A) Relative expression of mRNA that code stress-related proteins (B-type natriuretic peptide (BNP), NADPH oxidase subunit NOX2 and heme-oxygenase-1 (HO-1)) in hearts of mice was determined by quantitative polymerase-chain reaction (qRT-rtPCR) after 28-day noise exposure. (B) Relative mRNA expression of stress-related proteins copper-zinc-superoxide dismutase (Cu/Zn-SOD), endothelin-1 (ET-1) and phosphorylated myristoylated alanine-rich C-kinase substrate (p-MARCKS) in hearts of mice was determined using western blot method after 28-day noise exposure. (C) Relative expression of stress-related proteins endothelial NO-synthase (eNOS), HO-1, NADPH oxidase subunit p67phox, protein-kinase C alpha (PKCα) and cluster of differentiation 68 (CD68) in aortas of mice was determined by western blot after 28-day noise exposure. (D) Relative expression of 3-nitro tyrosine positive proteins (3-NT) in hearts of mice was determined by dot blot after 4-day noise exposure. The data are shown as jitter-plots (mean ± SD, n=4-6). Significance is indicated as * when $p < 0.05$.

3.1.3. Effects of noise on behaviour of mice

Open-field, light-dark chamber, Y-maze and social interaction tests were performed to evaluate the anxiety and cognitive capacities of mice after 4-day and 28-day noise exposure

(**Figures 19-26**). After 4-day noise-exposure no significant difference was observed for either of the open-field, light-dark chamber, social interaction or y-maze behavioural tests (**Figures 19-22**).

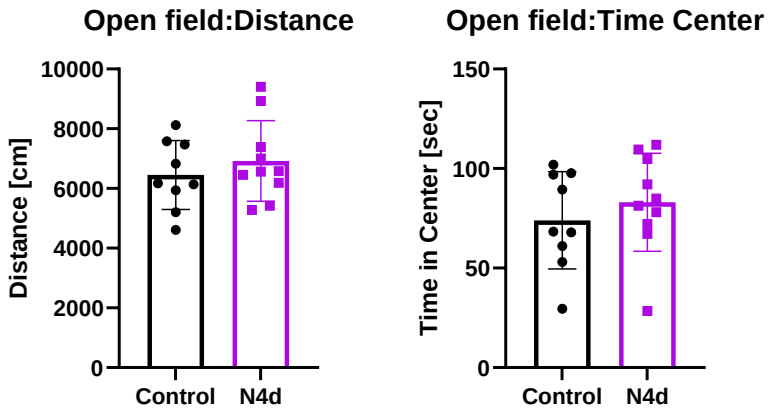

Figure 19. Open-field test results after 4-day noise exposure. The data are shown as jitter-plots (mean ± SD, n=9-10).

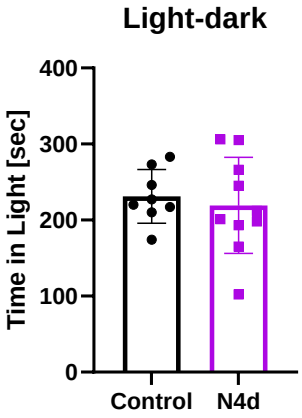

Figure 20. Light-dark chamber test results after 4-day noise exposure. The data are shown as a jitter-plot (mean ± SD, n=9-10).

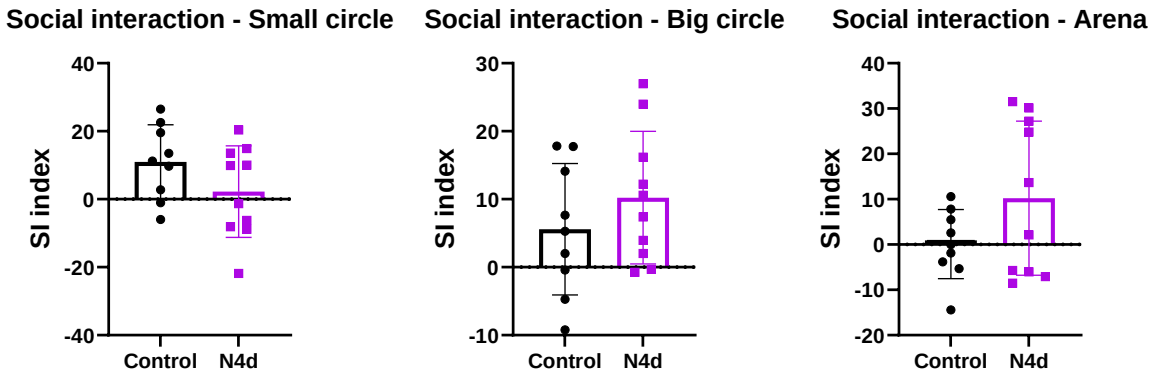

Figure 21. Social interaction test results after 4-day noise exposure. The data are shown as jitter-plots (mean ± SD, n=9-10).

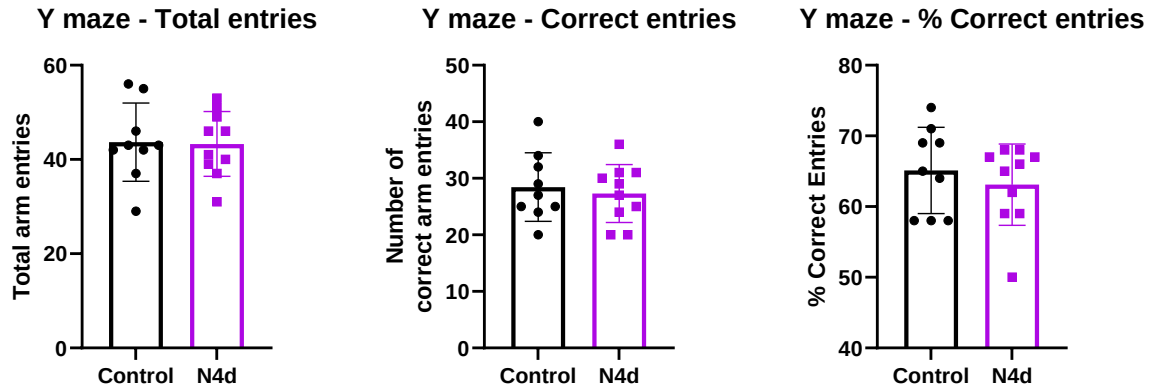

Figure 22. Y-maze test results after 4-day noise exposure. The data are shown as jitter-plots (mean ± SD, n=9-10).

After 28-day noise exposure, open-field test showed that noise-exposed mice travelled significantly higher distance and spent significantly more time in the centre of the open-field (**Figure 23**). Light-dark chamber test did not show any significant difference between 28-days noise-exposed and unexposed group (**Figure 24**). Social interaction test again showed that noise-exposed mice travelled significantly higher distance, and they also explored the stranger mice significantly less time when compared to control mice (**Figure 25**). Y-maze test showed significantly higher number of total entries into the arms of the maze and total distance

crossed, but significantly lower number of "correct" entries (entering a different arm of the maze from the one it was already entered) in the noise-exposed group (**Figure 26**).

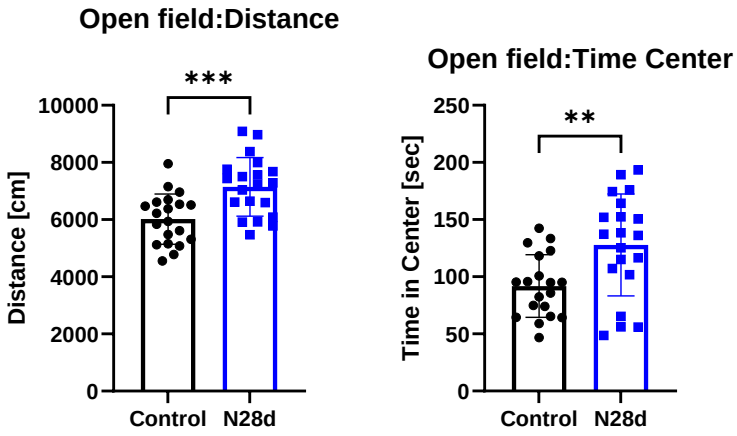

Figure 23. Open-field test results after 28-day noise exposure. The data are shown as jitter-plots (mean ± SD, n=20). Significance is indicated as ** and *** when $p < 0.01$ and $p < 0.001$ respectively.

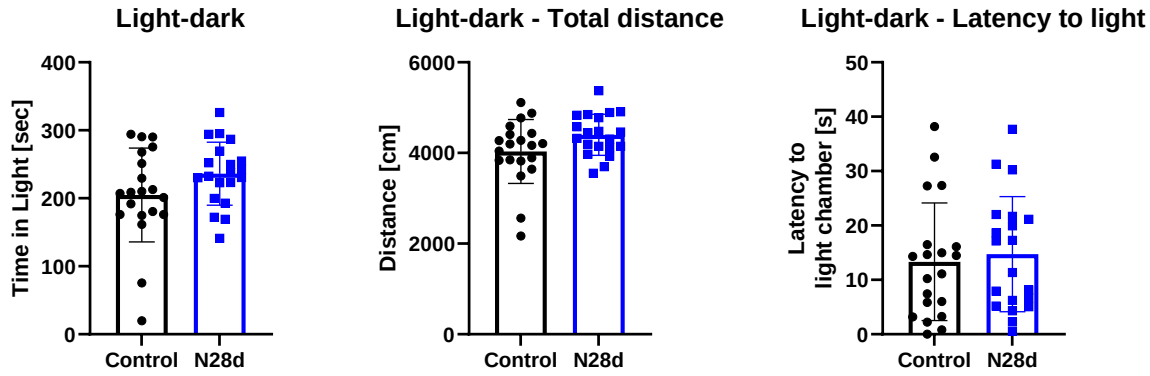

Figure 24. Light-dark chamber test results after 28-day noise exposure. The data are shown as jitter-plots (mean ± SD, n=20).

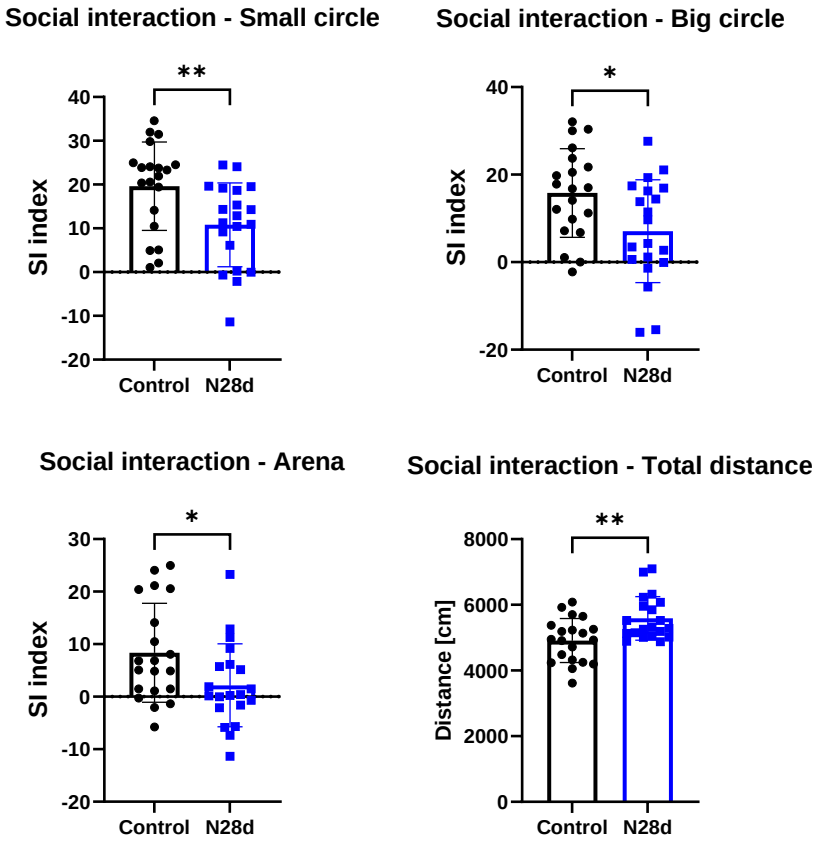

Figure 25. Social interaction test results after 28-day noise exposure. The data are shown as jitter-plots (mean ± SD, n=20). Significance is indicated as * and ** when $p < 0.05$ and $p < 0.01$ respectively.

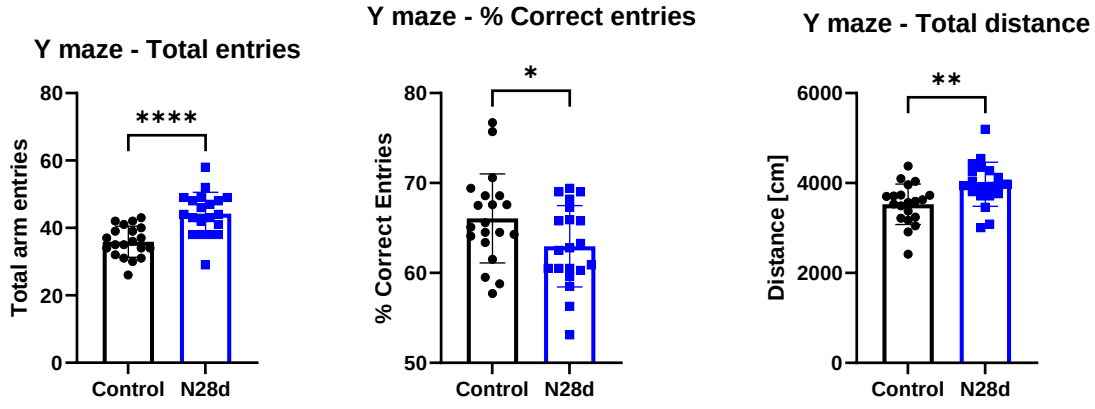

Figure 26. Y-maze test results after 28-day noise exposure. The data are shown as jitter-plots (mean ± SD, n=20). Significance is indicated as *, ** and **** when $p < 0.05$, $p < 0.01$ and $p < 0.0001$ respectively.

3.1.4. Effects of pharmacological intervention in noise-exposed mice

Clinical parameters, blood pressure and vascular relaxation, were tested in the noise-exposed mice with or without pharmacological intervention (**Figure 28**). Systolic blood pressure was significantly increased in the noise-exposed groups as well as in groups treated with propranolol, phenoxybenzamine and citalopram, but not in the diazepam treated group (**Figure 27** A and **28** A). Diastolic blood pressure remained unchanged in all of the exposed groups (**Figure 27** B and **28** B). All four pharmacological interventions mitigated the noise-induced endothelial dysfunction, shown as the right shift of the endothelium-dependent relaxation curve (**Figure 27** C and **28** C). Endothelium-independent relaxation curves with nitro-glycerine remained unchanged for all treatment groups (**Figure 27** D and **28** D).

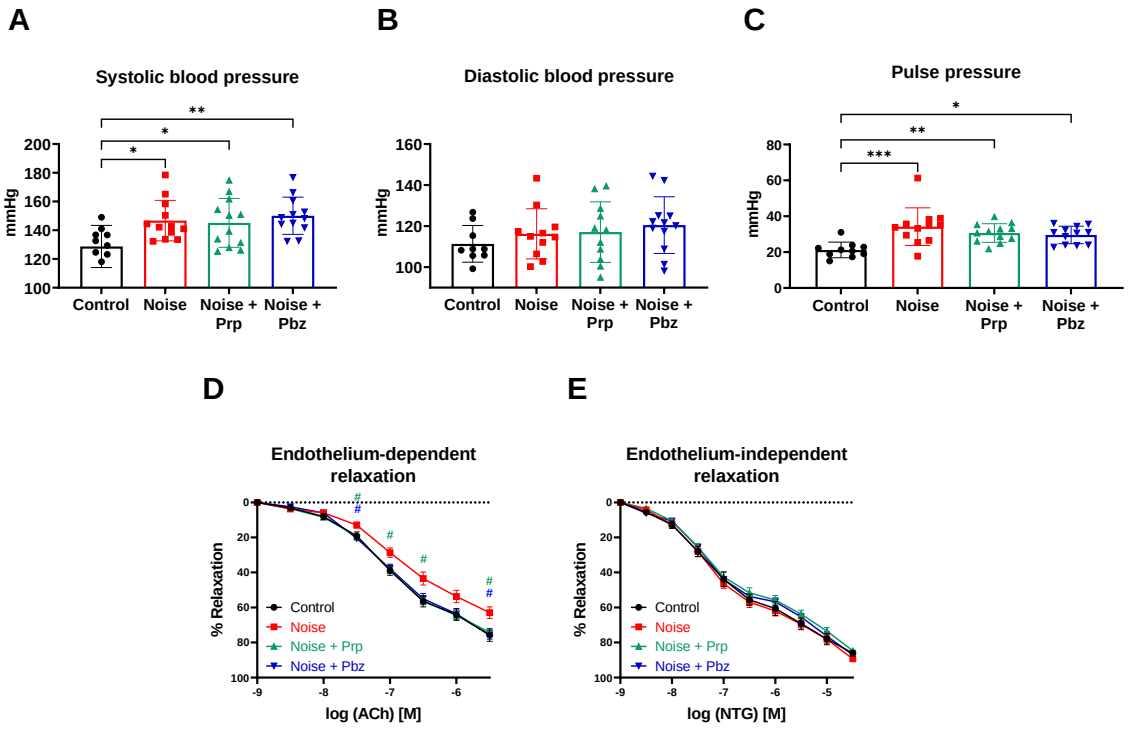

Figure 27. Effects of noise and cardiovascular pharmacological treatments on cardiovascular system of mice. (A, B, C) Blood pressure was measured via tail-cuff method, after the 4-day noise exposure with or without pharmacological treatments. The data are shown as a jitter-plot (A and B, mean ± SD, n = 12). Significance is indicated as *, ** and *** when $p < 0.05$, $p < 0.01$ and $p < 0.001$ respectively, between control group and exposed group. (C,D) Vascular function is measured as a percentage of relaxation of the aortic rings in the presence of acetylcholine (Ach, endothelium-dependent) or nitroglycerine (NTG, endothelium-independent) after noise-exposure and pharmacological treatments. The data are shows as an XY graph (C and D, mean ± SD, n = 12-16). Significance is indicated as # when

p < 0.05 between noise-exposed group and pharmacologically-treated group, as indicated by colour.

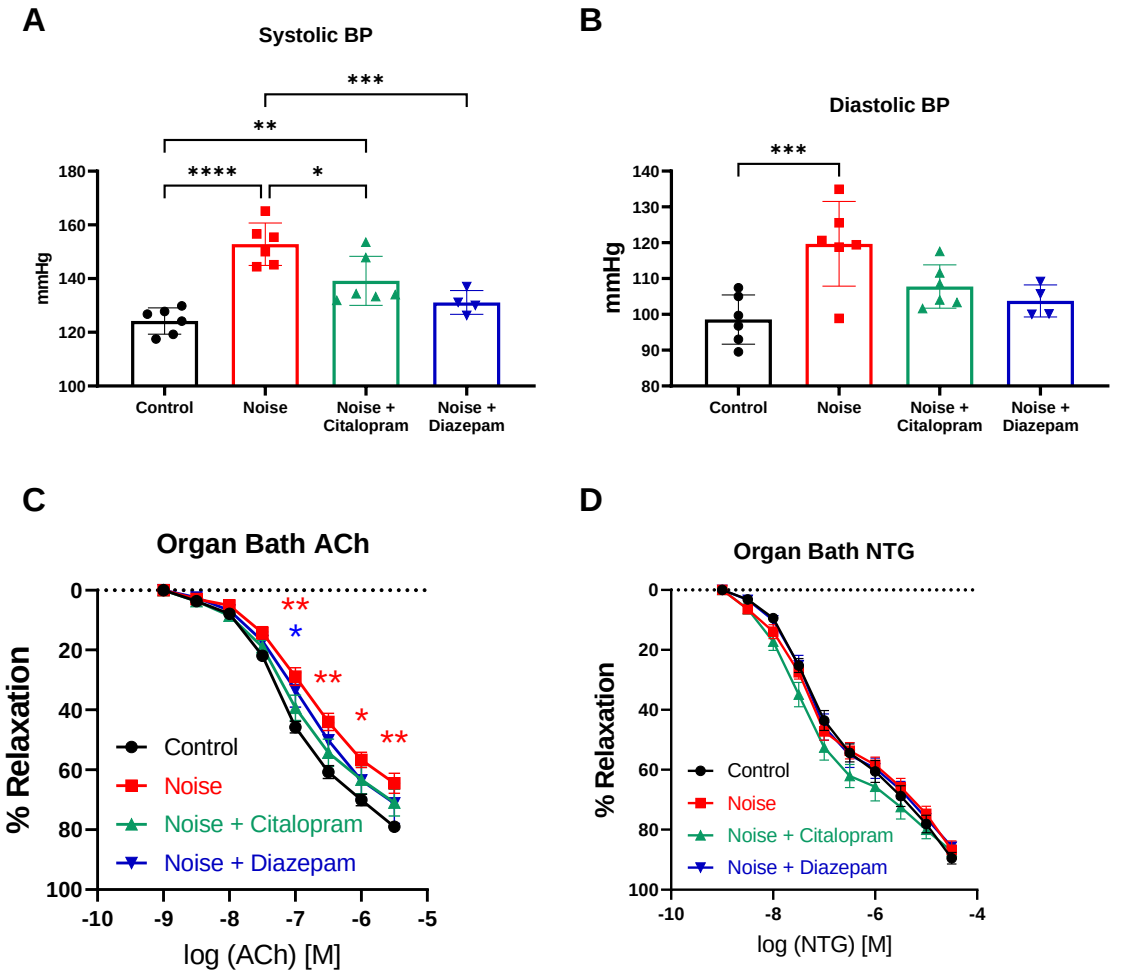

Figure 28. Effects of noise and neurological pharmacological treatments on cardiovascular system of mice. (A, B) Blood pressure was measured after the 4-day noise exposure with or without pharmacological treatments via tail-cuff method. The data are shown as a jitter-plot (A, mean ± SD, n = 6). Significance is indicated as *, **, *** and **** when p < 0.05, p < 0.01, p < 0.001 and p < 0.0001 respectively between control group and exposed group. (C, D) Vascular function is measured as a percentage of relaxation of the aortic rings in the presence of acetylcholine (Ach, endothelium-dependent) or nitroglycerine (NTG, endothelium-independent) after noise-exposure and pharmacological treatments. The data are shown as an XY graph (B, mean ± SD, n = 6-8). Significance is indicated as * and ** when p < 0.05 and p < 0.01 respectively, between control group and exposed group, as indicated by colour.

3.2. Effects of e-cigarettes on EA.hy 926 and RAW 264.7 cell cultures

3.2.1. Effects of acrolein and e-cigarette condensate on EA.hy 926 cells

Cell viability was determined by counting the cells with visible nuclei. Counting was performed every 24 h of the treatment, after removing the old medium and washing off the dead cells. EA.hy 926 cells treated with acrolein showed a concentration- and dose-dependent loss of viability, with the highest concentration of acrolein used (33 µM) having statistically significant impact on the cell viability from the first 24 h onward. After 72 h of cell exposure, 1 µM and 10 µM concentrations of acrolein also showed statistically significant reduction of cell viability (**Figure 29** A).

Same cell type was treated with e-cigarette vapour condensate, which also showed concentration- and time-dependent loss of viability, which became statistically significant after 24 h for two highest concentrations of e-cigarette vapour condensate. After 48 h of exposure, 1:75, 1:50 and 1:25 concentrations all displayed statistically significant reduction of cell viability, and the trend remained after 72 h of exposure as well (**Figure 29** B). This result was further tested by cell death detection assay (CDD) after 72 h exposure, and the results here were statistically significant for all treated groups (**Figure 29** C).

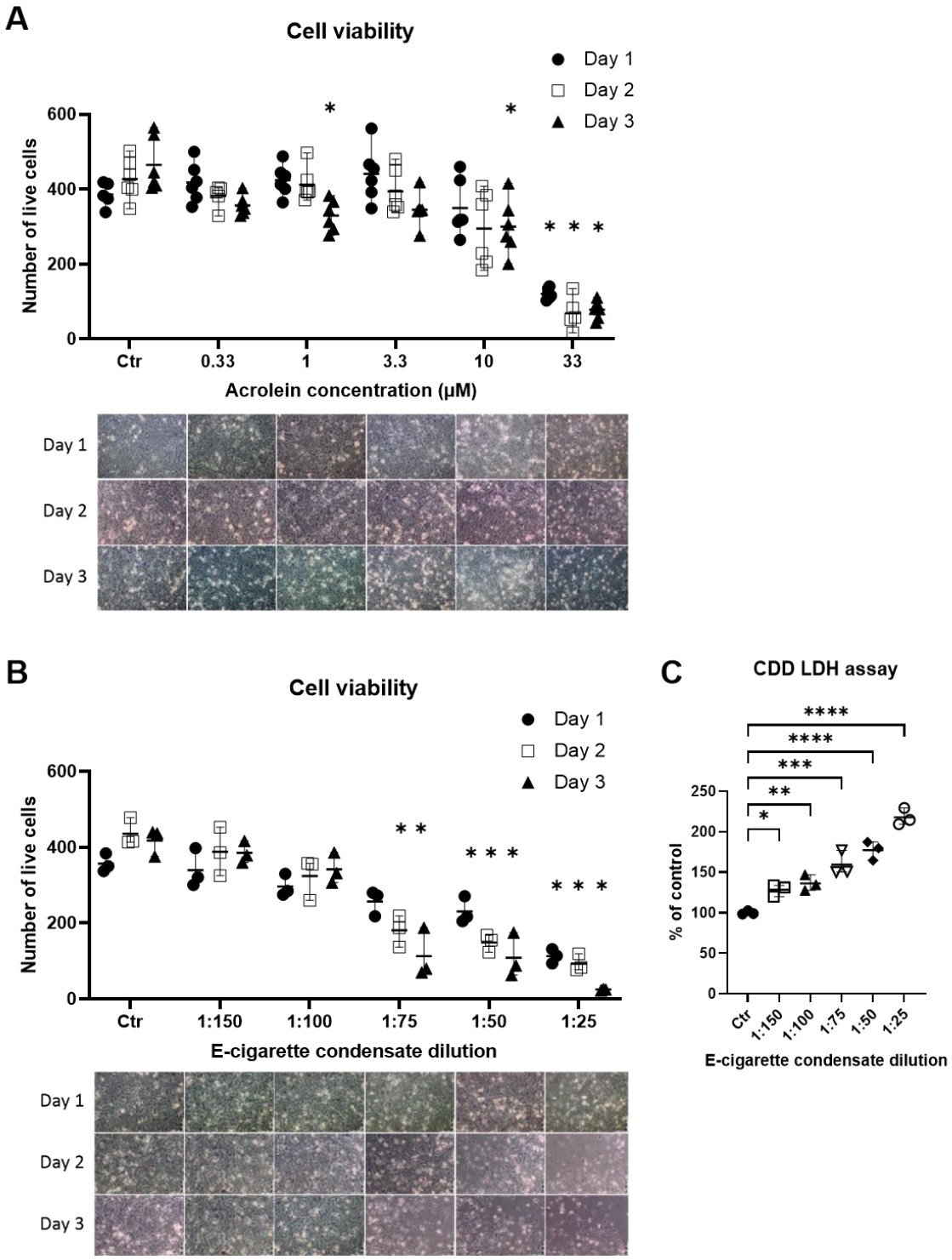

Figure 29. Effects of acrolein and e-cigarette condensate on EA.hy 926 cells. (A) The cells were incubated for three days with solvent only (1 % DMSO, named control (Ctr)) or different concentrations of acrolein in DMSO (0.33, 1, 3.3, 10, 33 µM) and the viability of the cells was determined each day as the number of cells with a visible nucleus (number of live cells). (B) The cells were incubated for three days with solvent only (1 % DMSO, named control (Ctr)) or e-cigarette condensate dilutions (1:150, 1:100, 1:75, 1:50, 1:25) and the viability of the cells was determined each day as the number of cells with a visible nucleus (number of live cells). The data are shown as jitter-plots (mean ± SD, n = 3-6). (**C**) Cell death (lactate dehydrogenase)

assay was performed on the collected cell medium of e-cigarette condensate exposed cells after the three-day exposure. The data are shown as jitter-plots (mean ± SD, n = 3). Significance is indicated as *, **, ***, and **** when $p < 0.05$, $p < 0.01$, $p < 0.001$ and $p < 0.0001$ respectively.

3.2.2. Effects of acrolein and e-cigarette condensate on RAW 264.7 macrophages

Cell viability of RAW 264.7 macrophages was assessed using a haemocytometer after the third exposure day. Macrophages were treated with acrolein what caused concentration-dependent loss of viability (**Figure 30** A). Highest concentration of acrolein used was too detrimental to cells, so they could not be used in further experiments. After the 3-day exposure, stimulation of oxidative burst was performed in the presence of zymosan A and kinetic traces show an increase in macrophage-derived ROS formation, likely measured in extracellular compartment by the assay (**Figure 30** B). Comparison at the 35-minute mark, which is a time point when kinetic traces reach plateau, shows statistically significant increase in the oxidative burst in the cells treated with 0.33, 3.3 and 10 µM acrolein compared to the control.

After the treatment with e-cigarette vapour condensate, RAW 264.7 macrophages showed also concentration-dependent loss of viability (**Figure 30** C). Cells treated with highest concentration of e-cigarette vapour condensate used (1:25) were affected too much to be able to give any result in further experiments so they were not used. Stimulation of oxidative burst was also performed after 3-day exposure and kinetic traces showed an increase in extracellular ROS formation in treated cells (**Figure 30** D). Comparison at the 60-minute mark (which is the time point when kinetic traces hit the highest point, as no plateau was observed this time) showed no statistically significant increase in the oxidative burst in the treated cells compared to control, but a clear trend.

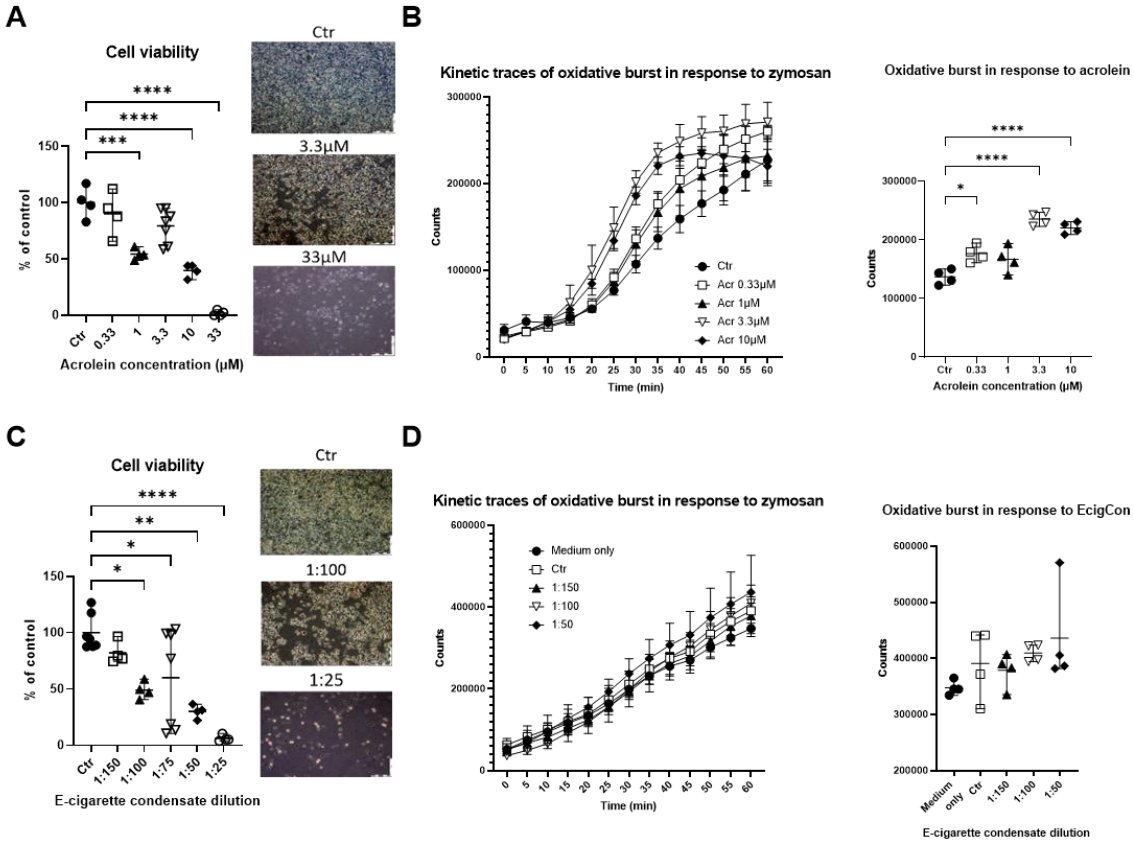

Figure 30. Effects of acrolein and e-cigarette condensate on RAW 264.7 cells. (A) The cells were incubated for three days with solvent only (1 % DMSO, named control (Ctr)) or different concentrations of acrolein in DMSO (0.33, 1, 3.3, 10, 33 µM) and the viability of the cells was determined each day. The data are shown as a bar graph (mean ± SD, n = 4). (B) After 3-day acrolein-exposure, oxidative burst was measured in whole cells after stimulation with zymosan A and shown as kinetic traces (XY graph, mean ± SD, n = 4 pooled samples) and as jitter-plots (mean ± SD, n = 4 pooled samples) at the time point when traces hit a plateau (35 min). (C) The cells were incubated for three days with solvent only (1 % DMSO, named control (Ctr)) or e-cigarette condensate (1:150, 1:100, 1:75, 1:50, 1:25) and the viability of the cells was determined each day. The data are shown as jitter-plots (mean ± SD, n = 4). (D) After 3-day acrolein-exposure, oxidative burst was measured in whole cells and shown as kinetic traces (XY graph, mean ± SD, n = 4 pooled samples) and as jitter-plots (mean ± SD, n = 4 pooled samples) at the last time point (60 min) (mean ± SD, n = 4). This time no plateau was observed. Significance is indicated as *, **, ***, and **** when $p < 0.05$, $p < 0.01$, $p < 0.001$ and $p < 0.0001$ respectively.

3.2.3. Effects of acrolein on intracellular ROS formation and NADPH oxidase complex

Intracellular ROS formation was determined using DHE staining of the cells. EA.hy cells treated with acrolein showed a trend-like increase in total ROS formation after staining with DHE, with the increase becoming significant in 1 µM, 3.3 µM and 10 µM groups (**Figure 31** A). RAW 264.7 macrophages showed an increase in total ROS formation after staining with DHE only in the 10 µM group (**Figure 31** B). Trend-like increase in the concentration of Rac1 protein in the membrane fraction of EA.hy cells, that became statistically significant in the 10 µM group, indicates activation of NADPH-oxidase complex (**Figure 31** C). Similar results were observed with the concentration of Rac1 protein in the membrane fraction of RAW macrophages. The data showed the same trend, reaching significance in the 10 µM exposure group (**Figure 31** D).

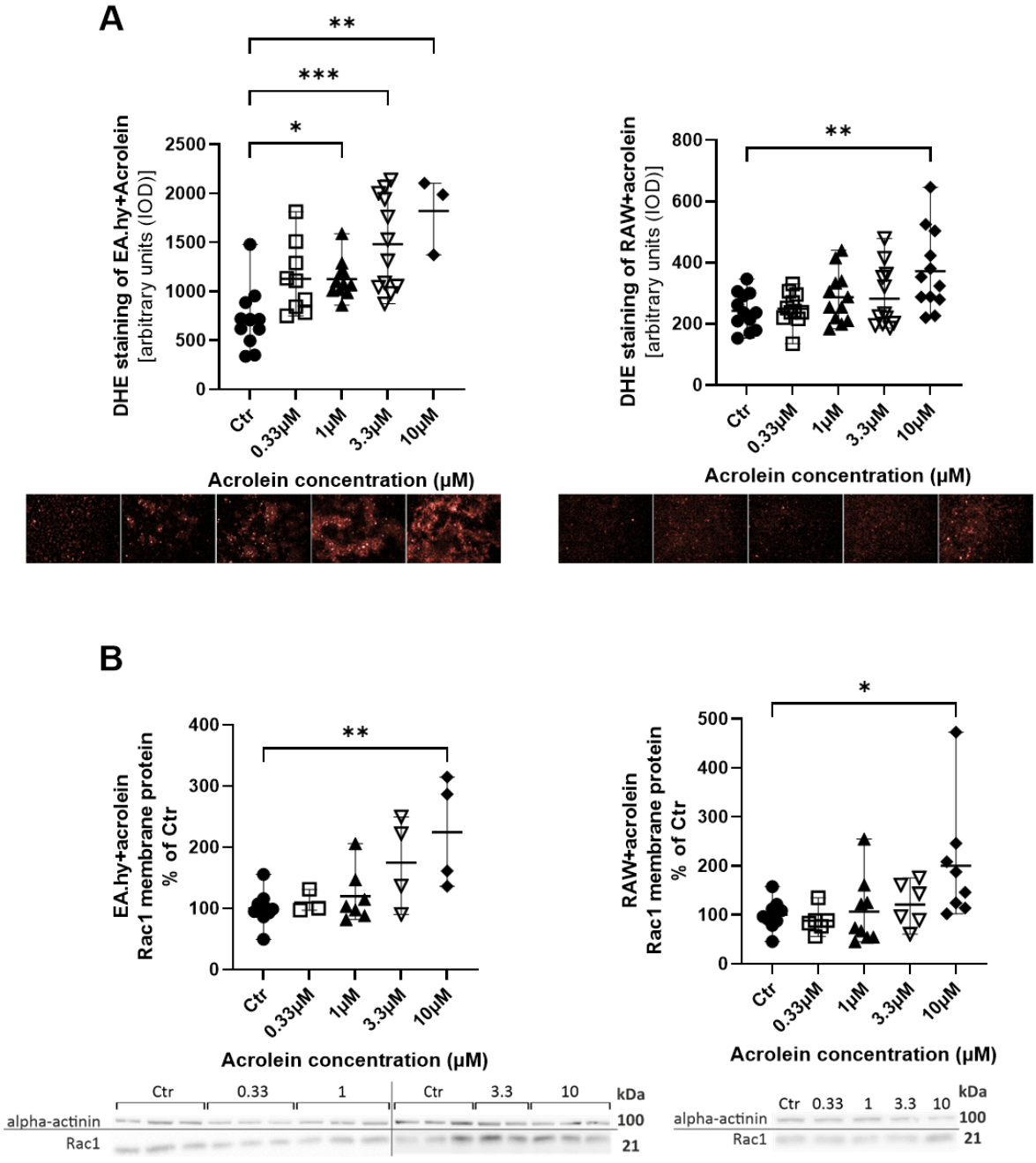

Figure 31. Effects of acrolein on intracellular ROS formation and membrane Rac1 protein content in EA.hy 926 cells and RAW 264.7 macrophages. (A) Cells were stained with dihydroethidium (DHE) whose degradation into its oxidation products (2-hydroxyethidium (2-HE, superoxide specific) and ethidium (E+, unspecific)) shows fluorescence. This fluorescence was then recorded under a fluorescent microscope (Exc. 510-520 nm/Ems. 580-610 nm) and the intensity was quantified and is shown in the graph as integrated optical density (IOD, arbitrary units, as mean ± SD). Representative images are presented in order of the increased concentrations underneath the DHE staining quantification**.** (B) Rac1 protein content in membrane fraction of the cells, after the incubation with acrolein. Original blots are presented in order underneath the densitometric quantification. Data are presented as jitter-plots as

percentage of control (mean ± SD, n = 3-12). Significance is indicated as *, ** and *** when $p < 0.05$, $p < 0.01$ and $p < 0.001$ respectively.

3.2.4. Effects of acrolein on extracellular ROS formation

Extracellular ROS formation is shown as an increase in formation of oxidation products of DHE, 2-HE and E+. The concentrations of oxidation products were measured by HPLC with fluorescence-based detection in the control group and the 33 µM acrolein-group. RAW cells showed an increase in extracellular ROS formation, however, the same result was absent in the EA.hy cells (**Figure 32** A and B). As a complementary assay, DLD1-HO1-prom cell line was treated with acrolein for 3 days and the results showed statistically significant increase in luciferase-dependent chemiluminescence light emission, as a read-out of heme-oxygenase-1 induction, when treated with 10 µM and 33 µM acrolein (**Figure 32** C). This result points to the activation of Nrf2-pathway, a significant part of a cells antioxidative defence.

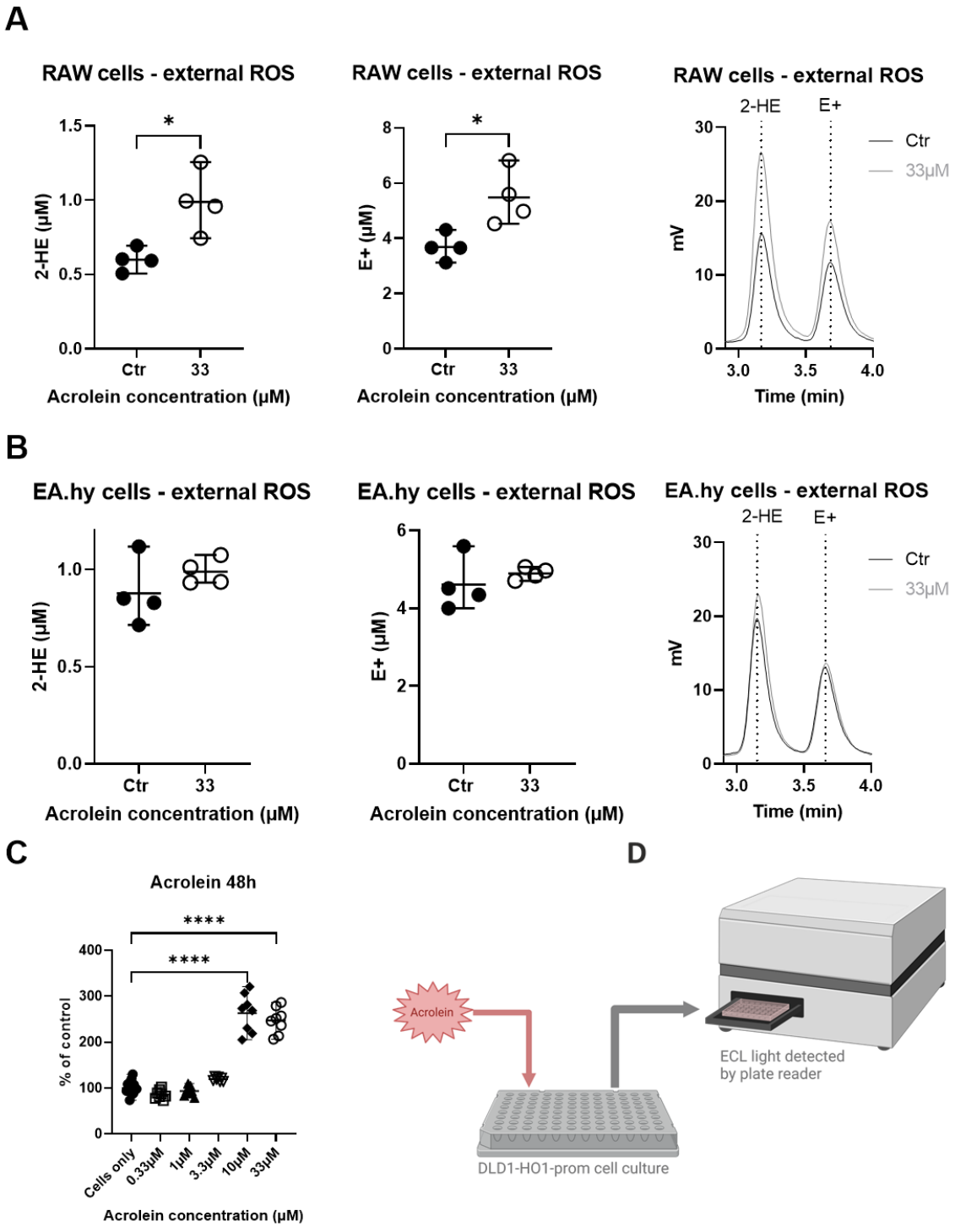

Figure 32. Effects of acrolein on extracellular ROS formation in RAW 264.7 and EA.hy 926 cells. After incubation with DHE, its oxidation products 2-HE and E+ were separated by HPLC in the cell culture medium. Concentrations of oxidation products of RAW (A) and EA.hy (B) cells are shown with the representative chromatograms. Data are shown as bar graphs (mean ± SD, n = 4). (C) Evaluation of Nrf2 activation in acrolein treated DLD1-HO1-prom cells luciferase assay was measured as chemiluminescence read-out. Data are shown as percentage

of control as jitter-plots (mean ± SD, n = 8-16). Significance is indicated as * and **** when $p < 0.05$ and $p < 0.0001$ respectively.

3.3. Effects of shisha smoking on cardiovascular system

3.3.1. Carbon monoxide exposure from shisha

Carbon monoxide is produced by burning of shisha tobacco, as well as burning of coal pieces while heating the tobacco. Carbon monoxide levels were measured in the smoke coming directly from the shisha mouthpiece. The amount of carbon monoxide in the shisha smoke is directly correlated to the number of coal pieces used to heat shisha tobacco (**Figure 33** A). Removing coal as a heater, by using electrical heater for the shisha tobacco, significantly reduces the amount of carbon monoxide produced, however, it does not remove carbon monoxide from the air completely (**Figure 33** A). For all further experiments, one piece of coal was used to heat the shisha tobacco, as the smoke produced by electrically heated shisha was uneven. Carbon monoxide levels in blood were tested as the levels of carboxyhaemoglobin in whole blood samples of 3-day shisha-exposed mice via UV-Vis spectrophotometry. Carboxyhaemoglobin levels in mice exposed to shisha heated with one piece of coal were significantly higher that carboxyhaemoglobin levels in control mice (**Figure 33** B).

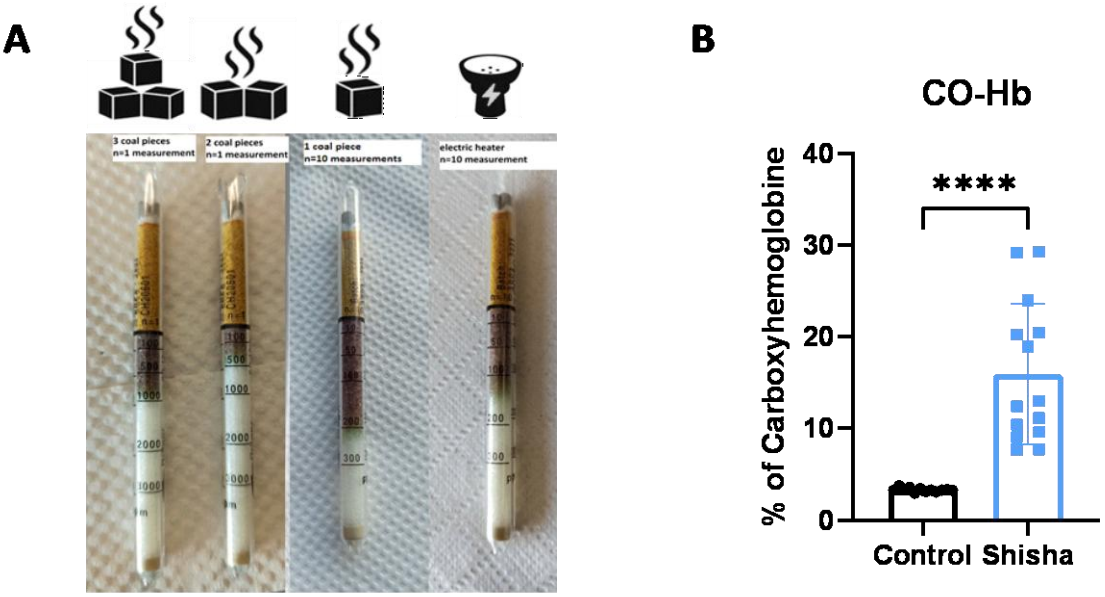

Figure 33. Carbon monoxide levels in shisha smoke. (A) The amount of carbon monoxide in shisha smoke (dark brown colour) depends on the number of coal pieces used to heat the shisha tobacco. (B) Carboxyhaemoglobin (CO-Hb) was determined from the peripheral blood.

Data are shown as jitter-plots (mean ± SD, n = 12-14). Significance is indicated as **** when $p < 0.0001$.

3.3.2. Effects of shisha on cardiovascular system and ROS production

Systolic blood pressure was measured via tail-cuff method and no significant difference was observed (**Figure 34** A). Oxidative stress in aortic rings was determined via lucigenin-enhanced chemiluminescence. Again, no significant difference was observed after 3-day shisha exposure (**Figure 34** B). Stimulation of oxidative burst in whole blood showed statistically significant difference at the 35-minute mark for zymosan-stimulated samples, whereas at the 20-minute mark for PDBu-stimulated samples the difference was not statistically significant (**Figure 34** C). Vascular function was assessed using isometric tension method. Here, both endothelium-dependent and endothelium-independent relaxation curves were dose dependently shifted to the right with several statistically significant points (**Figure 34**D).

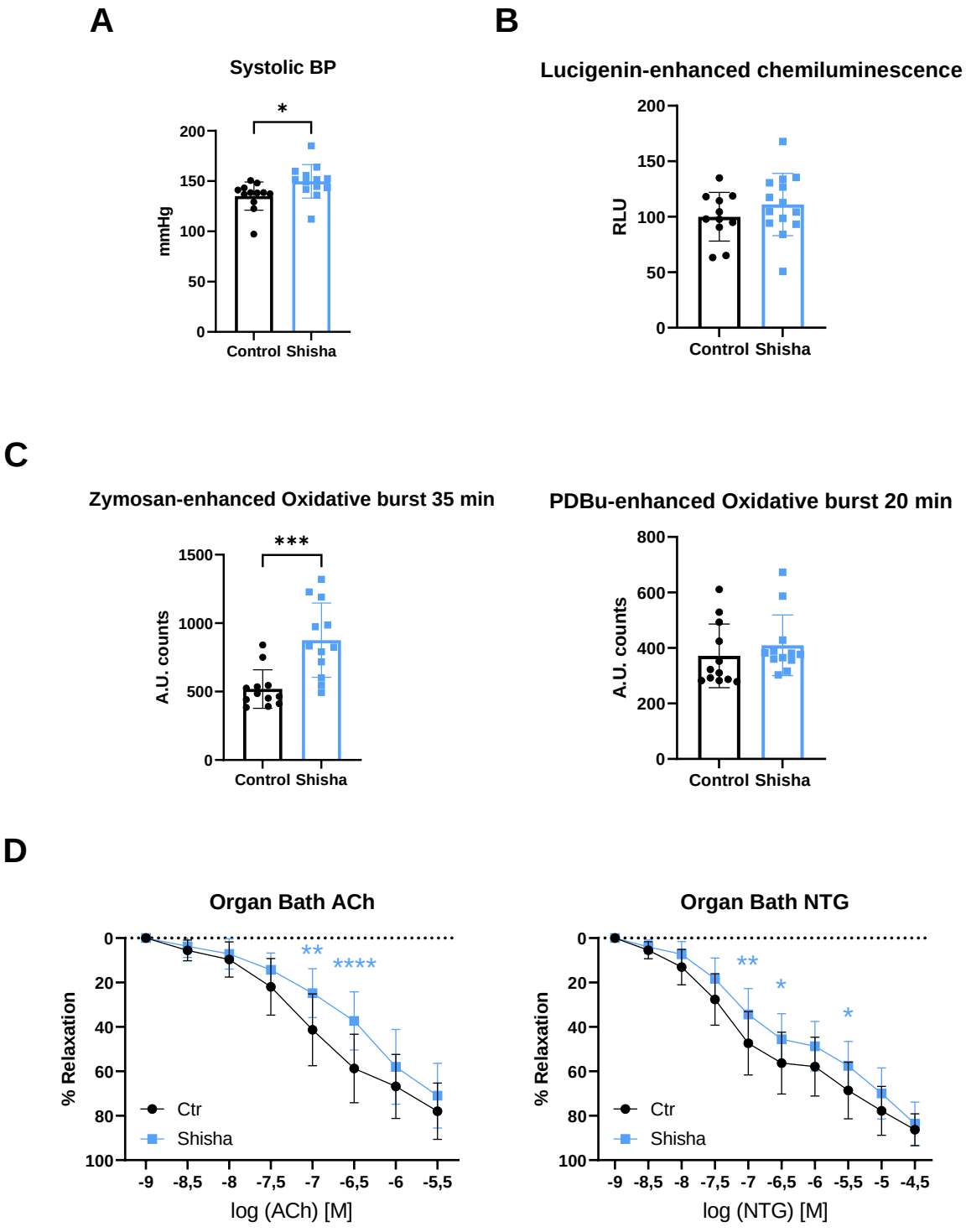

Figure 34. Effects of shisha smoke on cardiovascular system. (A) Blood pressure was measured via tail-cuff method after 3-day shisha exposure (jitter-plot, mean ± SD, n = 24). (B) Lucigenin-enhanced chemiluminescence was measured in aortic rings after 3-day shisha exposure. It is defined as percentage of control (jitter-plot, mean ± SD, n = 16-19). (C) Oxidative burst is determined in whole blood samples and the results are shown at the time points kinetic curves reach plateau (35-minute mark for zymosan-treated samples and 20-minute

mark for PDBu-treated samples; jitter-plots, mean ± SD, n = 12). (D) Endothelial function test is expressed as percentage of relaxation of the aortic rings using acetylcholine as endothelium-dependent vasodilator and nitro-glycerine as endothelium-independent vasodilator (XY graph, mean ± SD, n = 12-18). Significance is indicated as *, **, *** and **** when $p < 0.05$, $p < 0.01$, $p < 0.001$ and $p < 0.0001$ respectively.

3.3.3. Effects of shisha on relative expression of stress-related targets in heart, lung, brain and aorta

Oxidative stress in cortex, heart, lung aorta and blood plasma was determined by qRT-rtPCR, western blot, dot blot and DHE staining. Relative expression of mRNA that code NAD(P)H dehydrogenase quinone 1 (Nqo-1), glutathione peroxidase 1 (Gpx-1), thioredoxin-reductase 1 (Txnrd-1), peroxiredoxin-5 (Prdx-5), glutamate-cysteine ligase catalytic subunit (Gclc), monocyte chemoattractant protein 1 (Ccl-2), heme-oxygenase-1 (Hmox), Nitric Oxide Synthase 3 (Nos3), interleukin-1ß (IL-1ß), interleukin 6 (IL-6), NOX2, CD68, VCAM, cyclooxygenase 2 (COX-2), neuronal NOS (nNOS) and NOX1 proteins were measured in cortex. All of the results remained unchanged in shisha-exposed mice (**Figure 35**).

Relative expression of mRNA that code Nqo-1, Gpx-1, HO-1, NOX2, CD68, VCAM and NOX1 were measured in hearts of mice. Most of the results were significantly higher (Nqo-1, HO-1, NOX2, CD68 and VCAM) in shisha-exposed mice with the exception of NOX1 and Gpx-1 (**Figure 36** A). Relative expression of mRNA that code Gpx-1 and IL-1β were measured in lung and both were significantly higher in shisha-exposed mice than in controls (**Figure 36** B).

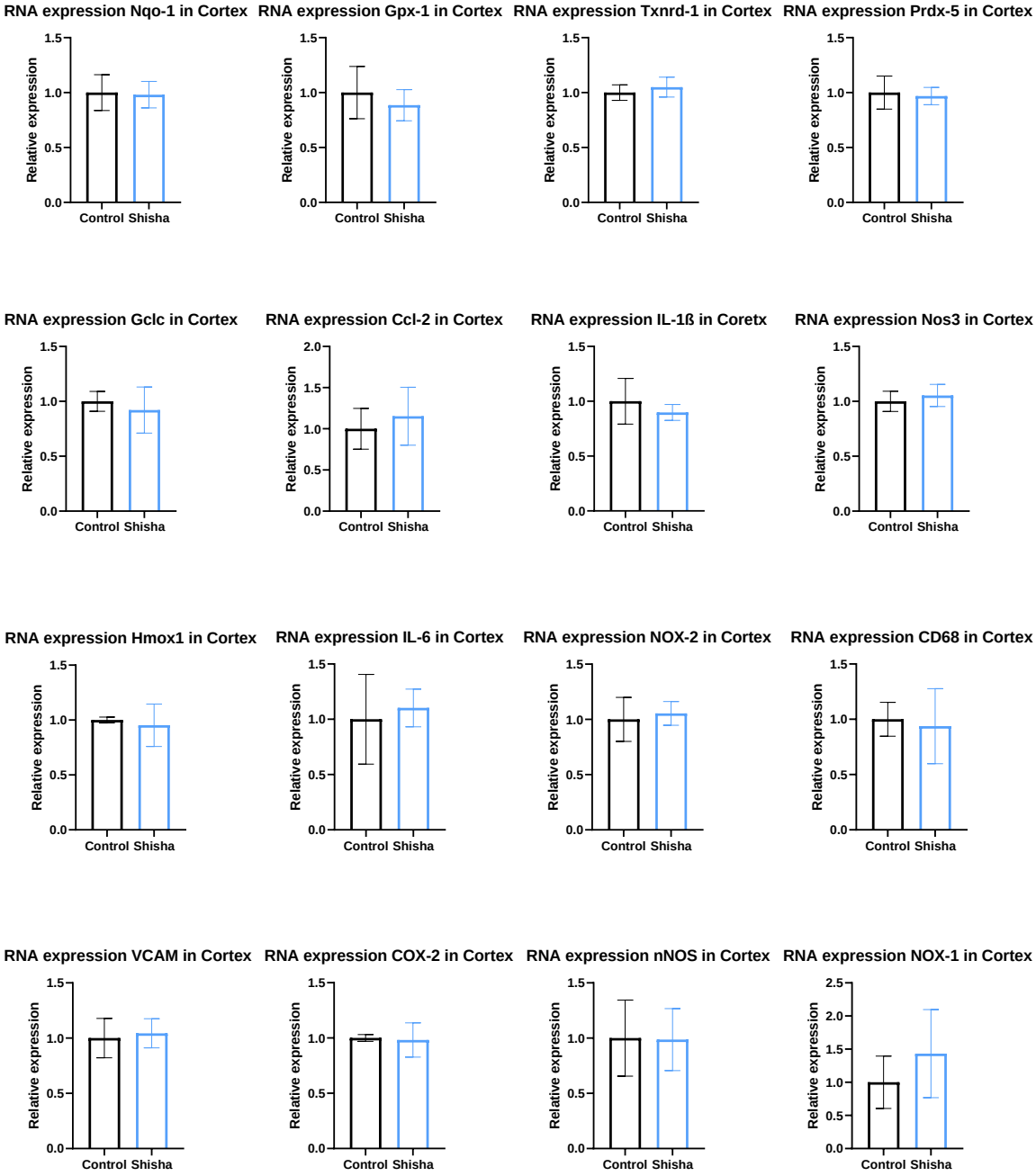

Figure 35. Effects of shisha on relative expression of RNAs that code stress-related proteins in cortex. Relative expression of mRNA in cortex was determined by qRT-rtPCR. NAD(P)H dehydrogenase quinone 1 (Nqo-1), glutathione peroxidase 1 (Gpx-1), thioredoxin-reductase 1 (Txnrd-1), peroxiredoxin-5 (Prdx-5), glutamate-cysteine ligase catalytic subunit (Gclc), monocyte chemoattractant protein 1 (Ccl-2), interleukin-1ß (IL-1ß), nitric oxide synthase 3 (Nos3), heme-oxygenase-1 (Hmox), interleukin 6 (IL-6), NADPH oxidase subunits NOX2 and NOX1, CD68, vascular cell adhesion molecule (VCAM), cyclooxygenase 2 (COX-2) and neuronal NOS (nNOS). The data are shown as bar graphs (mean ± SD, n = 3-6).

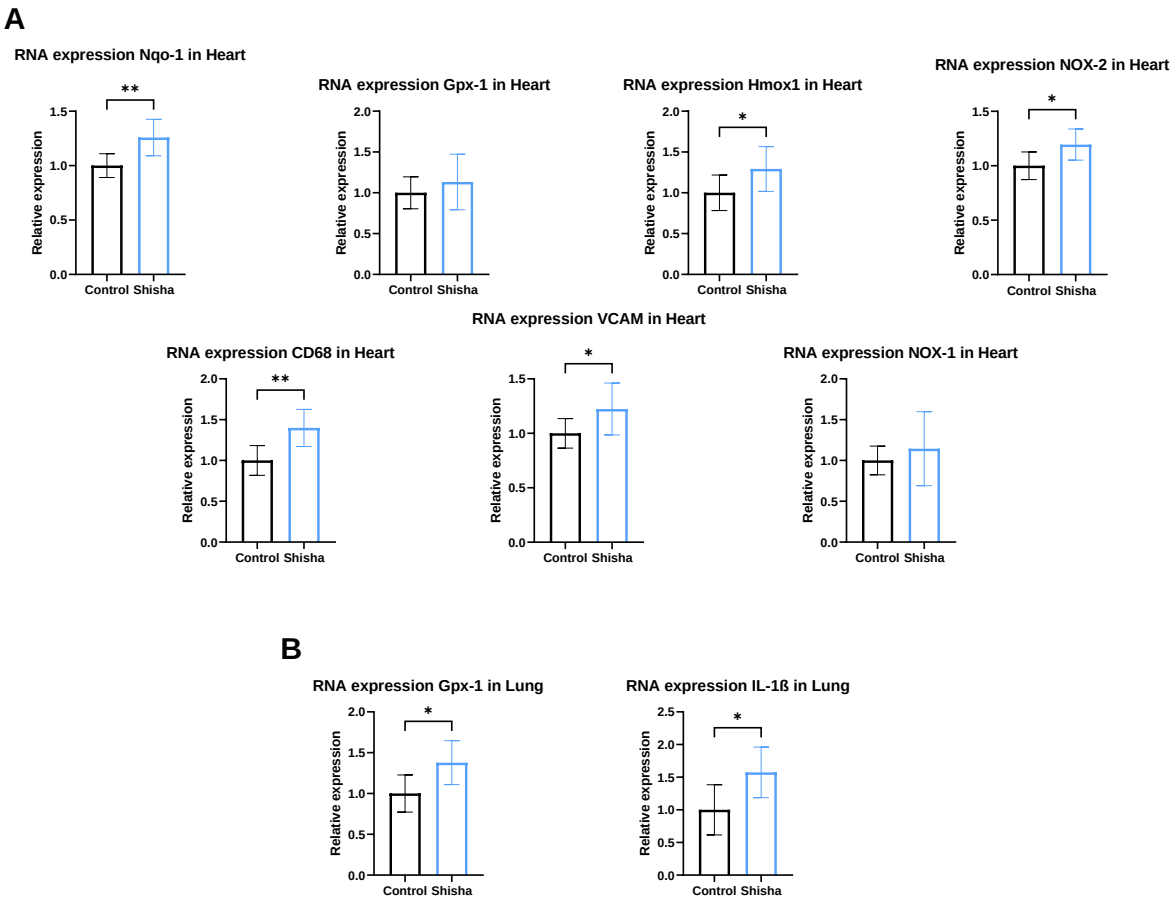

Figure 36. Effects of shisha on relative expression of RNAs that code stress-related proteins in heart and lung. Relative expression of RNAs in heart and lung tissues was determined by qRT-rtPCR. The data are shown as bar graphs (mean ± SD, n = 3-6). Significance is indicated as * and ** when $p < 0.05$ and $p < 0.01$ respectively.

Relative expression of VCAM, GCLC, eNOS, NOX2, HO-1, MCP-1 and COX2 proteins was measured in heart using western blot (**Figure 37** A). Only relative expression of MCP-1 was significantly higher in shisha-exposed mice. Relative expression of GCLC, eNOS, NOX2, HO-1 and MCP-1 proteins was measured in aorta by western blot (**Figure 37** B). Relative expression of MCP-1 again showed statistical significance in shisha-exposed mice.

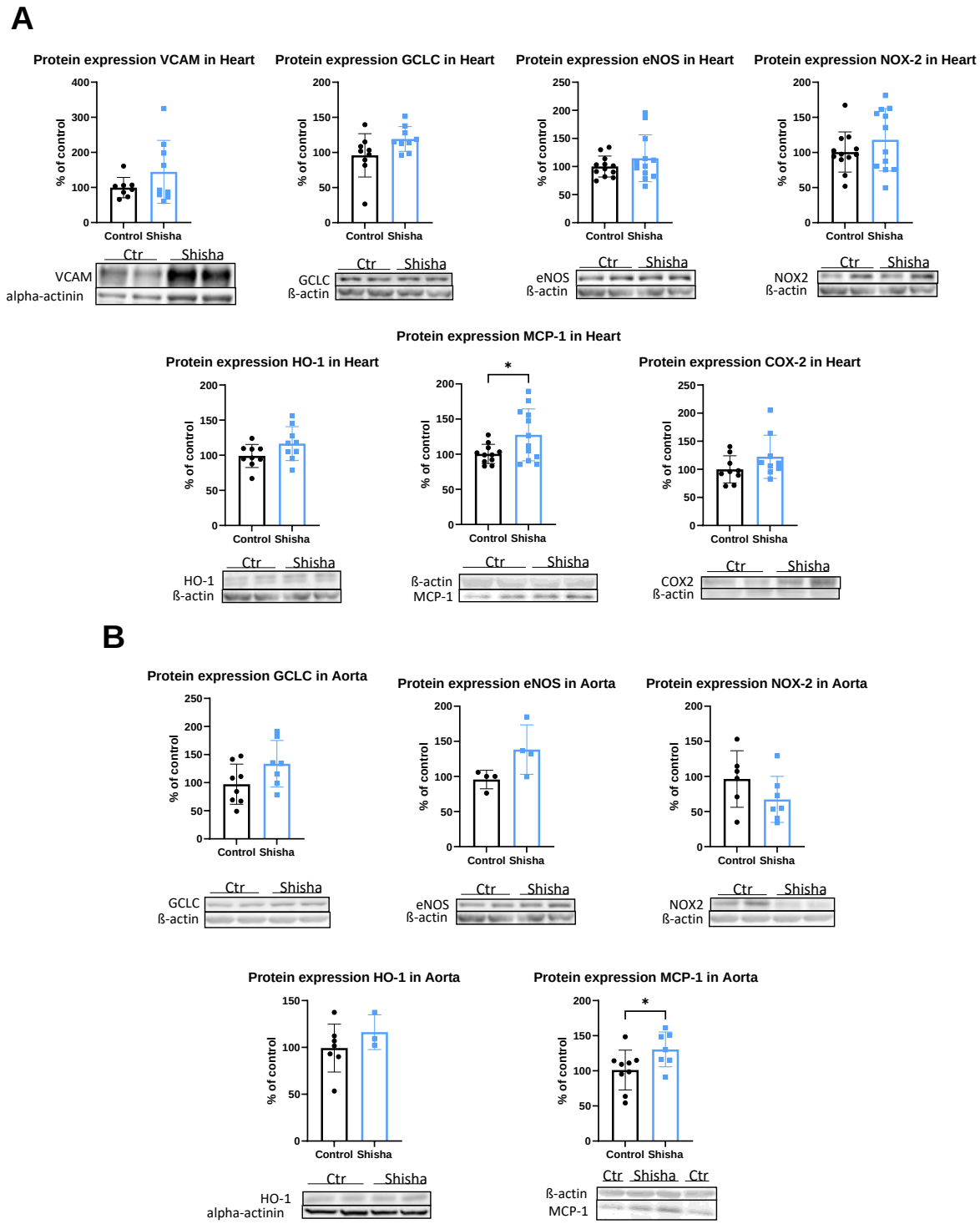

Figure 37. Effects of shisha on relative expressions of stress-related proteins. Relative expression of proteins in heart (A) and aorta (B) was determined by western blot. The data are shown as jitter-plots (mean ± SD, n = 3-12). Significance is indicated as * when $p < 0.05$.

Relative expression of stress-related markers 3-NT-positive proteins and IL-6 was measured in heart, lung and plasma of shisha-exposed mice using dot blot technique. 3-NT-poitive proteins in hearts of shisha-exposed mice did not change compared to control mice. On the other hand, IL-6 levels in hearts and lung of shisha-exposed mice were significantly higher. In blood plasma 3-NT positive proteins were increased only by trend (Figure 37).

Total ROS formation was determined by staining cortex, lung, aorta and heart tissue with DHE. Fluorescence of oxidation products 2-HE and E+ was evaluated under fluorescent microscope, and cortex and lung tissue showed a significant increase in ROS formation, whereas aortic and heart tissue showed trend-like increase in ROS formation, but it was not statistically different (**Figure 39**).

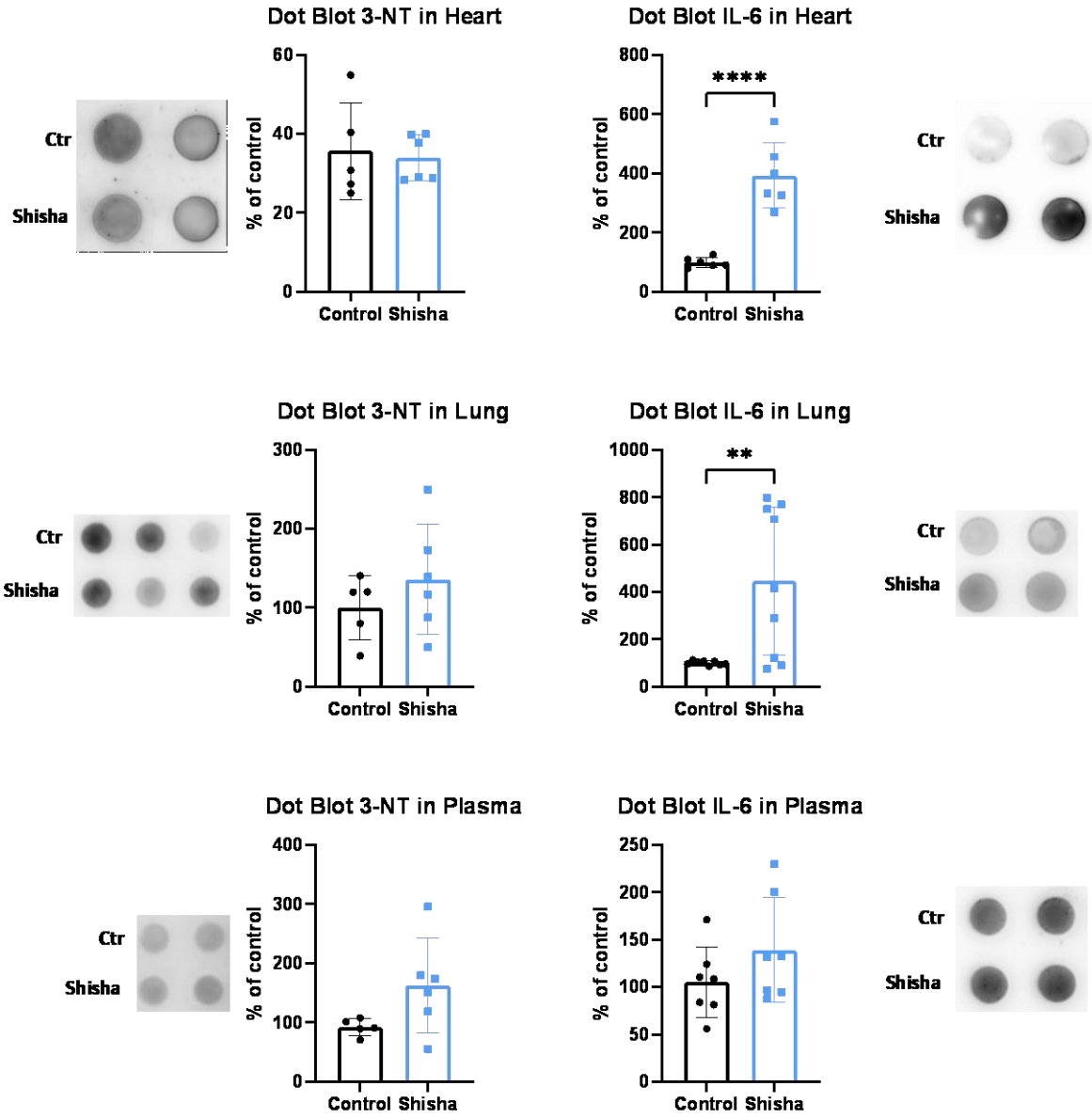

Figure 38. Effects of shisha on relative expressions of oxidative stress markers in heart and lung tissues and plasma. Relative expression of 3-NT and IL-6 proteins in hearts, lungs and plasma of mice was assessed by dot blot. The data are shown as jitter-plots (mean ± SD, n = 3-10). Significance is indicated as **, and **** when $p < 0.01$ and $p < 0.0001$ respectively.

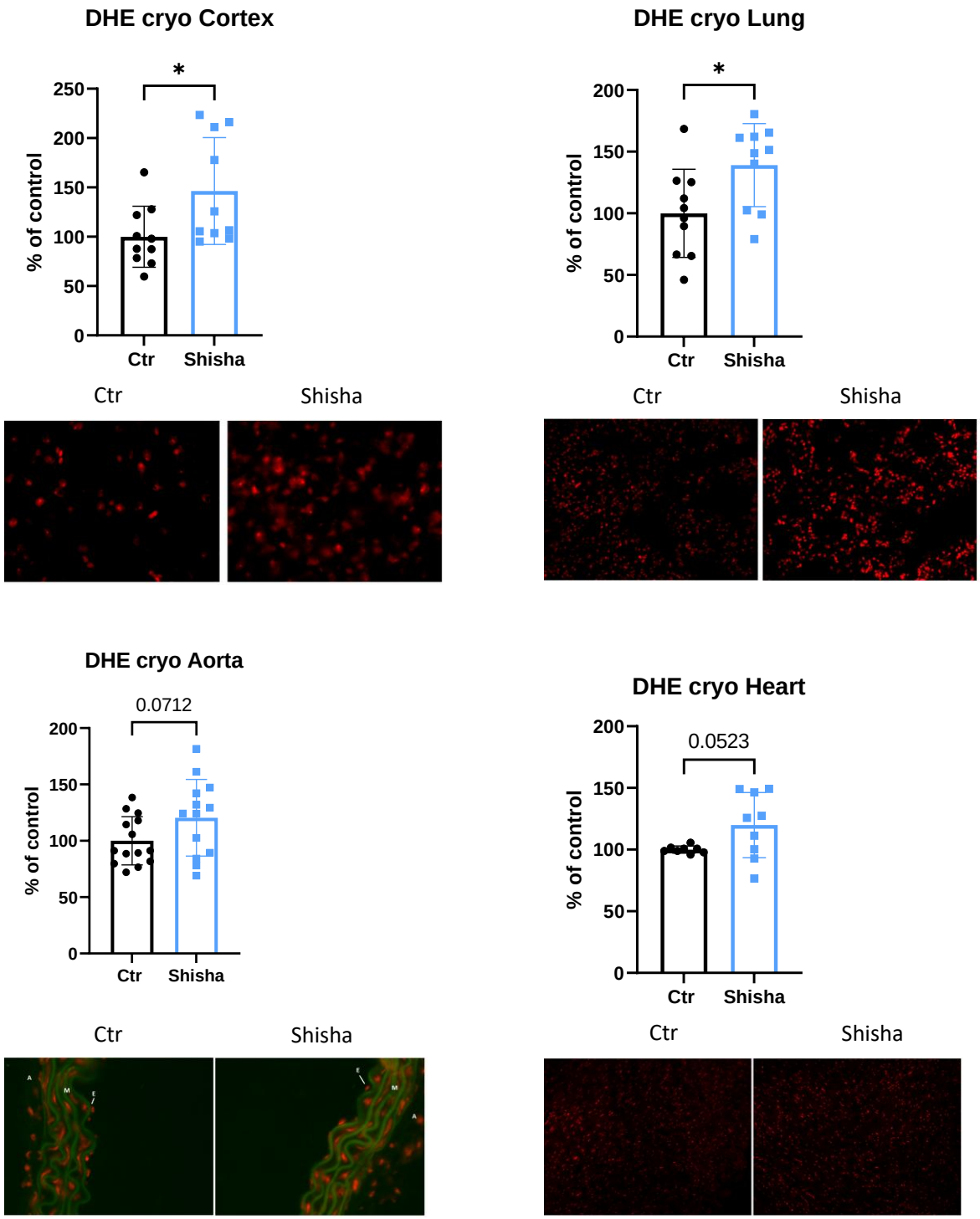

Figure 39. Effects of shisha on ROS formation in cortex, lung, aortic and heart tissues. ROS formation in cortex, lung, aorta and heart was evaluated using DHE staining. Representative fluorescence images are shown below the quantifications. The data are shown as jitter plots (mean ± SD, n = 3-10). Significance is indicated as * when $p < 0.05$.

3.3.4. Effects of particulate matter on Nrf2 induction in DLD1-HO1-promotor cells

DLD1-HO1-prom cell line was treated with particulate matter for 48 hours and the results showed trend-like increase in luciferase-dependent chemiluminescence light emission, as a read-out of heme-oxygenase-1 induction, that became statistically significant when treated with 22, 66 and 200 µg/mL particulate matter (**Figure 40** A). When we treated the same cells with highest concentration of particulate matter (200 µg/mL) and one of the Nrf2 inhibitors (ML385 or AEM1), chemiluminescence subsided significantly (**Figure 40** B).

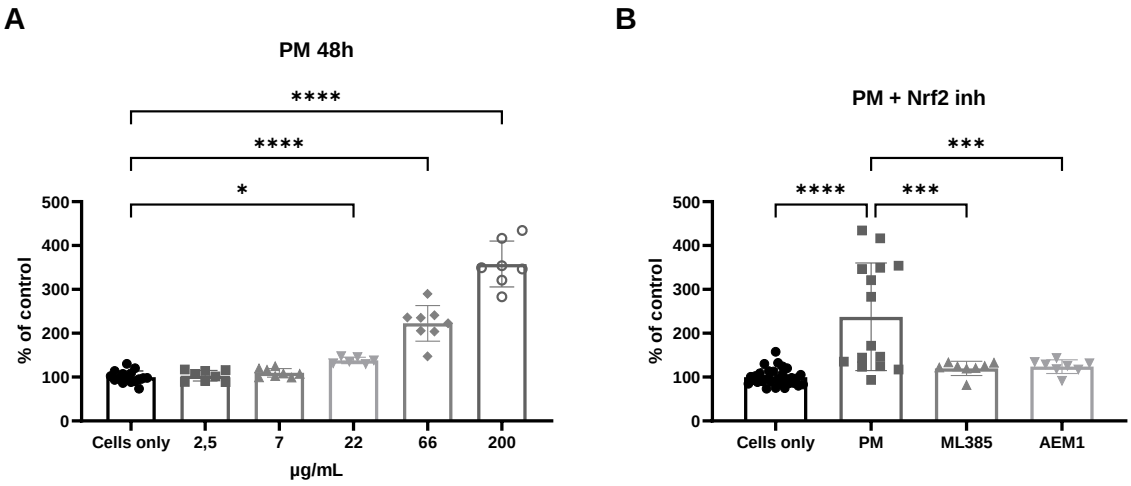

Figure 40. **Effects of particulate matter (NIST SRM1648a) on DLD1-HO1-prom cells.** Activation of Nrf2-pathway was tested using luciferase-dependent chemiluminescence light emission of the DLD1-HO1-prom cell line. (A) Chemiluminescence emitted when cells are treated with particulate matter (PM). (B) Chemiluminescence when cells are treated with both particulate matter and one of the Nrf2-inhibitors, ML385 or AEM1. The data are shown as jitter-plots (mean ± SD, n = 7-15). Significance is indicated as *, *** and **** when $p < 0.05$, $p < 0.001$ and $p < 0.0001$ respectively.

4. Discussion

The principal aim of my thesis was to determine the molecular mechanisms behind the cardiovascular effects that are caused by behavioural and environmental risk factors. The thesis focuses on three different environmental and behavioural factors with increasing prevalence in today's world (noise, e-cigarettes and shisha) in three separate studies. The first study focused on the role of noise on behavioural and neuronal changes in mice, as well as protective effects of cardiovascular and neuroactive medicines. Second study focused on molecular mechanisms behind e-cigarette-induced vascular oxidative stress, namely activation of NADPH-oxidase complex and counter-regulatory activation of the Nrf2-signaling pathway. Third study was a pilot study on cardiovascular effects of shisha exposure of mice, with specific focus on oxidative stress and inflammation markers in cardiac, vascular, neuronal and lung tissue.

4.1. Noise

Noise was firstly labelled as a "public health hazard" by American Speech and Hearing Association in 1970 [210]. It is now a known risk factor for multiple cardiovascular and metabolic diseases, recognised by both World Health Organisation (WHO) [7] and European Environment Agency [211]. Environmental noise has previously been associated with cardiovascular diseases in multiple studies [32, 77, 79, 80, 212-214]. Road traffic noise was strongly correlated with ischemic heart disease in a 2018 systematic review and guideline paper by van Kempen et al, where every 10 dB increase in noise exposure showed the relative risk of 1.08 for ischemic heart disease [7]. Proposed mechanisms behind the adverse effects of noise are noise-induced psychological stress [74-76], sleep disturbance [13, 14], oxidative stress [76, 80, 97, 105, 163] and inflammation [80, 97]. However, not all noise is considered similarly harmful. WHO reports focus on both daytime and night-time noise exposure, whereas night-time noise exposure is the one primarily connected with the onset of cardiovascular diseases [215]. Additionally, even different types of noise are perceived differently at the same noise levels - aircraft noise was perceived as more annoying than road traffic or rail traffic noise [216]. Noise exposure system used in our lab is a 24-hour (whole-day) aircraft noise-exposure system with an intermittent exposure protocol, with an average sound pressure level of 72 dB and peak noise levels of 85 dB. This level of noise is still

considered as a “no risk for hearing damage” level by WHO, but that it “may cause sleep disturbance” during a night-time exposure [217].

Aircraft noise is a long studied environmental risk factor in my group, with a very well established exposure model for mice. Noise effects on oxidative stress and inflammation markers were previously tested previously, however, the effects on mice behaviour and the potentially beneficial effects of neuroactive drugs were not addressed so far. Here, we tested the effects of both short-term (4 days) and long-term (28 days) noise exposure on behaviour of mice in addition to some metabolic and cardiovascular effects, as well as protective effects of citalopram (selective serotonin reuptake inhibitor), diazepam (sedative benzodiazepine), propranolol (beta-blocker) and phenoxybenzamine (alpha-blocker).

In the present study, mice were exposed to aircraft noise for either 4 days or 28 days, and both exposures showed a significant increase in blood pressure (**Figure 17** A and B), with the significance remaining for the full 28-days of noise exposure. Traffic noise has been connected to the primary hypertension multiple times before, [218, 219] with the most recently reported relative risk of 1.018 per every 10 dB of increased sound pressure levels [218].

Aside from cardiovascular clinical parameters, metabolic clinical parameters glycosylated haemoglobin (HbA1C) and body weight were tested in 28-day noise-exposed mice. Blood glucose levels were previously tested in short-term noise exposure [220], as well as glucose tolerance and insulin resistance in both short-term and long-term noise exposure [221, 222] and it was found that noise might disturb glucose metabolism during short-term noise exposure. The effects were specifically attributed to oxidative stress and inflammation [221]. However, in the present study, reduced glycosylated haemoglobin levels were observed in mice after long-term noise-exposure (**Figure 17** E).

Adverse cardiovascular and metabolic effects of noise are mostly related to increased oxidative stress and inflammation [214, 221]. Multiple oxidative stress and inflammation markers were tested in the present study, and most of them were elevated by trend, while HO-1 levels in aorta were significantly higher in noise-exposed groups (**Figure 18**). Higher levels of 8-OHG are present after ROS-mediated damage of DNA, and they are specifically connected to the cardiovascular diseases [223].

Mouse behaviour after long-term noise exposure was also tested before, however, it was, so far, connected only to the anxiety-like behaviour [224-226] and impaired cognitive function [227]. Present results show no difference in behaviour of mice after short-term noise exposure

(**Figures 19-22**). Long-term (28 days) noise-exposure lead to mice hyperactivity (defined by significant increase in the distance travelled and time spent in the centre of the open-field test (**Figure 23**), significant increase in distance travelled in the social interaction test (**Figure 25**) and significant increase in total amount of entries into the arms of the Y-maze test (**Figure 26**)), social withdrawal (defined by significant decrease in the social interaction index (**Figure 25**)) and working memory deficit (defined by significant decrease in percentage of correct entries of the arms of Y-maze (**Figure 26**). Noise was previously connected to the reduced memory and cognitive abilities in children [228-230] and learning abilities in mice [231] , similarly to the results presented here. Hyperactivity, memory impairment and reduced social activity are symptoms connected to the schizophrenia-like behaviour in mice [232]. Similarly, one spatial study connected closeness to the traffic noise to the onset of schizophrenia-like symptoms [233], while other pointed to the worsening of the working memory in both healthy subjects and schizophrenia patients [234]. Taken together, these results may point to the onset of schizophrenia-like symptoms in mice when exposed to noise. Present long-term noise exposure results so far do not point to the anxiety-like behaviour observed previously (defined by light-dark test, **Figure 24**).

As hypertension was demonstrated in short-term noise-exposed mice both in this study and other studies before [80, 163, 214, 218], antihypertensive treatments were tested for their potential protective effects on cardiovascular system. Propranolol, widely used beta-blocker, and phenoxybenzamine, alpha-blocker used in treatment of paroxysmal hypertension were used. Antihypertensive treatments did not show improvement in blood pressure measurements (**Figure 27**A). These two treatments exert their effects through reducing the activation of sympathetic nervous system [235], which is only one of the mechanisms involved in noise-induced hypertension, as discussed before. Reducing the activity of sympathetic nervous system did not, however, reduce blood pressure back to normal, as other mechanisms involved were probably still active enough to mask the effects of antihypertensive medications. Propranolol has immediate effects on cardiac output and heart rate, however, it takes some time (7-10 days) to display full effect on blood pressure [236, 237], so the results presented here should be analysed with the time-course in mind. Two neuroactive treatments, diazepam, a benzodiazepine hypnotic, and citalopram, a selective serotonin reuptake inhibitor, were also tested. Those two treatments reverted systolic blood pressure to normal (**Figure 28** A). Hypertension was previously connected to the sleep

disturbance [238], so the improvement of the blood pressure levels may be attributed to the hypnotic effect of diazepam [239, 240], as well as citalopram in mice [241, 242]. Interestingly, all of the treatments showed an improvement of endothelial-dependent relaxation curve, pointing to the protective effects of antihypertensive and neuroactive treatments on the vascular function (**Figure 27** C and 28 C). This is in line with the fast onset of protective effects of propranolol on endothelial function [243] even though the blood pressure was not significantly changed. Overall mechanisms and pathways are shown in **Figure 41**.

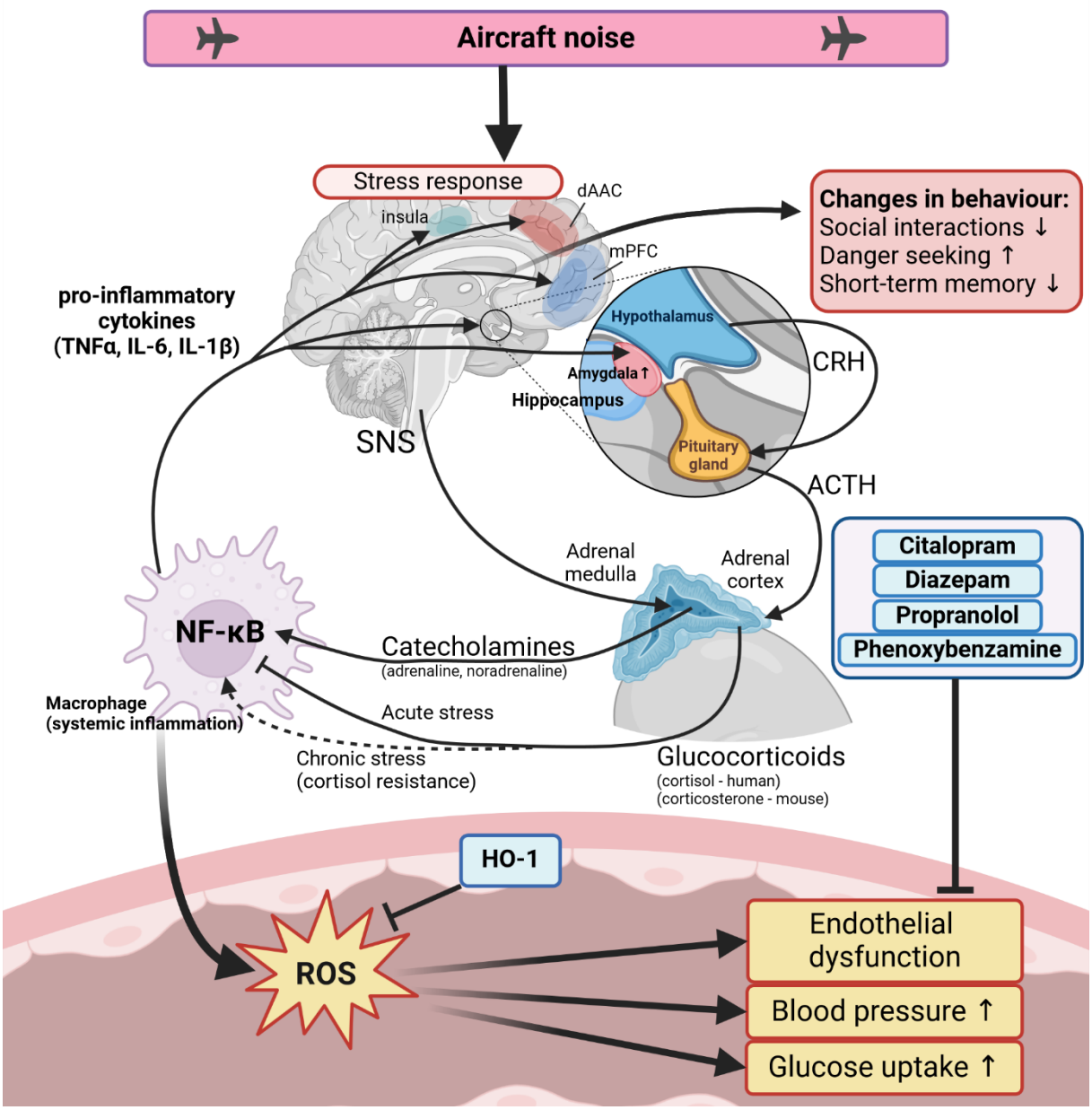

Figure 41. Effects of aircraft noise on the stress response pathway and vascular inflammation and oxidative stress. Aircraft noise exposure altered the behaviour of mice resulting in lower social interaction and impaired short-term memory. Pharmacological treatments with diazepam, citalopram, propranolol and phenoxybenzamine improved endothelial function of noise-exposed mice, whereas blood pressure, protein expression and

oxidative stress parameters were improved to a different extend by the various drugs. Figure created with BioRender.com

4.2. E-cigarettes

As one of the most debated topics of this generation, smoking of e-cigarettes or "vaping" pervades the public discourse since the devices first hit the mass market in the early 21st century. e-cigarettes as a research topic showed sudden increase in popularity after 2015, when the devices started being marketed as a smoking-cessation device, with most of the research being highly oriented towards this outcome [244]. When used as a smoking-cessation device in comparison to other nicotine-replacement therapy, e-cigarettes proved to be more efficient. However, the improvement reported was short-term (after one year), with no follow-up [38]. Second focus of research seems to be adolescent usage of e-cigarettes, with specific orientation toward short-term negative effects on respiratory system, largely because of misuse of the devices [245]. Both of the main outcomes are directly patient-oriented, with the emphasis on short-term usage. Less discussed, but still an open topic, was the effect of long-term e-cigarette usage, mainly on cardiovascular health. These results seem to be less positive and point toward the increased risk of high blood pressure, endothelial dysfunction and myocardial infarction [54, 60, 246]. In the end, the research that was done so far was deemed "inconclusive" and remains an open topic [244], with significant lack of preclinical studies to define the mechanisms lying behind the perceived consequences. In the present study the role of NADPH-oxidase complex in detrimental effects and the counter-regulatory protection via activation of the Nrf2-pathway of e-cigarette vapour condensate and its main component acrolein was tested in cultured endothelial cells and macrophages.

My group proposed oxidative stress as the leading mechanism behind adverse cardiovascular effects connected with vaping [106]. The aim of the present research was to determine specific processes whose over-activation leads to oxidative stress observed in previous animal and human studies [93, 106, 247]. It was previously established that e-cigarette vapour on its own is a source of high levels of ROS [248], however, the production of ROS from the vascular tissue is still not fully elucidated. Human endothelial cells and macrophages were chosen as in vitro models because of their importance in vascular homeostasis. Previous study in HUVEC (human umbilical vein endothelial) cells showed induction of ROS formation by e-cigarette aerosol extract [249]. Similarly, a study on alveolar

macrophages showed an increase in ROS production after e-cigarette aerosol extract exposure [250]. Incubation of the cells with different concentrations of e-cigarette vapour condensate showed significant impact on viability of the cells (**Figure 29** and **Figure 30**), in accordance to the previous work of my group. Loss of viability was concentration- and time-dependent, as stated previously [106].

The base of e-cigarette liquid consists of propylene-glycol and glycerine, with added nicotine and aromas to provide wanted effects and approve sensory characteristics. Propylene-glycol and glycerine are considered non-reactive and non-toxic compounds by the FDA [251], so the toxicity of e-cigarette vapour condensate is typically attributed to nicotine and added aromas. However, studies performed with nicotine-free and flavour-free e-cigarette liquids still showed cytotoxic [252], pro-oxidative and pro-inflammatory effects [253, 254]. When tested separately, glycerine showed more pronounced pro-oxidative and pro-inflammatory effects than propylene-glycol [185, 254]. E-cigarette vapour was also tested previously, using different analytical methods, and the relative glycerine quantities in the e-cigarette liquid correlated with the acrolein concentration in the e-cigarette vapour [255, 256]. Acrolein is a water-soluble α,β-unsaturated aldehyde and a strong electrophilic compound [257]. It is a product of thermal degradation of glycerine, which gives a sweet smell to the produced vapour [258, 259]. As an electrophile, acrolein reacts with nucleophilic residues on protein and DNA strands via Michael addition or Schiff base formation, specifically with deoxyguanosine and amino acid side chain residues that contain thiol or amino groups, such as cysteine, histidine or lysine [260-262]. The main elimination pathway for acrolein is through conjugation with glutathione, which may deplete glutathione as an antioxidant and increase the toxicity of both acrolein and other substances that rely on conjugation with glutathione to be eliminated from the organism [262].

As a product of glycerine degradation and the main toxic component found in e-cigarette vapour condensate, acrolein was used here independently to determine whether it produces the same toxic effects as e-cigarette vapour condensate. Indeed, the cell viability obtained from incubation with acrolein showed similar time- and concentration-dependent trend as the viability obtained from incubation with e-cigarette vapour condensate (**Figure 29** and **Figure 30**). To determine whether oxidative stress was the reason behind the perceived cytotoxicity, several tests that show oxidative burden in the cells were performed. Live cells, as well as cell supernatant was analysed after 3-day incubation, to define pathways activated

by exposure to acrolein. Unspecific DHE staining of the cells showed an increased intracellular ROS production in both types of cells by trend, with the highest concentration of acrolein used (10 µM) producing a significant effect (**Figure 31** A). Accordingly, oxidative stress shows a similar trend as compared to the viability of the cells, although on a smaller scale. This was expected, as acrolein is not the only toxic component of the e-cigarette vapour condensate, thus carrying only a part of detrimental effects vaping may have [106]. As there were not enough viable cells left to determine oxidative burden after incubation with 33 µM acrolein, we analysed cell supernatant only. Supernatant was incubated with DHE and we separated its two oxidation products using HPLC. This experiment showed a significant increase in both superoxide production (as portrayed by the production of 2-HE) and unspecific ROS production (as portrayed by the production of E+) (**Figure 32** A and B).

Mechanism of acrolein effects on ROS formation was studied previously and one of the proposed mechanisms was activation of NADPH-oxidase complex activity [263]. Curiously, even though acrolein was labelled as an NADPH-oxidase complex activator, it was also found that it may inhibit the activity of the active complex via binding to the p47phox subunit of the complex, thus averting it to bind to other subunits and activate the complex [264]. NADPH-oxidase complex is a known contributor to the production of ROS [116, 157]. It plays a prominent role in the development of cardiovascular diseases and is linked with the promotion of atherosclerosis, small vessel disease, hypertension and dysfunction of the endothelium [116, 265-267]. Here, the activity of NADPH-oxidase complex was tested by determining the Rac1 subunit translocation to the cell membrane, which shows an activation of NADPH-oxidase complex and its role in ROS production. We demonstrated Rac1 translocation to the cell membrane by trend, becoming significant in the group exposed to the highest concentration of acrolein (10 µM) (**Figure 31** B), as well as increased production of ROS extracellularly, as manifested by oxidative burst in cultured macrophages (**Figure 30** B). Oxidative burst in macrophages treated with e-cigarette vapour condensate showed a similar trend in production of ROS, as manifested by oxidative burst by acrolein, which again suggests that the effects of e-cigarette vapour condensate on cultured cells are highly related to the acrolein content (**Figure 30** D). It was previously proposed that acrolein, besides cytotoxic effects, expresses cytostatic effects too. This question was raised after finding out that acrolein is one of the metabolites of the anticancer drug cyclophosphamide. However, a study done in mice showed that the chemical variant of cyclophosphamide that releases both

acrolein and phosphoramide-mustard happened to be the one with cytostatic effects, and the chemical variant of cyclophosphamide that releases only acrolein didn't show cytostatic effects [268]. On the other hand, a study on endothelial cells showed that extracellular treatment with cyclophosphamide had no cytotoxic effects, whereas treatment with acrolein did [269]. These findings are in line with presented results, where inhaled e-cigarette-derived acrolein had a severe impact on viability of the cells. Summary of all of the findings is presented in **Figure 42**.

By using up glutathione reserves to be removed from the organism, acrolein has an indirect impact on certain transcription factors of NADPH-oxidase subunits, such as activator protein 1 (AP-1) and nuclear factor kappa-light-chain enhancer of activated B cells (NF-κB) [270-272]. These factors are also redox regulated, making them a target of acrolein-derived ROS formation. AP-1 activity is directly increased by acrolein through activation of c-jun and activator transcription factor-2 (ATF-2) via stress-activated protein kinases / jun amino-terminal kinases (SAPK/JNK) and p38 mitogen-activated protein kinases (p38MAPK) [91, 273]. Additionally, activation of Nrf2, a widely distributed transcription factor is dependent on GSH/GSSG ratio [274] that is impaired by acrolein. Nrf2 via its regulator Keap1 can be activated by a broad range of electrophiles including ROS such as hydrogen peroxide and peroxynitrite. DLD-HO1-prom cells used here as a model for Nrf2 activation and subsequent induction of heme-oxygenase-1 gene and protein expression, showed a significant increase in luciferase-dependent chemiluminescence light emission (as a read-out of HO-1 promoter activation by Nrf2) with incubation with 10 µM and 33 µM acrolein (**Figure 30** C).

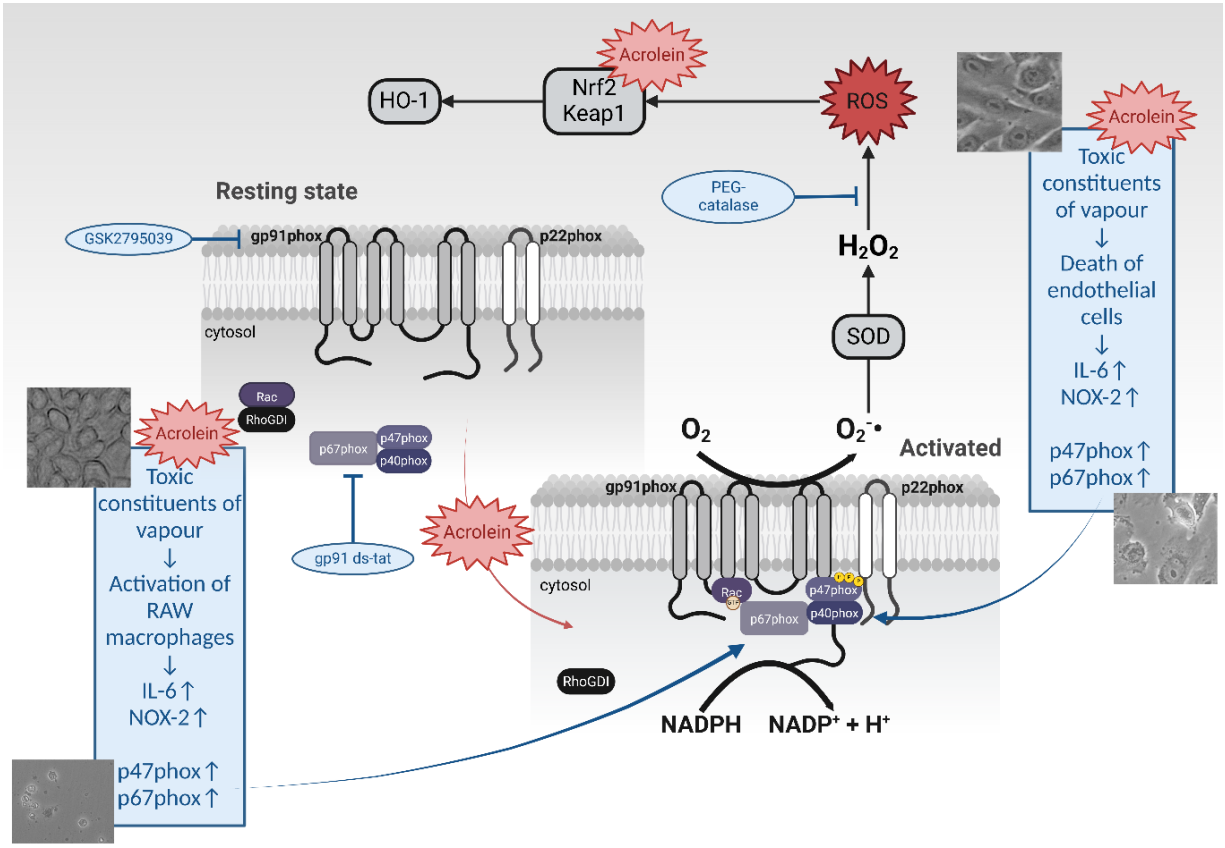

Figure 42. Mechanism of NADPH oxidase activation by acrolein and e-cigarette condensate. The overlapping effects of acrolein and e-cigarette condensate on the activation of NADPH oxidase provide a strong indication that e-cigarette vapour-derived acrolein is responsible for a significant part of the observed oxidative stress. Own figure reused from [50].

4.3. Shisha

As standard tobacco smoking in form of cigarettes became recognised as a huge risk factor for lung, cardiovascular and nervous diseases, shisha (waterpipe, hookah or narghile) smoking became another alternative way to enjoy nicotine effects, much like e-cigarettes. Even though shisha existed for decades, even centuries, and is a part of culture in Middle East and North Africa, it is now becoming spread worldwide and more popular each day. The prevalence of ever use raised by 41.9 % in the USA, 28.5 % in the UK and 8.9 % in Germany in only ten years [56]. Increased prevalence of use among adolescents seems to be of the biggest concern, as it can negatively affect adolescent's health later in life [275]. Although shisha smoking is considered an alternative and safer way of inhaling nicotine than cigarette smoking, previous research proves it is a misconception. Biomarkers of exposure to shisha smoke are proven to be similar to the biomarkers of exposure to cigarette smoke, both first-hand and second-hand [276]. Nicotine levels in blood after smoking shisha are similar as after smoking cigarettes

[277]. Shisha smoking is even connected to the higher levels of carbon monoxide and particulate matter inhaled when compared to cigarette smoking, as well as general smoke exposure [277, 278]. These results are contributed to by the charcoal used to heat the shisha tobacco and assessed only on a short-term scale, as the half-time of carbon monoxide in blood is about an hour [279]. A study of comparison of exposure to carcinogens between shisha smoking and cigarette smoking found that the carcinogen profiles are different between those two different ways of inhaling nicotine and that clinical cancer risk profile should be assessed accordingly [280]. Same study specifically mentioned the risk of leukaemia as a major outcome that shisha smoking is a big risk factor for [280]. In the present pilot study of shisha exposure, we tested the effects of full-body shisha exposure on cardiac, vascular, neuronal and lung tissue of mice, as well as some metabolic and inflammation markers in blood of the exposed mice.

Cardiovascular effects of shisha have been tested multiple times before, and the results are not always conclusive. Systematic review of the cardiovascular effects of shisha pointed towards multiple negative effects, such as increased blood pressure and heart rate, higher levels of high-density lipoprotein (HDL), triglycerides and blood glucose, and lower levels of low-density lipoproteins (LDL), similarly to cigarette smoking [281]. On the other hand, endothelial function, as measured as flow mediated dilation (FMD), was impaired in some of the studies [282], unchanged in some [283], and improved in the others [147]. Preclinical studies regarding shisha smoking were mostly oriented toward respiratory effects, with only a minority of studies regarding the cardiovascular system, all of them lacking a mechanistic insight into the observed effects [284-287]. Present experiments were performed on mice, and the results did not fully correspond to the effects observed in humans. Systolic blood pressure was moderately increased (**Figure 34** B), as well as oxidative stress produced in aorta by trend, as visualised by lucigenin-enhanced chemiluminescence (**Figure 34** C). However, levels of carboxyhaemoglobin were significantly higher in mice treated with shisha than in control mice (**Figure 33** A), which may lower blood pressure acutely [288]. On the other hand, both endothelium-dependent and endothelium-independent relaxation of isolated aortic rings was reduced, which points to the dysfunction of the endothelium (**Figure 34** D).

Several previous studies tested inflammation and oxidative stress markers after shisha exposure [286, 287]. We tested several of those inflammation and oxidative stress markers in heart, lung and aortic tissues, as well as in plasma of shisha exposed mice. Relative RNA

expression of Nqo-1, HO-1, NOX2, CD68 and VCAM were elevated in heart tissue, as well as Gpx-1 and IL-1β, pointing to the induction of inflammation and counter-regulatory activation of Nrf2-signaling pathway in heart of shisha smoke exposed mice (**Figure 36**). Similarly, monocyte-chemoattractant protein-1 (MCP-1), a known marker of inflammation [289], was elevated in both heart and aortic tissue of shisha exposed mice compared to the untreated mice (**Figure 37**). Additionally, dot blot analysis of IL-6, a pro-inflammatory cytokine, showed significant increase in relative expression of the protein in heart and lung tissues (**Figure 38** A). Nitrated proteins in heart tissue of shisha exposed mice did not significantly change (**Figure 38** A). This result was not expected, since the 3-nitrotyrosine-positive proteins were previously connected with endothelial dysfunction and increased oxidative stress [106]. However, this result could be explained by the activation of the antioxidant defence system via the Nrf2-pathway with subsequent upregulation of the protective genes and proteins, HO-1, SOD, HIF-1 [290].

High levels of circulating markers of oxidative stress, such as malondialdehyde (MDA) and 8-epi-prostaglandin-F2α were also observed in several human studies after shisha smoking [291], as well as reduced total antioxidant capacity [281]. Here, production of ROS in several different tissues (cortex, lung, aorta and heart) was examined and increased ROS production in cortex and lung was found, as envisioned by oxidised DHE fluorescence (**Figure 39**). Oxidative burst in leukocytes of shisha smoke treated mice was enhanced in the presence of zymosan A, pointing to priming of leukocytes towards a pro-inflammatory state (**Figure 34** D). Summary of all of the effects of shisha smoke on vascular function and the similarities with e-cigarette exposure are presented in **Figure 43**.

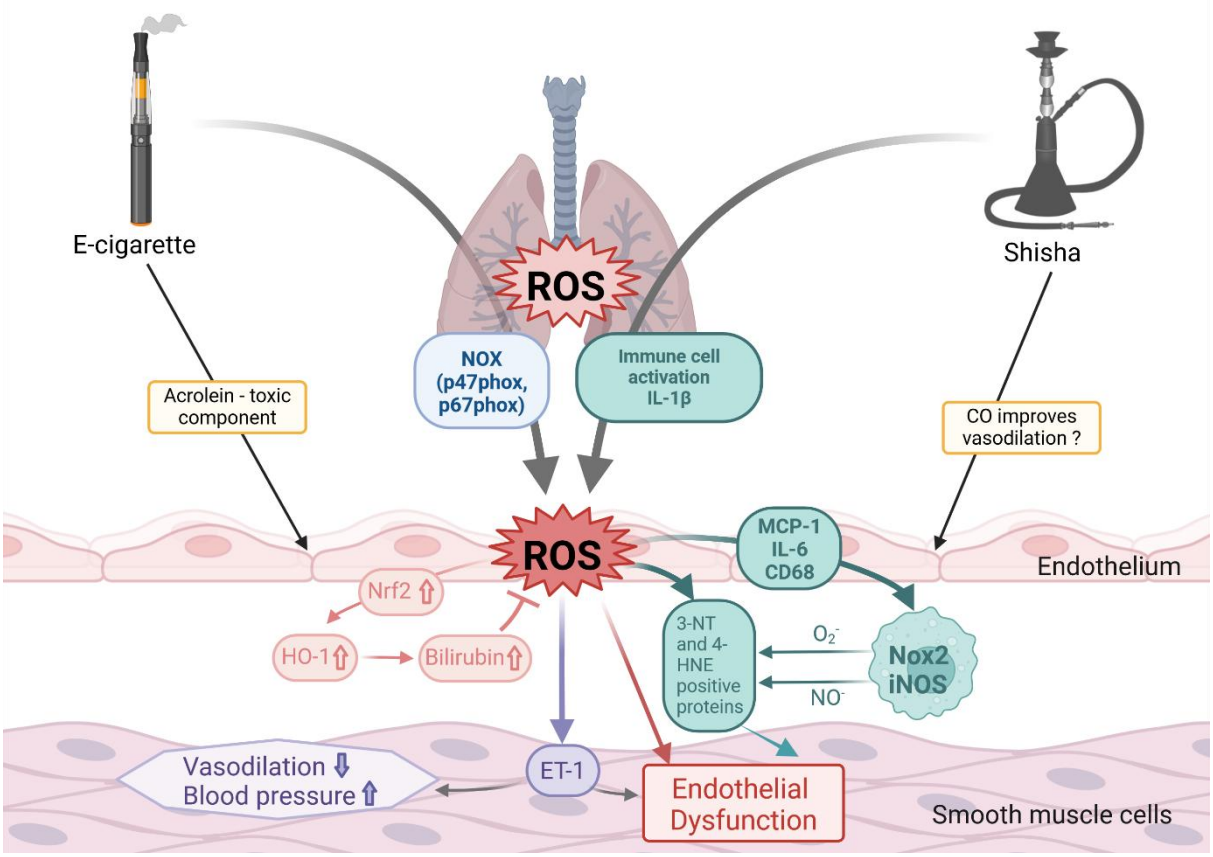

Figure 43. Similarities between e-cigarette and shisha effects on vascular function oxidative stress and inflammation. Figure created with BioRender.com

Carbon monoxide (CO) is defined as a known toxic component of cigarette smoke. The contribution of CO to the overall health effects of shisha smoke was previously evaluated in shisha smokers [292, 293], but only in a form of case studies. Inhaling carbon monoxide causes functional anaemia, as it binds to haemoglobin instead of oxygen. CO has higher affinity to haemoglobin than oxygen, and when bound in the form of carboxyhaemoglobin it makes the binding of oxygen to haemoglobin impossible, decreasing the oxygen supply to tissues and causing oxygen starvation of the cells [294, 295]. CO also acts as a signalling molecule, regulating enzymes with haeme prosthetic group [296]. Direct regulation of eNOS, guanylyl cyclase and potassium channels by CO has beneficial effects on vascular function [297-300]. Oxidative stress is also suppressed by CO in general, e.g. by inhibition of NADPH-oxidase complex, whereas inhibition of haem-dependent mitochondrial enzymes may increase mtROS formation to induce autophagy and other protective processes [301]. Because of the overall beneficial effects of CO this molecule could be considered a masking factor of the real toxic

effects of shisha smoking [147]. CO in shisha smoke is produced not only by burning of the tobacco, as in cigarettes, but also by burning coal to heat the molasses.

In order to address the importance and contribution of particulate matter in shisha smoke, e.g. coming from the coal pieces as well as burning of the tobacco itself, to the CO effects again the exposure of cultured HO-1 promoter reporter cells were used. Particulate matter exposure induced HO-1 promoter activity (and accordingly Hmox-1 gene expression) in a concentration-dependent manner, which could be blocked by Nrf2 inhibitors (see **Figure 39**). Accordingly, besides CO being produced by the coal used for tobacco burning as an external source, also induction of HO-1 in a Nrf2-dependent fashion contributes to the formation of endogenous CO. Both processes will ultimately mask the toxic effects of shisha smoke by the beneficial effects of CO as well as bilirubin and ferritin originating from HO-1 activity.

4.4. Conclusion

The work presented in this thesis examines the role of three known stress risk factors present in the modern society that are much talked about, but not explored enough. Noise, as an environmental risk factor, and e-cigarettes and shisha smoking as behavioural risk factors have shared biochemical mechanisms (oxidative stress and inflammation) that result in pathological effects (here discussed are cardiovascular and behavioural effects). Many of the markers of oxidative stress were increased in all three of the studies, as well as some inflammation markers, showing the underlying causes of the negative clinical effects, such as hypertension and endothelial dysfunction, observed in my work as well as multiple times before. Studies such as these ones prove how important the exposome concept is and how much of an effect both the environment and lifestyle have on our health and wellbeing. Studying all of the factors that affect us directly and indirectly is imperative to be able to improve the life and living conditions of people around the globe. Noise is a recognised risk factor with multiple guidelines already in place, providing recommended daily and yearly noise levels that should not be exceeded. However, these are only guidelines, not required nor enforced anywhere in the world. Adding proof to the already acquired knowledge can and should put pressure on lawmakers to start applying the guidelines. Lack of regulations surrounding e-cigarettes and shisha consumption continually proves to be a big problem not only for the health of individuals, but also for the researchers that try to invent better ways to examine all of the effects these risk factors may have. This thesis is a small contribution to the overall understanding of how noise, e-cigarettes, and shisha smoking negatively influence our lives and provides new insights into the underlying molecular mechanisms. However, it is also a beacon of hope, offering a direction we should follow to mitigate these effects and better the lives of millions.

5. References

1. Lu, S., F. Wei, and G. Li, *The evolution of the concept of stress and the framework of the stress system.* Cell Stress, 2021. **5**(6): p. 76-85.
2. Selye, H., *What Is Stress.* Metabolism-Clinical and Experimental, 1956. **5**(5): p. 525-530.
3. Selye, H., *Stress and the General Adaptation Syndrome.* British Medical Journal, 1950. **1**(4667): p. 1383-1392.
4. Wild, C.P., *Complementing the genome with an "exposome": the outstanding challenge of environmental exposure measurement in molecular epidemiology.* Cancer Epidemiol Biomarkers Prev, 2005. **14**(8): p. 1847-50.
5. Daiber, A., et al., *Das Exposom charakterisiert die Auswirkungen unserer Umwelt auf Stoffwechsel und Gesundheit.* Aktuelle Kardiologie, 2021. **10**(06): p. 502-508.
6. Vrijheid, M., *The exposome: a new paradigm to study the impact of environment on health.* Thorax, 2014. **69**(9): p. 876-8.
7. Kempen, E.V., et al., *WHO Environmental Noise Guidelines for the European Region: A Systematic Review on Environmental Noise and Cardiovascular and Metabolic Effects: A Summary.* Int J Environ Res Public Health, 2018. **15**(2).
8. WHO, *Burden of Disease from Environmental Noise: Quantification of Healthy Life Years Lost in Europe.* 2011.
9. Farooqi, Z.U.R., et al., *Types, sources, socioeconomic impacts, and control strategies of environmental noise: a review.* Environ Sci Pollut Res Int, 2022. **29**(54): p. 81087-81111.
10. Wunderli, J.M., et al., *Intermittency ratio: A metric reflecting short-term temporal variations of transportation noise exposure.* J Expo Sci Environ Epidemiol, 2016. **26**(6): p. 575-585.
11. Sari, D., et al., *Measuring the levels of noise at the Istanbul Ataturk Airport and comparisons with model simulations.* Sci Total Environ, 2014. **482-483**: p. 472-9.
12. Brink, M., et al., *A survey on exposure-response relationships for road, rail, and aircraft noise annoyance: Differences between continuous and intermittent noise.* Environ Int, 2019. **125**: p. 277-290.
13. Brink, M., et al., *Self-Reported Sleep Disturbance from Road, Rail and Aircraft Noise: Exposure-Response Relationships and Effect Modifiers in the SiRENE Study.* Int J Environ Res Public Health, 2019. **16**(21).
14. Basner, M., M. Witte, and S. McGuire, *Aircraft Noise Effects on Sleep-Results of a Pilot Study Near Philadelphia International Airport.* Int J Environ Res Public Health, 2019. **16**(17).
15. Becker, A.B., et al., *Effects of jet engine noise and performance feedback on perceived workload in a monitoring task.* Int J Aviat Psychol, 1995. **5**(1): p. 49-62.
16. Hahad, O., et al., *Noise and mental health: evidence, mechanisms, and consequences.* J Expo Sci Environ Epidemiol, 2024.
17. Sorensen, M., et al., *Health position paper and redox perspectives - Disease burden by transportation noise.* Redox Biol, 2024. **69**: p. 102995.
18. Sorensen, M., et al., *Long-term exposure to residential transportation noise and mortality: A nationwide cohort study.* Environ Pollut, 2023. **328**: p. 121642.
19. Grady, S.T., et al., *Associations between long-term aircraft noise exposure, cardiovascular disease, and mortality in US cohorts of female nurses.* Environ Epidemiol, 2023. **7**(4): p. e259.
20. Agency, E.E. *Noise*. 2024 30.06.2024.]; Available from: https://www.eea.europa.eu/en/topics/in-depth/noise?activeTab=fa515f0c-9ab0-493c-b4cd-58a32dfaae0a.
21. Sorensen, M., et al., *Road traffic noise and incident myocardial infarction: a prospective cohort study.* PLoS One, 2012. **7**(6): p. e39283.
22. Babisch, W., *Cardiovascular effects of noise.* Noise Health, 2011. **13**(52): p. 201-4.
23. Agency, E.E. *Environmental Noise in Europe.* . No 22/2019 2020.
24. Munzel, T., et al., *Cardiovascular effects of environmental noise exposure.* Eur Heart J, 2014. **35**(13): p. 829-36.

25. Munzel, T., et al., *The Adverse Effects of Environmental Noise Exposure on Oxidative Stress and Cardiovascular Risk.* Antioxid Redox Signal, 2018. **28**(9): p. 873-908.
26. Munzel, T., et al., *Environmental stressors and cardio-metabolic disease: part I-epidemiologic evidence supporting a role for noise and air pollution and effects of mitigation strategies.* Eur Heart J, 2017. **38**(8): p. 550-556.
27. Daiber, A., et al., *Targeting vascular (endothelial) dysfunction.* Br J Pharmacol, 2017. **174**(12): p. 1591-1619.
28. Miedema, H.M. and C.G. Oudshoorn, *Annoyance from transportation noise: relationships with exposure metrics DNL and DENL and their confidence intervals.* Environ Health Perspect, 2001. **109**(4): p. 409-16.
29. Rosenlund, M., et al., *Increased prevalence of hypertension in a population exposed to aircraft noise.* Occup Environ Med, 2001. **58**(12): p. 769-73.
30. Babisch, W., et al., *Traffic noise and cardiovascular risk. The Caerphilly study, first phase. Outdoor noise levels and risk factors.* Arch Environ Health, 1988. **43**(6): p. 407-14.
31. Beelen, R., et al., *The joint association of air pollution and noise from road traffic with cardiovascular mortality in a cohort study.* Occup Environ Med, 2009. **66**(4): p. 243-50.
32. Sorensen, M., et al., *Road traffic noise and stroke: a prospective cohort study.* Eur Heart J, 2011. **32**(6): p. 737-44.
33. Halonen, J.I., et al., *Road traffic noise is associated with increased cardiovascular morbidity and mortality and all-cause mortality in London.* Eur Heart J, 2015. **36**(39): p. 2653-61.
34. Eriksson, C., et al., *Long-term aircraft noise exposure and body mass index, waist circumference, and type 2 diabetes: a prospective study.* Environ Health Perspect, 2014. **122**(7): p. 687-94.
35. Sorensen, M., et al., *Combined effects of road traffic noise and ambient air pollution in relation to risk for stroke?* Environ Res, 2014. **133**: p. 49-55.
36. Hahad, O., et al., *Midregional pro atrial natriuretic peptide: a novel important biomarker for noise annoyance-induced cardiovascular morbidity and mortality?* Clin Res Cardiol, 2021. **110**(1): p. 29-39.
37. CDC. *Cigarette smoking in the U.S.* 2023 30.06.2024.]; Available from: https://www.cdc.gov/tobacco/data_statistics/fact_sheets/fast_facts/cigarette-smoking-in-the-us.html.
38. Hajek, P., et al., *A Randomized Trial of E-Cigarettes versus Nicotine-Replacement Therapy.* N Engl J Med, 2019. **380**(7): p. 629-637.
39. Ibrahim, S., M. Habiballah, and I.E. Sayed, *Efficacy of Electronic Cigarettes for Smoking Cessation: A Systematic Review and Meta-Analysis.* Am J Health Promot, 2021. **35**(3): p. 442-455.
40. Wang, R.J., S. Bhadriraju, and S.A. Glantz, *E-Cigarette Use and Adult Cigarette Smoking Cessation: A Meta-Analysis.* Am J Public Health, 2021. **111**(2): p. 230-246.
41. Eisenberg, M.J., et al., *Effect of e-Cigarettes Plus Counseling vs Counseling Alone on Smoking Cessation: A Randomized Clinical Trial.* JAMA, 2020. **324**(18): p. 1844-1854.
42. Initiative, T. *Truth Initiative: Action needed: E-cigarettes*. 2021 30.06.2024.]; Available from: https://truthinitiative.org/research-resources/emerging-tobacco-products/action-needed-e-cigarettes.
43. Cullen, K.A., et al., *e-Cigarette Use Among Youth in the United States, 2019.* JAMA, 2019. **322**(21): p. 2095-2103.
44. Statista. *U.S. teens more likely top use e-cigarettes that cigarettes*. 2019 30.06.2024.]; Available from: https://www.statista.com/chart/18633/use-of-cigarettes-and-e-cigarettes-among-us-teens.
45. Statista. *U.S. smoking rate falls to record low*. 2018 30.06.2024.]; Available from: https://www.statista.com/chart/14879/us-smoking-rate-falls-to-record-low.
46. Kuntic, M., et al., *Lebensstil und kardiovaskuläre Gesundheit – wie schädlich sind E-Zigaretten und Shisha-Rauchen?* Aktuelle Kardiologie, 2021. **10**(06): p. 537-542.

47. Shao, X.M. and T.C. Friedman, *Pod-mod vs. conventional e-cigarettes: nicotine chemistry, pH, and health effects.* J Appl Physiol (1985), 2020. **128**(4): p. 1056-1058.
48. Zhao, D., et al., *Effects of e-liquid flavor, nicotine content, and puff duration on metal emissions from electronic cigarettes.* Environ Res, 2022. **204**(Pt C): p. 112270.
49. Lee, Y.J., et al., *Quantitative insights into major constituents contained in or released by electronic cigarettes: Propylene glycol, vegetable glycerin, and nicotine.* Sci Total Environ, 2020. **703**: p. 134567.
50. Kuntic, I., et al., *The role of acrolein for E-cigarette vapour condensate mediated activation of NADPH oxidase in cultured endothelial cells and macrophages.* Pflugers Arch, 2023. **475**(7): p. 807-821.
51. Chaumont, M., et al., *Differential Effects of E-Cigarette on Microvascular Endothelial Function, Arterial Stiffness and Oxidative Stress: A Randomized Crossover Trial.* Sci Rep, 2018. **8**(1): p. 10378.
52. Chaumont, M., et al., *Fourth generation e-cigarette vaping induces transient lung inflammation and gas exchange disturbances: results from two randomized clinical trials.* Am J Physiol Lung Cell Mol Physiol, 2019. **316**(5): p. L705-L719.
53. Farsalinos, K.E., et al., *Is e-cigarette use associated with coronary heart disease and myocardial infarction? Insights from the 2016 and 2017 National Health Interview Surveys.* Ther Adv Chronic Dis, 2019. **10**: p. 2040622319877741.
54. D'Ruiz, C.D., et al., *Measurement of cardiovascular and pulmonary function endpoints and other physiological effects following partial or complete substitution of cigarettes with electronic cigarettes in adult smokers.* Regul Toxicol Pharmacol, 2017. **87**: p. 36-53.
55. Moheimani, R.S., et al., *Sympathomimetic Effects of Acute E-Cigarette Use: Role of Nicotine and Non-Nicotine Constituents.* J Am Heart Assoc, 2017. **6**(9).
56. Jawad, M., et al., *The prevalence and trends of waterpipe tobacco smoking: A systematic review.* PLoS One, 2018. **13**(2): p. e0192191.
57. Maziak, W., et al., *The global epidemiology of waterpipe smoking.* Tob Control, 2015. **24 Suppl 1**(Suppl 1): p. i3-i12.
58. Kadhum, M., et al., *Measuring the acute cardiovascular effects of shisha smoking: a cross-sectional study.* JRSM Open, 2014. **5**(6): p. 2054270414531127.
59. El-Zaatari, Z.M., H.A. Chami, and G.S. Zaatari, *Health effects associated with waterpipe smoking.* Tob Control, 2015. **24 Suppl 1**(Suppl 1): p. i31-i43.
60. Munzel, T., et al., *Effects of tobacco cigarettes, e-cigarettes, and waterpipe smoking on endothelial function and clinical outcomes.* Eur Heart J, 2020. **41**(41): p. 4057-4070.
61. Sepetdjian, E., N. Saliba, and A. Shihadeh, *Carcinogenic PAH in waterpipe charcoal products.* Food Chem Toxicol, 2010. **48**(11): p. 3242-5.
62. Badran, M. and I. Laher, *Waterpipe (shisha, hookah) smoking, oxidative stress and hidden disease potential.* Redox Biol, 2020. **34**: p. 101455.
63. Al-Kazwini, A.T., A.J. Said, and S. Sdepanian, *Compartmental analysis of metals in waterpipe smoking technique.* BMC Public Health, 2015. **15**: p. 153.
64. *<Kadhum2015.pdf>.*
65. Darawshy, F., et al., *Waterpipe smoking: a review of pulmonary and health effects.* Eur Respir Rev, 2021. **30**(160).
66. Wu, F., et al., *A prospective study of tobacco smoking and mortality in Bangladesh.* PLoS One, 2013. **8**(3): p. e58516.
67. Sibai, A.M., et al., *Lifetime cumulative exposure to waterpipe smoking is associated with coronary artery disease.* Atherosclerosis, 2014. **234**(2): p. 454-60.
68. Waziry, R., et al., *The effects of waterpipe tobacco smoking on health outcomes: an updated systematic review and meta-analysis.* Int J Epidemiol, 2017. **46**(1): p. 32-43.
69. Khabour, O.F., et al., *Acute exposure to waterpipe tobacco smoke induces changes in the oxidative and inflammatory markers in mouse lung.* Inhal Toxicol, 2012. **24**(10): p. 667-75.

70. Nemmar, A., et al., *Cardiovascular effects of nose-only water-pipe smoking exposure in mice.* Am J Physiol Heart Circ Physiol, 2013. **305**(5): p. H740-6.
71. Selim, G.M., H. Fouad, and S. Ezzat, *Impact of shisha smoking on the extent of coronary artery disease in patients referred for coronary angiography.* Anadolu Kardiyol Derg, 2013. **13**(7): p. 647-54.
72. Hakim, F., et al., *The acute effects of water-pipe smoking on the cardiorespiratory system.* Chest, 2011. **139**(4): p. 775-781.
73. Kadhum, M., et al., *A review of the health effects of smoking shisha.* Clin Med (Lond), 2015. **15**(3): p. 263-6.
74. Babisch, W., *The Noise/Stress Concept, Risk Assessment and Research Needs.* Noise Health, 2002. **4**(16): p. 1-11.
75. Daiber, A., et al., *Environmental noise induces the release of stress hormones and inflammatory signaling molecules leading to oxidative stress and vascular dysfunction-Signatures of the internal exposome.* Biofactors, 2019. **45**(4): p. 495-506.
76. Said, M.A. and O.A. El-Gohary, *Effect of noise stress on cardiovascular system in adult male albino rat: implication of stress hormones, endothelial dysfunction and oxidative stress.* Gen Physiol Biophys, 2016. **35**(3): p. 371-7.
77. Munzel, T., M. Sorensen, and A. Daiber, *Transportation noise pollution and cardiovascular disease.* Nat Rev Cardiol, 2021. **18**(9): p. 619-636.
78. Peterson, E.A., et al., *Noise raises blood pressure without impairing auditory sensitivity.* Science, 1981. **211**(4489): p. 1450-2.
79. Babisch, W., et al., *Noise annoyance--a modifier of the association between noise level and cardiovascular health?* Sci Total Environ, 2013. **452-453**: p. 50-7.
80. Munzel, T., et al., *Effects of noise on vascular function, oxidative stress, and inflammation: mechanistic insight from studies in mice.* Eur Heart J, 2017. **38**(37): p. 2838-2849.
81. Benowitz, N.L. and A.D. Burbank, *Cardiovascular toxicity of nicotine: Implications for electronic cigarette use.* Trends Cardiovasc Med, 2016. **26**(6): p. 515-23.
82. Piao, W.H., et al., *Nicotine and inflammatory neurological disorders.* Acta Pharmacol Sin, 2009. **30**(6): p. 715-22.
83. Grines, C.L., et al., *Effect of cigarette smoking on outcome after thrombolytic therapy for myocardial infarction.* Circulation, 1995. **91**(2): p. 298-303.
84. Guslandi, M., *Nicotine treatment for ulcerative colitis.* Br J Clin Pharmacol, 1999. **48**(4): p. 481-4.
85. Farsalinos, K.E., et al., *Tobacco-Specific Nitrosamines in Electronic Cigarettes: Comparison between Liquid and Aerosol Levels.* Int J Environ Res Public Health, 2015. **12**(8): p. 9046-53.
86. Yalcin, E. and S. de la Monte, *Tobacco nitrosamines as culprits in disease: mechanisms reviewed.* J Physiol Biochem, 2016. **72**(1): p. 107-20.
87. Konstantinou, E., et al., *Tobacco-specific nitrosamines: A literature review.* Food Chem Toxicol, 2018. **118**: p. 198-203.
88. Na, C.J., et al., *The transfer characteristics of heavy metals in electronic cigarette liquid.* Environ Res, 2019. **174**: p. 152-159.
89. Tchounwou, P.B., et al., *Heavy metal toxicity and the environment.* Exp Suppl, 2012. **101**: p. 133-64.
90. in *E-Cigarette Use Among Youth and Young Adults: A Report of the Surgeon General*. 2016: Atlanta (GA).
91. Moghe, A., et al., *Molecular mechanisms of acrolein toxicity: relevance to human disease.* Toxicol Sci, 2015. **143**(2): p. 242-55.
92. Kassem, N.O.F., et al., *Acrolein Exposure in Hookah Smokers and Non-Smokers Exposed to Hookah Tobacco Secondhand Smoke: Implications for Regulating Hookah Tobacco Products.* Nicotine Tob Res, 2018. **20**(4): p. 492-501.

93. Glynos, C., et al., *Comparison of the effects of e-cigarette vapor with cigarette smoke on lung function and inflammation in mice.* Am J Physiol Lung Cell Mol Physiol, 2018. **315**(5): p. L662-L672.
94. Whitnall, M.H., *Regulation of the hypothalamic corticotropin-releasing hormone neurosecretory system.* Prog Neurobiol, 1993. **40**(5): p. 573-629.
95. Smith, S.M. and W.W. Vale, *The role of the hypothalamic-pituitary-adrenal axis in neuroendocrine responses to stress.* Dialogues Clin Neurosci, 2006. **8**(4): p. 383-95.
96. Sandeep Kumar, V. and E.M. Schneider, *Depression: An Insight and Need for Personalized Psychological Stress Monitoring and Management.* Journal of Basic & Applied Sciences, 2014. **10**: p. 177-182.
97. Daiber, A., et al., *Oxidative stress and inflammation contribute to traffic noise-induced vascular and cerebral dysfunction via uncoupling of nitric oxide synthases.* Redox Biol, 2020. **34**: p. 101506.
98. Lob, H.E., et al., *Induction of hypertension and peripheral inflammation by reduction of extracellular superoxide dismutase in the central nervous system.* Hypertension, 2010. **55**(2): p. 277-83, 6p following 283.
99. Mendelson, J.H., et al., *Effects of smoking successive low- and high-nicotine cigarettes on hypothalamic-pituitary-adrenal axis hormones and mood in men.* Neuropsychopharmacology, 2008. **33**(4): p. 749-60.
100. Rohleder, N. and C. Kirschbaum, *The hypothalamic-pituitary-adrenal (HPA) axis in habitual smokers.* Int J Psychophysiol, 2006. **59**(3): p. 236-43.
101. Sies, H., *Oxidative stress: a concept in redox biology and medicine.* Redox Biol, 2015. **4**: p. 180-3.
102. Bedard, K. and K.H. Krause, *The NOX family of ROS-generating NADPH oxidases: physiology and pathophysiology.* Physiol Rev, 2007. **87**(1): p. 245-313.
103. Kurutas, E.B., *The importance of antioxidants which play the role in cellular response against oxidative/nitrosative stress: current state.* Nutr J, 2016. **15**(1): p. 71.
104. Sies, H. and E. Cadenas, *Oxidative stress: damage to intact cells and organs.* Philos Trans R Soc Lond B Biol Sci, 1985. **311**(1152): p. 617-31.
105. Golbidi, S., H. Li, and I. Laher, *Oxidative Stress: A Unifying Mechanism for Cell Damage Induced by Noise, (Water-Pipe) Smoking, and Emotional Stress-Therapeutic Strategies Targeting Redox Imbalance.* Antioxid Redox Signal, 2018. **28**(9): p. 741-759.
106. Kuntic, M., et al., *Short-term e-cigarette vapour exposure causes vascular oxidative stress and dysfunction: evidence for a close connection to brain damage and a key role of the phagocytic NADPH oxidase (NOX-2).* Eur Heart J, 2020. **41**(26): p. 2472-2483.
107. Panday, A., et al., *NADPH oxidases: an overview from structure to innate immunity-associated pathologies.* Cell Mol Immunol, 2015. **12**(1): p. 5-23.
108. Dusting, G.J., S. Selemidis, and F. Jiang, *Mechanisms for suppressing NADPH oxidase in the vascular wall.* Mem Inst Oswaldo Cruz, 2005. **100 Suppl 1**: p. 97-103.
109. Koshkin, V. and E. Pick, *Superoxide production by cytochrome b559. Mechanism of cytosol-independent activation.* FEBS Lett, 1994. **338**(3): p. 285-9.
110. Miyano, K. and H. Sumimoto, *Role of the small GTPase Rac in p22phox-dependent NADPH oxidases.* Biochimie, 2007. **89**(9): p. 1133-44.
111. Kanai, F., et al., *The PX domains of p47phox and p40phox bind to lipid products of PI(3)K.* Nat Cell Biol, 2001. **3**(7): p. 675-8.
112. Karathanassis, D., et al., *Binding of the PX domain of p47(phox) to phosphatidylinositol 3,4-bisphosphate and phosphatidic acid is masked by an intramolecular interaction.* EMBO J, 2002. **21**(19): p. 5057-68.
113. Nisimoto, Y., et al., *The p67(phox) activation domain regulates electron flow from NADPH to flavin in flavocytochrome b(558).* J Biol Chem, 1999. **274**(33): p. 22999-3005.

114. Fuchs, A., M.C. Dagher, and P.V. Vignais, *Mapping the domains of interaction of p40phox with both p47phox and p67phox of the neutrophil oxidase complex using the two-hybrid system.* J Biol Chem, 1995. **270**(11): p. 5695-7.
115. Heyworth, P.G., et al., *Regulation of NADPH oxidase activity by Rac GTPase activating protein(s).* Mol Biol Cell, 1993. **4**(11): p. 1217-23.
116. Daiber, A., et al., *Crosstalk of mitochondria with NADPH oxidase via reactive oxygen and nitrogen species signalling and its role for vascular function.* Br J Pharmacol, 2017. **174**(12): p. 1670-1689.
117. Groemping, Y. and K. Rittinger, *Activation and assembly of the NADPH oxidase: a structural perspective.* Biochem J, 2005. **386**(Pt 3): p. 401-16.
118. El-Benna, J., P.M. Dang, and M.A. Gougerot-Pocidalo, *Priming of the neutrophil NADPH oxidase activation: role of p47phox phosphorylation and NOX2 mobilization to the plasma membrane.* Semin Immunopathol, 2008. **30**(3): p. 279-89.
119. Hallett, M.B. and D. Lloyds, *Neutrophil priming: the cellular signals that say 'amber' but not 'green'.* Immunol Today, 1995. **16**(6): p. 264-8.
120. Belambri, S.A., et al., *NADPH oxidase activation in neutrophils: Role of the phosphorylation of its subunits.* Eur J Clin Invest, 2018. **48 Suppl 2**: p. e12951.
121. Kroller-Schon, S., et al., *Crucial role for Nox2 and sleep deprivation in aircraft noise-induced vascular and cerebral oxidative stress, inflammation, and gene regulation.* Eur Heart J, 2018. **39**(38): p. 3528-3539.
122. Nguyen Dinh Cat, A., et al., *Angiotensin II, NADPH oxidase, and redox signaling in the vasculature.* Antioxid Redox Signal, 2013. **19**(10): p. 1110-20.
123. Kim, M., C.H. Han, and M.Y. Lee, *NADPH oxidase and the cardiovascular toxicity associated with smoking.* Toxicol Res, 2014. **30**(3): p. 149-57.
124. Nemmar, A., et al., *Nose-only water-pipe smoking effects on airway resistance, inflammation, and oxidative stress in mice.* J Appl Physiol (1985), 2013. **115**(9): p. 1316-23.
125. Hadi, H.A., C.S. Carr, and J. Al Suwaidi, *Endothelial dysfunction: cardiovascular risk factors, therapy, and outcome.* Vasc Health Risk Manag, 2005. **1**(3): p. 183-98.
126. Shaito, A., et al., *Oxidative Stress-Induced Endothelial Dysfunction in Cardiovascular Diseases.* Front Biosci (Landmark Ed), 2022. **27**(3): p. 105.
127. Forstermann, U. and W.C. Sessa, *Nitric oxide synthases: regulation and function.* Eur Heart J, 2012. **33**(7): p. 829-37, 837a-837d.
128. Knowles, R.G. and S. Moncada, *Nitric oxide synthases in mammals.* Biochem J, 1994. **298 (Pt 2)**(Pt 2): p. 249-58.
129. Dong, J., et al., *Insights into human eNOS, nNOS and iNOS structures and medicinal indications from statistical analyses of their interactions with bound compounds.* Biophys Rep, 2023. **9**(3): p. 159-175.
130. Fleming, I., et al., *Ca2+-independent activation of the endothelial nitric oxide synthase in response to tyrosine phosphatase inhibitors and fluid shear stress.* Circ Res, 1998. **82**(6): p. 686-95.
131. Matsubara, M., K. Titani, and H. Taniguchi, *Interaction of calmodulin-binding domain peptides of nitric oxide synthase with membrane phospholipids: regulation by protein phosphorylation and Ca(2+)-calmodulin.* Biochemistry, 1996. **35**(46): p. 14651-8.
132. Dudzinski, D.M., et al., *The regulation and pharmacology of endothelial nitric oxide synthase.* Annu Rev Pharmacol Toxicol, 2006. **46**: p. 235-76.
133. Forstermann, U. and T. Munzel, *Endothelial nitric oxide synthase in vascular disease: from marvel to menace.* Circulation, 2006. **113**(13): p. 1708-14.
134. Munzel, T., et al., *Vascular consequences of endothelial nitric oxide synthase uncoupling for the activity and expression of the soluble guanylyl cyclase and the cGMP-dependent protein kinase.* Arterioscler Thromb Vasc Biol, 2005. **25**(8): p. 1551-7.
135. Steven, S., et al., *Vascular Inflammation and Oxidative Stress: Major Triggers for Cardiovascular Disease.* Oxid Med Cell Longev, 2019. **2019**: p. 7092151.

136. Mollnau, H., et al., *Effects of angiotensin II infusion on the expression and function of NAD(P)H oxidase and components of nitric oxide/cGMP signaling.* Circ Res, 2002. **90**(4): p. E58-65.
137. Landmesser, U., et al., *Oxidation of tetrahydrobiopterin leads to uncoupling of endothelial cell nitric oxide synthase in hypertension.* J Clin Invest, 2003. **111**(8): p. 1201-9.
138. Hink, U., et al., *Mechanisms underlying endothelial dysfunction in diabetes mellitus.* Circ Res, 2001. **88**(2): p. E14-22.
139. Warnholtz, A., et al., *Increased NADH-oxidase-mediated superoxide production in the early stages of atherosclerosis: evidence for involvement of the renin-angiotensin system.* Circulation, 1999. **99**(15): p. 2027-33.
140. Sorescu, D., et al., *Superoxide production and expression of nox family proteins in human atherosclerosis.* Circulation, 2002. **105**(12): p. 1429-35.
141. Ohara, Y., T.E. Peterson, and D.G. Harrison, *Hypercholesterolemia increases endothelial superoxide anion production.* J Clin Invest, 1993. **91**(6): p. 2546-51.
142. Vergnani, L., et al., *Effect of native and oxidized low-density lipoprotein on endothelial nitric oxide and superoxide production : key role of L-arginine availability.* Circulation, 2000. **101**(11): p. 1261-6.
143. Munzel, T. and A. Daiber, *Vascular Redox Signaling, Endothelial Nitric Oxide Synthase Uncoupling, and Endothelial Dysfunction in the Setting of Transportation Noise Exposure or Chronic Treatment with Organic Nitrates.* Antioxid Redox Signal, 2023. **38**(13-15): p. 1001-1021.
144. Herzog, J., et al., *Acute exposure to nocturnal train noise induces endothelial dysfunction and pro-thromboinflammatory changes of the plasma proteome in healthy subjects.* Basic Res Cardiol, 2019. **114**(6): p. 46.
145. El-Mahdy, M.A., et al., *Electronic cigarette exposure causes vascular endothelial dysfunction due to NADPH oxidase activation and eNOS uncoupling.* Am J Physiol Heart Circ Physiol, 2022. **322**(4): p. H549-H567.
146. Rammah, M., et al., *In vitro effects of waterpipe smoke condensate on endothelial cell function: a potential risk factor for vascular disease.* Toxicol Lett, 2013. **219**(2): p. 133-42.
147. Rezk-Hanna, M., et al., *High Carbon Monoxide Levels from Charcoal Combustion Mask Acute Endothelial Dysfunction Induced by Hookah (Waterpipe) Smoking in Young Adults.* Circulation, 2019. **139**(19): p. 2215-2224.
148. Diab, O.A., E.M. Abdelrahim, and M. Esmail, *Effect of water pipe tobacco smoking on plasma high sensitivity C reactive protein level and endothelial function compared to cigarette smoking.* The Egyptian Heart Journal, 2015. **67**(3): p. 233-241.
149. Bennett, J.M., et al., *Inflammation-Nature's Way to Efficiently Respond to All Types of Challenges: Implications for Understanding and Managing "the Epidemic" of Chronic Diseases.* Front Med (Lausanne), 2018. **5**: p. 316.
150. Chen, H., et al., *Maternal E-Cigarette Exposure in Mice Alters DNA Methylation and Lung Cytokine Expression in Offspring.* Am J Respir Cell Mol Biol, 2018. **58**(3): p. 366-377.
151. Cicchinelli, S., et al., *PAMPs and DAMPs in Sepsis: A Review of Their Molecular Features and Potential Clinical Implications.* Int J Mol Sci, 2024. **25**(2).
152. Kyriakis, J.M. and J. Avruch, *Mammalian mitogen-activated protein kinase signal transduction pathways activated by stress and inflammation.* Physiol Rev, 2001. **81**(2): p. 807-69.
153. Turner, M.D., et al., *Cytokines and chemokines: At the crossroads of cell signalling and inflammatory disease.* Biochim Biophys Acta, 2014. **1843**(11): p. 2563-2582.
154. Karbach, S., et al., *eNOS uncoupling in cardiovascular diseases--the role of oxidative stress and inflammation.* Curr Pharm Des, 2014. **20**(22): p. 3579-94.
155. Wenzel, P., et al., *Redox regulation of cardiovascular inflammation - Immunomodulatory function of mitochondrial and Nox-derived reactive oxygen and nitrogen species.* Free Radic Biol Med, 2017. **109**: p. 48-60.

156. Howson, J.M.M., et al., *Fifteen new risk loci for coronary artery disease highlight arterial-wall-specific mechanisms.* Nat Genet, 2017. **49**(7): p. 1113-1119.
157. Kroller-Schon, S., et al., *Molecular mechanisms of the crosstalk between mitochondria and NADPH oxidase through reactive oxygen species-studies in white blood cells and in animal models.* Antioxid Redox Signal, 2014. **20**(2): p. 247-66.
158. Murakami, A. and H. Ohigashi, *Targeting NOX, INOS and COX-2 in inflammatory cells: chemoprevention using food phytochemicals.* Int J Cancer, 2007. **121**(11): p. 2357-63.
159. Bellezza, I., et al., *Nrf2-Keap1 signaling in oxidative and reductive stress.* Biochim Biophys Acta Mol Cell Res, 2018. **1865**(5): p. 721-733.
160. Harijith, A., D.L. Ebenezer, and V. Natarajan, *Reactive oxygen species at the crossroads of inflammasome and inflammation.* Front Physiol, 2014. **5**: p. 352.
161. Wassmann, S., et al., *Interleukin-6 induces oxidative stress and endothelial dysfunction by overexpression of the angiotensin II type 1 receptor.* Circ Res, 2004. **94**(4): p. 534-41.
162. Osborne, M.T., et al., *A neurobiological mechanism linking transportation noise to cardiovascular disease in humans.* Eur Heart J, 2020. **41**(6): p. 772-782.
163. Bayo Jimenez, M.T., et al., *Noise-Induced Vascular Dysfunction, Oxidative Stress, and Inflammation Are Improved by Pharmacological Modulation of the NRF2/HO-1 Axis.* Antioxidants (Basel), 2021. **10**(4).
164. Frenis, K., et al., *Ablation of lysozyme M-positive cells prevents aircraft noise-induced vascular damage without improving cerebral side effects.* Basic Res Cardiol, 2021. **116**(1): p. 31.
165. Patrick, D.M. and D.G. Harrison, *Nocturnal noise knocks NOS by Nox: mechanisms underlying cardiovascular dysfunction in response to noise pollution.* Eur Heart J, 2018. **39**(38): p. 3540-3542.
166. Sugama, S. and Y. Kakinuma, *Stress and brain immunity: Microglial homeostasis through hypothalamus-pituitary-adrenal gland axis and sympathetic nervous system.* Brain Behav Immun Health, 2020. **7**: p. 100111.
167. Park, J.A., L.E. Crotty Alexander, and D.C. Christiani, *Vaping and Lung Inflammation and Injury.* Annu Rev Physiol, 2022. **84**: p. 611-629.
168. Chatterjee, S., et al., *Acute exposure to e-cigarettes causes inflammation and pulmonary endothelial oxidative stress in nonsmoking, healthy young subjects.* Am J Physiol Lung Cell Mol Physiol, 2019. **317**(2): p. L155-L166.
169. Mohammadi, L., et al., *Chronic E-Cigarette Use Impairs Endothelial Function on the Physiological and Cellular Levels.* Arterioscler Thromb Vasc Biol, 2022. **42**(11): p. 1333-1350.
170. Biondi-Zoccai, G., et al., *Acute Effects of Heat-Not-Burn, Electronic Vaping, and Traditional Tobacco Combustion Cigarettes: The Sapienza University of Rome-Vascular Assessment of Proatherosclerotic Effects of Smoking (SUR - VAPES) 2 Randomized Trial.* J Am Heart Assoc, 2019. **8**(6): p. e010455.
171. Nocella, C., et al., *Impact of Tobacco Versus Electronic Cigarette Smoking on Platelet Function.* Am J Cardiol, 2018. **122**(9): p. 1477-1481.
172. Chaumont, M., et al., *Short halt in vaping modifies cardiorespiratory parameters and urine metabolome: a randomized trial.* Am J Physiol Lung Cell Mol Physiol, 2020. **318**(2): p. L331-L344.
173. Husari, A., et al., *Acute Exposure to Electronic and Combustible Cigarette Aerosols: Effects in an Animal Model and in Human Alveolar Cells.* Nicotine Tob Res, 2016. **18**(5): p. 613-9.
174. Crotty Alexander, L.E., et al., *Chronic inhalation of e-cigarette vapor containing nicotine disrupts airway barrier function and induces systemic inflammation and multiorgan fibrosis in mice.* Am J Physiol Regul Integr Comp Physiol, 2018. **314**(6): p. R834-R847.
175. Wetendorf, M., et al., *E-Cigarette Exposure Delays Implantation and Causes Reduced Weight Gain in Female Offspring Exposed In Utero.* J Endocr Soc, 2019. **3**(10): p. 1907-1916.
176. Alsaad, A.M., et al., *Genotoxic impact of long-term cigarette and waterpipe smoking on DNA damage and oxidative stress in healthy subjects.* Toxicol Mech Methods, 2019. **29**(2): p. 119-127.

177. Khan, N.A., et al., *Systemic biomarkers of inflammation, oxidative stress and tissue injury and repair among waterpipe, cigarette and dual tobacco smokers.* Tob Control, 2020. **29**(Suppl 2): p. s102-s109.
178. Khabour, O.F., et al., *The effect of chronic exposure to waterpipe tobacco smoke on airway inflammation in mice.* Life Sci, 2018. **200**: p. 110-114.
179. Taati, B., H. Arazi, and K. Suzuki, *Oxidative Stress and Inflammation Induced by Waterpipe Tobacco Smoking Despite Possible Protective Effects of Exercise Training: A Review of the Literature.* Antioxidants (Basel), 2020. **9**(9).
180. Tebay, L.E., et al., *Mechanisms of activation of the transcription factor Nrf2 by redox stressors, nutrient cues, and energy status and the pathways through which it attenuates degenerative disease.* Free Radic Biol Med, 2015. **88**(Pt B): p. 108-146.
181. Panieri, E. and L. Saso, *Potential Applications of NRF2 Inhibitors in Cancer Therapy.* Oxid Med Cell Longev, 2019. **2019**: p. 8592348.
182. Wang, X., et al., *NRF2/HO-1 pathway activation by ATF3 in a noise-induced hearing loss murine model.* Arch Biochem Biophys, 2022. **721**: p. 109190.
183. Fetoni, A.R., et al., *Rosmarinic acid up-regulates the noise-activated Nrf2/HO-1 pathway and protects against noise-induced injury in rat cochlea.* Free Radic Biol Med, 2015. **85**: p. 269-81.
184. Wu, F., et al., *CFTR potentiator ivacaftor protects against noise-induced hair cell loss by increasing Nrf2 and reducing oxidative stress.* Biomed Pharmacother, 2023. **166**: p. 115399.
185. Escobar, Y.H., et al., *In Vitro Toxicity and Chemical Characterization of Aerosol Derived from Electronic Cigarette Humectants Using a Newly Developed Exposure System.* Chem Res Toxicol, 2020. **33**(7): p. 1677-1688.
186. Hamadi, N., et al., *Impact of prolonged exposure to occasional and regular waterpipe smoke on cardiac injury, oxidative stress and mitochondrial dysfunction in male mice.* Front Physiol, 2024. **15**: p. 1286366.
187. Nemmar, A., et al., *Waterpipe Tobacco Smoke Inhalation Triggers Thrombogenicity, Cardiac Inflammation and Oxidative Stress in Mice: Effects of Flavouring.* Int J Mol Sci, 2020. **21**(4).
188. Nemmar, A., et al., *Waterpipe Smoke Exposure Triggers Lung Injury and Functional Decline in Mice: Protective Effect of Gum Arabic.* Oxid Med Cell Longev, 2019. **2019**: p. 8526083.
189. Nemmar, A., et al., *Gum Arabic Ameliorates Impaired Coagulation and Cardiotoxicity Induced by Water-Pipe Smoke Exposure in Mice.* Front Physiol, 2019. **10**: p. 53.
190. Kubo, H., et al., *Astaxanthin Suppresses Cigarette Smoke-Induced Emphysema through Nrf2 Activation in Mice.* Mar Drugs, 2019. **17**(12).
191. Zhang, Y., et al., *Nrf2/HO-1 signaling activation alleviates cigarette smoke-induced inflammation in chronic obstructive pulmonary disease by suppressing NLRP3-mediated pyroptosis.* J Cardiothorac Surg, 2024. **19**(1): p. 58.
192. Karbach, S., et al., *Hyperglycemia and oxidative stress in cultured endothelial cells--a comparison of primary endothelial cells with an immortalized endothelial cell line.* J Diabetes Complications, 2012. **26**(3): p. 155-62.
193. Steven, S., et al., *The Endothelin Receptor Antagonist Macitentan Improves Isosorbide-5-Mononitrate (ISMN) and Isosorbide Dinitrate (ISDN) Induced Endothelial Dysfunction, Oxidative Stress, and Vascular Inflammation.* Oxid Med Cell Longev, 2018. **2018**: p. 7845629.
194. Schuhmacher, S., et al., *Vascular dysfunction in experimental diabetes is improved by pentaerithrityl tetranitrate but not isosorbide-5-mononitrate therapy.* Diabetes, 2011. **60**(10): p. 2608-16.
195. Turner, J.G., et al., *Hearing in laboratory animals: strain differences and nonauditory effects of noise.* Comp Med, 2005. **55**(1): p. 12-23.
196. Hensel, E.C., et al., *A Proposed Waterpipe Emissions Topography Protocol Reflecting Natural Environment User Behaviour.* Int J Environ Res Public Health, 2019. **17**(1).
197. Gather, F., et al., *Regulation of human inducible nitric oxide synthase expression by an upstream open reading frame.* Nitric Oxide, 2019. **88**: p. 50-60.

198. Beutler, E. and C. West, *Simplified determination of carboxyhemoglobin.* Clin Chem, 1984. **30**(6): p. 871-4.
199. Oelze, M., et al., *Nebivolol inhibits superoxide formation by NADPH oxidase and endothelial dysfunction in angiotensin II-treated rats.* Hypertension, 2006. **48**(4): p. 677-684.
200. Wenzel, P., et al., *AT1-receptor blockade by telmisartan upregulates GTP-cyclohydrolase I and protects eNOS in diabetic rats.* Free Radic Biol Med, 2008. **45**(5): p. 619-26.
201. Kielkopf, C.L., W. Bauer, and I.L. Urbatsch, *Bradford Assay for Determining Protein Concentration.* Cold Spring Harb Protoc, 2020. **2020**(4): p. 102269.
202. Christensen, J.S., et al., *Road Traffic and Railway Noise Exposures and Adiposity in Adults: A Cross-Sectional Analysis of the Danish Diet, Cancer, and Health Cohort.* Environ Health Perspect, 2016. **124**(3): p. 329-35.
203. Colombo, E., et al., *The K63 deubiquitinase CYLD modulates autism-like behaviors and hippocampal plasticity by regulating autophagy and mTOR signaling.* Proc Natl Acad Sci U S A, 2021. **118**(47).
204. Kraeuter, A.K., P.C. Guest, and Z. Sarnyai, *The Open Field Test for Measuring Locomotor Activity and Anxiety-Like Behavior.* Methods Mol Biol, 2019. **1916**: p. 99-103.
205. Bourin, M. and M. Hascoet, *The mouse light/dark box test.* Eur J Pharmacol, 2003. **463**(1-3): p. 55-65.
206. Crawley, J.N., P. Skolnick, and S.M. Paul, *Absence of intrinsic antagonist actions of benzodiazepine antagonists on an exploratory model of anxiety in the mouse.* Neuropharmacology, 1984. **23**(5): p. 531-7.
207. Rein, B., K. Ma, and Z. Yan, *A standardized social preference protocol for measuring social deficits in mouse models of autism.* Nat Protoc, 2020. **15**(10): p. 3464-3477.
208. Kraeuter, A.K., P.C. Guest, and Z. Sarnyai, *The Y-Maze for Assessment of Spatial Working and Reference Memory in Mice.* Methods Mol Biol, 2019. **1916**: p. 105-111.
209. Jiang, F., et al., *Assessment of the performance of A1CNow(+) and development of an error grid analysis graph for comparative hemoglobin A1c measurements.* Diabetes Technol Ther, 2014. **16**(6): p. 363-9.
210. Fletcher, J.L., *Proceedings of Conference - Noise as a Public Health Hazard - Ward,Wd and Fricke,Je.* Journal of Speech and Hearing Disorders, 1970. **35**(2): p. 198-199.
211. Dobruszkes, F. and M. Efthymiou, *When environmental indicators are not neutral: Assessing aircraft noise assessment in Europe.* Journal of Air Transport Management, 2020. **88**.
212. Cai, Y., et al., *Long-term exposure to road traffic noise, ambient air pollution, and cardiovascular risk factors in the HUNT and lifelines cohorts.* Eur Heart J, 2017. **38**(29): p. 2290-2296.
213. *<Babisch2003.pdf>.*
214. Munzel, T., et al., *Environmental Noise and the Cardiovascular System.* J Am Coll Cardiol, 2018. **71**(6): p. 688-697.
215. Munzel, T., et al., *Adverse Cardiovascular Effects of Traffic Noise with a Focus on Nighttime Noise and the New WHO Noise Guidelines.* Annu Rev Public Health, 2020. **41**: p. 309-328.
216. Guski, R., D. Schreckenberg, and R. Schuemer, *WHO Environmental Noise Guidelines for the European Region: A Systematic Review on Environmental Noise and Annoyance.* Int J Environ Res Public Health, 2017. **14**(12).
217. *WHO/Europe Environmental Noise Guidelines.* Acoustics Australia, 2018. **46**(3): p. 291-291.
218. Dzhambov, A.M. and D.D. Dimitrova, *Residential road traffic noise as a risk factor for hypertension in adults: Systematic review and meta-analysis of analytic studies published in the period 2011-2017.* Environ Pollut, 2018. **240**: p. 306-318.
219. Huang, J., et al., *Road Traffic Noise and Incidence of Primary Hypertension: A Prospective Analysis in UK Biobank.* JACC Adv, 2023. **2**(2): p. None.
220. Wu, S., et al., *Effect of chronic noise exposure on glucose and lipid metabolism in mice via modulating gut microbiota and regulating CREB/CRTC2 and SREBP1/SCD pathway.* Ecotoxicol Environ Saf, 2024. **270**: p. 115887.

221. Liu, L., et al., *The effect of noise exposure on insulin sensitivity in mice may be mediated by the JNK/IRS1 pathway.* Environ Health Prev Med, 2018. **23**(1): p. 6.
222. Liu, L., et al., *Effects of Noise Exposure on Systemic and Tissue-Level Markers of Glucose Homeostasis and Insulin Resistance in Male Mice.* Environ Health Perspect, 2016. **124**(9): p. 1390-8.
223. Di Minno, A., et al., *8-Hydroxy-2-Deoxyguanosine Levels and Cardiovascular Disease: A Systematic Review and Meta-Analysis of the Literature.* Antioxid Redox Signal, 2016. **24**(10): p. 548-55.
224. Di, G. and Y. Xu, *Influences of combined traffic noise on anxiety in mice.* Sci Total Environ, 2017. **579**: p. 1439-1445.
225. Di, G. and L. He, *Behavioral and plasma monoamine responses to high-speed railway noise stress in mice.* Noise Health, 2013. **15**(65): p. 217-23.
226. Peng, X., et al., *Characterization of Anxiety-Like Behaviors and Neural Circuitry following Chronic Moderate Noise Exposure in Mice.* Environ Health Perspect, 2023. **131**(10): p. 107004.
227. Di, G.Q. and Z.Q. Qin, *Influences of combined traffic noise on the ability of learning and memory in mice.* Noise Health, 2018. **20**(92): p. 9-15.
228. Stansfeld, S.A. and M.P. Matheson, *Noise pollution: non-auditory effects on health.* British Medical Bulletin, 2003. **68**: p. 243-257.
229. Porto, L., J. Wouters, and A. van Wieringen, *Speech perception in noise, working memory, and attention in children: A scoping review.* Hear Res, 2023. **439**: p. 108883.
230. Shield, B.M. and J.E. Dockrell, *The effects of environmental and classroom noise on the academic attainments of primary school children.* J Acoust Soc Am, 2008. **123**(1): p. 133-44.
231. Zhang, Y., et al., *Environmental noise degrades hippocampus-related learning and memory.* Proc Natl Acad Sci U S A, 2021. **118**(1).
232. Jones, C.A., D.J. Watson, and K.C. Fone, *Animal models of schizophrenia.* Br J Pharmacol, 2011. **164**(4): p. 1162-94.
233. Cruz, J., et al., *Association of environmental and socioeconomic indicators with serious mental illness diagnoses identified from general practitioner practice data in England: A spatial Bayesian modelling study.* PLoS Med, 2022. **19**(6): p. e1004043.
234. Wright, B., et al., *Effects of environmental noise on cognitive (dys)functions in schizophrenia: A pilot within-subjects experimental study.* Schizophr Res, 2016. **173**(1-2): p. 101-8.
235. Starke, K. and H.J. Schumann, *Interactions of angiotensin, phenoxybenzamine and propranolol on noradrenaline release during sympathetic nerve stimulation.* Eur J Pharmacol, 1972. **18**(1): p. 27-30.
236. Tarazi, R.C., H.P. Dustan, and E.L. Bravo, *Haemodynamic effects of propranolol in hypertension: a review.* Postgrad Med J, 1976. **52 Suppl 4**: p. 92-100.
237. Prichard, B.N., et al., *Heart and catecholamines.* Acta Cardiol, 1991. **46**(3): p. 309-22.
238. Hahad, O., et al., *Acute exposure to simulated nocturnal traffic noise and cardiovascular complications and sleep disturbance-results from a pooled analysis of human field studies.* Clin Res Cardiol, 2023. **112**(11): p. 1690-1698.
239. McKillop, L.E., et al., *Diazepam effects on local cortical neural activity during sleep in mice.* Biochem Pharmacol, 2021. **191**: p. 114515.
240. Tobler, I., et al., *Diazepam-induced changes in sleep: role of the alpha 1 GABA(A) receptor subtype.* Proc Natl Acad Sci U S A, 2001. **98**(11): p. 6464-9.
241. Misrani, A., et al., *Differential effects of citalopram on sleep-deprivation-induced depressive-like behavior and memory impairments in mice.* Prog Neuropsychopharmacol Biol Psychiatry, 2019. **88**: p. 102-111.
242. Saadati, N., et al., *The effects of citalopram, SB-334867 and orexin-1, alone or in various combinations, on the anxiogenic-like effects of REM sleep deprivation in male mice.* Behav Pharmacol, 2022. **33**(8): p. 559-566.

243. Ozyilmaz, E., et al., *Early propranolol treatment ameliorates endothelial dysfunction in experimental septic lung.* Adv Clin Exp Med, 2019. **28**(3): p. 291-297.
244. Hong, S., et al., *Research progress of E-cigarette-A bibliometric analysis during 2010-2022.* Front Public Health, 2022. **10**: p. 928059.
245. Li, X., et al., *Mapping of Global Research on Electronic Cigarettes: A Bibliometric Analysis.* Front Public Health, 2022. **10**: p. 856257.
246. Middlekauff, H.R. and J. Gornbein, *Association of Electronic Cigarette Use With Myocardial Infarction: Persistent Uncertainty.* Am J Prev Med, 2019. **56**(1): p. 159-160.
247. Yu, X., et al., *E-cigarette aerosol exacerbates cardiovascular oxidative stress in mice with an inactive aldehyde dehydrogenase 2 enzyme.* Redox Biol, 2022. **54**: p. 102369.
248. Lerner, C.A., et al., *Vapors produced by electronic cigarettes and e-juices with flavorings induce toxicity, oxidative stress, and inflammatory response in lung epithelial cells and in mouse lung.* PLoS One, 2015. **10**(2): p. e0116732.
249. Anderson, C., et al., *E-Cigarette Aerosol Exposure Induces Reactive Oxygen Species, DNA Damage, and Cell Death in Vascular Endothelial Cells.* Toxicol Sci, 2016. **154**(2): p. 332-340.
250. Scott, A., et al., *Pro-inflammatory effects of e-cigarette vapour condensate on human alveolar macrophages.* Thorax, 2018. **73**(12): p. 1161-1169.
251. FDA,(2022) *Substances Generally Recognized as Safe*, D.o.H.a.H.S. Food and Drug Administration, Editor: https://www.fda.gov/food/food-ingredients-packaging/generally-recognized-safe-gras.
252. Sancilio, S., et al., *Cytotoxicity and apoptosis induction by e-cigarette fluids in human gingival fibroblasts.* Clin Oral Investig, 2016. **20**(3): p. 477-83.
253. Schweitzer, K.S., et al., *Endothelial disruptive proinflammatory effects of nicotine and e-cigarette vapor exposures.* Am J Physiol Lung Cell Mol Physiol, 2015. **309**(2): p. L175-87.
254. Scheffler, S., et al., *Evaluation of E-cigarette liquid vapor and mainstream cigarette smoke after direct exposure of primary human bronchial epithelial cells.* Int J Environ Res Public Health, 2015. **12**(4): p. 3915-25.
255. Conklin, D.J., et al., *Electronic cigarette-generated aldehydes: The contribution of e-liquid components to their formation and the use of urinary aldehyde metabolites as biomarkers of exposure.* Aerosol Sci Technol, 2018. **52**(11): p. 1219-1232.
256. El Mubarak, M.A., et al., *Development and validation of analytical methodology for the quantification of aldehydes in e-cigarette aerosols using UHPLC-UV.* Food Chem Toxicol, 2018. **116**(Pt B): p. 147-151.
257. Witz, G., *Biological interactions of alpha,beta-unsaturated aldehydes.* Free Radic Biol Med, 1989. **7**(3): p. 333-49.
258. Berzelius, J.J., *Lehrbuch der chemie*. Vol. 1. 1831.
259. Redtenbacher, J., *Ueber die zerlegungsprodukte des glyceryloxydes durch trockene destillation.* Justus Liebigs Annalen der Chemie, 1843. **47**(2): p. 113-148.
260. Cai, J., A. Bhatnagar, and W.M. Pierce, Jr., *Protein modification by acrolein: formation and stability of cysteine adducts.* Chem Res Toxicol, 2009. **22**(4): p. 708-16.
261. Sanchez, A.M., et al., *Formation of inter- and intrastrand imine type DNA-DNA cross-links through secondary reactions of aldehydic adducts.* Chem Res Toxicol, 2005. **18**(11): p. 1683-90.
262. Stevens, J.F. and C.S. Maier, *Acrolein: Sources, metabolism, and biomolecular interactions relevant to human health and disease.* Molecular Nutrition & Food Research, 2008. **52**(1): p. 7-25.
263. Jaimes, E.A., et al., *Stable compounds of cigarette smoke induce endothelial superoxide anion production via NADPH oxidase activation.* Arterioscler Thromb Vasc Biol, 2004. **24**(6): p. 1031-6.
264. Nguyen, H., et al., *Cigarette smoke impairs neutrophil respiratory burst activation by aldehyde-induced thiol modifications.* Toxicology, 2001. **160**(1-3): p. 207-217.

265. Guzik, T.J., et al., *Vascular superoxide production by NAD(P)H oxidase: association with endothelial dysfunction and clinical risk factors.* Circ Res, 2000. **86**(9): p. E85-90.
266. McCarty, M.F., *NADPH Oxidase Activity in Cerebral Arterioles Is a Key Mediator of Cerebral Small Vessel Disease-Implications for Prevention.* Healthcare (Basel), 2015. **3**(2): p. 233-51.
267. Landmesser, U., et al., *Role of p47(phox) in vascular oxidative stress and hypertension caused by angiotensin II.* Hypertension, 2002. **40**(4): p. 511-5.
268. Wrabetz, E., G. Peter, and H.J. Hohorst, *Does acrolein contribute to the cytotoxicity of cyclophosphamide?* J Cancer Res Clin Oncol, 1980. **98**(2): p. 119-26.
269. Lau, S., et al., *Effects of acrolein in comparison to its prodrug cyclophosphamide on human primary endothelial cells in vitro.* Toxicol In Vitro, 2020. **62**: p. 104685.
270. Manea, A., et al., *AP-1-dependent transcriptional regulation of NADPH oxidase in human aortic smooth muscle cells: role of p22phox subunit.* Arterioscler Thromb Vasc Biol, 2008. **28**(5): p. 878-85.
271. Manea, A., et al., *Transcriptional regulation of NADPH oxidase isoforms, Nox1 and Nox4, by nuclear factor-kappaB in human aortic smooth muscle cells.* Biochem Biophys Res Commun, 2010. **396**(4): p. 901-7.
272. Li, L., R.F. Hamilton, Jr., and A. Holian, *Effect of acrolein on human alveolar macrophage NF-kappaB activity.* Am J Physiol, 1999. **277**(3): p. L550-7.
273. Ranganna, K., et al., *Acrolein activates mitogen-activated protein kinase signal transduction pathways in rat vascular smooth muscle cells.* Mol Cell Biochem, 2002. **240**(1-2): p. 83-98.
274. Dinkova-Kostova, A.T., et al., *Direct evidence that sulfhydryl groups of Keap1 are the sensors regulating induction of phase 2 enzymes that protect against carcinogens and oxidants.* Proc Natl Acad Sci U S A, 2002. **99**(18): p. 11908-13.
275. Klosterhalfen, S., et al., *Waterpipe Use among Adolescents in Germany: Prevalence, Associated Consumer Characteristics, and Trends (German Health Interview and Examination Survey for Children and Adolescents, KiGGS).* International Journal of Environmental Research and Public Health, 2020. **17**(21).
276. Yan, Y.Y., et al., *Biomarkers of Waterpipe Tobacco Smoke Exposure: A Systematic Review and Meta-Analysis.* Nicotine Tob Res, 2024. **26**(6): p. 655-662.
277. Eissenberg, T. and A. Shihadeh, *Waterpipe tobacco and cigarette smoking: direct comparison of toxicant exposure.* Am J Prev Med, 2009. **37**(6): p. 518-23.
278. Cobb, C.O., et al., *Waterpipe tobacco smoking and cigarette smoking: a direct comparison of toxicant exposure and subjective effects.* Nicotine Tob Res, 2011. **13**(2): p. 78-87.
279. Weaver, L.K., et al., *Carboxyhemoglobin half-life in carbon monoxide-poisoned patients treated with 100% oxygen at atmospheric pressure.* Chest, 2000. **117**(3): p. 801-8.
280. Jacob, P., 3rd, et al., *Comparison of nicotine and carcinogen exposure with water pipe and cigarette smoking.* Cancer Epidemiol Biomarkers Prev, 2013. **22**(5): p. 765-72.
281. Al Ali, R., et al., *Cardiovascular effects of waterpipe smoking: a systematic review and meta-analysis.* Rev Cardiovasc Med, 2020. **21**(3): p. 453-468.
282. Gaber, R. and M. Hamesa, *The effects of pipe water smoking on endothelial function in healthy non smoker volunteers.* Artery Research, 2016. **15**: p. 1-5.
283. Bentur, L., et al., *Laboratory and Clinical Acute Effects of Active and Passive Indoor Group Water-Pipe (Narghile) Smoking.* Chest, 2014. **145**(4): p. 803-809.
284. Nakhaee, M.R., et al., *Effects of Endurance Exercise Training on Cardiac Dysfunction Induced by Waterpipe Tobacco Smoking.* Addict Health, 2019. **11**(2): p. 100-109.
285. Nemmar, A., et al., *Chronic exposure to water-pipe smoke induces cardiovascular dysfunction in mice.* Am J Physiol Heart Circ Physiol, 2017. **312**(2): p. H329-H339.
286. Rababa'h, A.M., et al., *Waterpipe tobacco smoke distresses cardiovascular biomarkers in mice: alterations in protein expression of metalloproteinases, endothelin and myeloperoxidase.* Inhal Toxicol, 2019. **31**(3): p. 99-106.

287. Alarabi, A.B., et al., *Short-Term Exposure to Waterpipe/Hookah Smoke Triggers a Hyperactive Platelet Activation State and Increases the Risk of Thrombogenesis.* Arterioscler Thromb Vasc Biol, 2020. **40**(2): p. 335-349.
288. Kobayashi, A., et al., *Synergetic antioxidant and vasodilatory action of carbon monoxide in angiotensin II - induced cardiac hypertrophy.* Hypertension, 2007. **50**(6): p. 1040-8.
289. Deshmane, S.L., et al., *Monocyte chemoattractant protein-1 (MCP-1): an overview.* J Interferon Cytokine Res, 2009. **29**(6): p. 313-26.
290. Chu, L.M., et al., *Carbon monoxide and a change of heart.* Redox Biol, 2021. **48**: p. 102183.
291. Wolfram, R.M., et al., *Narghile (water pipe) smoking influences platelet function and (iso-)eicosanoids.* Life Sci, 2003. **74**(1): p. 47-53.
292. Dorey, A., et al., *Acute and Chronic Carbon Monoxide Toxicity from Tobacco Smoking.* Mil Med, 2020. **185**(1-2): p. e61-e67.
293. Veen, M., *Carbon Monoxide Poisoning Caused by Water Pipe Smoking: A Case Series.* J Emerg Med, 2016. **51**(3): p. e41-4.
294. Haldane, J., *The Action of Carbonic Oxide on Man.* J Physiol, 1895. **18**(5-6): p. 430-62.
295. Ernst, A. and J.D. Zibrak, *Carbon monoxide poisoning.* N Engl J Med, 1998. **339**(22): p. 1603-8.
296. Ryter, S.W. and A.M. Choi, *Targeting heme oxygenase-1 and carbon monoxide for therapeutic modulation of inflammation.* Transl Res, 2016. **167**(1): p. 7-34.
297. Herman, Z.S., *Carbon monoxide: a novel neural messenger or putative neurotransmitter?* Pol J Pharmacol, 1997. **49**(1): p. 1-4.
298. Wang, R. and L. Wu, *The chemical modification of KCa channels by carbon monoxide in vascular smooth muscle cells.* J Biol Chem, 1997. **272**(13): p. 8222-6.
299. Verma, A., et al., *Carbon monoxide: a putative neural messenger.* Science, 1993. **259**(5093): p. 381-4.
300. Wegiel, B., et al., *Nitric oxide-dependent bone marrow progenitor mobilization by carbon monoxide enhances endothelial repair after vascular injury.* Circulation, 2010. **121**(4): p. 537-48.
301. Boczkowski, J., J.J. Poderoso, and R. Motterlini, *CO-metal interaction: Vital signaling from a lethal gas.* Trends Biochem Sci, 2006. **31**(11): p. 614-21.

Curriculum vitae

List of own publications

1. Ksenija Vujacic-Mirski, Matthias Oelze, **Ivana Kuntic**, Marin Kuntic, Sanela Kalinovic, Huige Li, Jacek Zielonka, Thomas Münzel and Andreas Daiber, Measurement of Tetrahydrobiopterin in Animal Tissue Samples by HPLC with Electrochemical Detection—Protocol Optimization and Pitfalls, Antioxidants, 11(6), 1182, 16 June 2022, https://doi.org/10.3390/antiox11061182
2. Marin Kuntic, **Ivana Kuntic**, Roopesh Krishnankutty, Adrian Gericke, Matthias Oelze, Tristan Junglas, Maria Teresa Bayo Jimenez, Paul Stamm, Margaret Nandudu, Omar Hahad, Karin Keppeler, Steffen Daub, Ksenija Vujacic-Mirski, Sanela Rajlic, Lea Strohm, Henning Ubbens, Qi Tang, Subao Jiang, Yue Ruan, Kenneth G. Macleod, Thomas Münzel, Co-exposure to urban particulate matter and aircraft noise adversely impacts the cerebro-pulmonary-cardiovascular axis in mice, Redox Biology, Volume 59, February 2023, https://doi.org/10.1016/j.redox.2022.102580
3. Omar Hahad, Marin Kuntic, **Ivana Kuntic**, Andreas Daiber & Thomas Münzel, Tobacco smoking and vascular biology and function: evidence from human studies, Pflügers Arch - European Journal of Physiology, Volume 475, pages 797–805, 24 March 2023, https://doi.org/10.1007/s00424-023-02805-z
4. **Ivana Kuntic**, Marin Kuntic, Matthias Oelze, Paul Stamm, Angelica Karpi, Hartmut Kleinert, Omar Hahad, Thomas Münzel & Andreas Daiber, The role of acrolein for E-cigarette vapour condensate mediated activation of NADPH oxidase in cultured endothelial cells and macrophages, Pflügers Arch - European Journal of Physiology, Volume 475, pages 807–821, 07 June 2023, https://doi.org/10.1007/s00424-023-02825-9
5. Maria Teresa Bayo Jimenez, Adrian Gericke, Katie Frenis, Sanela Rajlic, Miroslava Kvandova, Swenja Kröller-Schön, Matthias Oelze, Marin Kuntic, **Ivana Kuntic**, Dominika Mihalikova, Qi Tang, Subao Jiang, Yue Ruan, Georg Daniel Duerr, Sebastian Steven, Michael J. Schmeisser, Omar Hahad, Huige Li, Andreas Daiber, Thomas Münzel, Effects of aircraft noise cessation on blood pressure, cardio- and cerebrovascular endothelial function, oxidative stress, and inflammation in an experimental animal model, Science of The Total Environment, Volume 903, 10 December 2023, https://doi.org/10.1016/j.scitotenv.2023.166106
6. Marin Kuntic, **Ivana Kuntic**, Omar Hahad, Jos Lelieveld, Thomas Münzel, Andreas Daiber, Impact of air pollution on cardiovascular aging, Mechanisms of Ageing and Development, Volume 214, September 2023, https://doi.org/10.1016/j.mad.2023.111857

7. Omar Hahad, Marin Kuntic, Sadeer Al-Kindi, **Ivana Kuntic**, Donya Gilan, Katja Petrowski, Andreas Daiber & Thomas Münzel, Noise and mental health: evidence, mechanisms, and consequences, Journal of Exposure Science & Environmental Epidemiology, 26 January 2024, https://doi.org/10.1038/s41370-024-00642-5
8. Karin Keppeler, Aline Pesi, Simon Lange, Johanna Helmstädter, Lea Strohm, Henning Ubbens, Marin Kuntić, **Ivana Kuntić**, Dominika Mihaliková, Ksenija Vujačić-Mirski, Alexandra Rosenberger, Leonie Küster, Charlotte Frank, Matthias Oelze, Stefanie Finger, Agnieszka Zakrzewska, Elena Verdu, Johannes Wild, Susanne Karbach, Philip Wenzel, Philipp Wild, David Leistner, Thomas Münzel, Andreas Daiber, Detlef Schuppan and Sebastian Steven, Vascular dysfunction and arterial hypertension in experimental celiac disease are mediated by gut-derived inflammation and oxidative stress, Redox Biology, Volume 70, April 2024, https://doi.org/10.1016/j.redox.2024.103071

Acknowledgments

Declarations

This work has not been submitted to any other university, foreign or German, for the conferral of an academic degree.

I declare I have not unsuccessfully ended another doctoral program in the subject of this current doctoral program.

I hereby declare that I wrote the dissertation submitted without any unauthorized external assistance and used only sources acknowledged in the work. All textual passages, which are appropriated verbatim or paraphrased from published and unpublished texts, as well as all information obtained from oral sources are duly indicated and listed in accordance with bibliographical rules. In carrying out this research, I complied with the rules of standard scientific practice as formulated in the statutes of Johannes Gutenberg-University Mainz to insure standard scientific practice.

Signature of Candidate Ivana Kuntić